

**University of Alberta**

**NEW SIGNAL PROCESSING TECHNIQUES FOR MIMO PHYSICAL LAYER**

by

**Damith Nivantha Senaratne**

A thesis submitted to the Faculty of Graduate Studies and Research  
in partial fulfillment of the requirements for the degree of

**Doctor of Philosophy**

in

Communications

Department of Electrical and Computer Engineering

©Damith Nivantha Senaratne

Fall 2012

Edmonton, Alberta

Permission is hereby granted to the University of Alberta Libraries to reproduce single copies of this thesis and to lend or sell such copies for private, scholarly or scientific research purposes only. Where the thesis is converted to, or otherwise made available in digital form, the University of Alberta will advise potential users of the thesis of these terms.

The author reserves all other publication and other rights in association with the copyright in the thesis and, except as herein before provided, neither the thesis nor any substantial portion thereof may be printed or otherwise reproduced in any material form whatsoever without the author's prior written permission.

*Dedicated to my beloved parents...*

# Abstract

Multiple-input multiple-output (MIMO) systems, characterized by multiple antenna transceivers, add a ‘space’ dimension to signal processing for wireless communication. Conventionally, the degrees of freedom (DoFs), i.e., the number of independent data streams that can be transmitted or received, available in the space dimension are utilized to improve the quality-of-service and the data rates. In other words, the spatial DoFs are exploited to gain diversity and multiplexing benefits. However, these DoFs may be used for other purposes (including multicasting, duplexing, and multipath resolution), which are conceivable given the emerging trend of accommodating more and more antennas in wireless terminals. Developing new physical layer signal processing techniques to realize such non-conventional benefits and ascertaining their viability through performance analysis are the main goals of this thesis. GSVD beamforming, which generalizes eigenmode transmission and zero forcing beamforming techniques for two-user MIMO downlink channels, and spatial multipath resolution, a unique application of spatial signal processing to mitigate multipath fading, are proposed here for the first time. Moreover, beamforming techniques for physical-layer multicasting and space division duplexing are developed in detail; the exact performance of channel inversion power allocation over eigenmode transmission is characterized. This thesis develops each of those contributions in detail.

# Acknowledgement

I express my heartfelt gratitude and respect to my advisor, Dr. Chintha Tellambura, who supported me as his student. He gave me the freedom to define and conduct my research, while also guiding me whenever I needed his advice. He was a constant source of inspiration and knowledge, a kind and caring person, and a true professional.

I also wish to thank the Alberta Innovates Technology Futures (AITF) and the Alberta Informatics Circle of Research Excellence (iCORE) for the financial support I received in the form of an AITF Graduate Scholarship.

I am also grateful to the faculty and the staff of the ECE for their support and for creating an environment conducive to research excellence. Special thanks go to professors Dr. Norman Beaulieu, Dr. Witold Krzymien, Dr. Masoud Ardakani, and Dr. Sergiy Vorobyov, with whom I took graduate-level courses, and to Ms. Pinder Bains, the ECE graduate student advisor. My thanks also go to members of my PhD candidacy committee and PhD examining committee.

I would also like to thank Dr. Himlal Suraweera for his invaluable feedback and collaboration while coauthoring publications, and my labmates, including Gayan Amarasuriya, Prasanna Kalansuriya, Gongpu Wang, and Madushanka Soysa, for the fruitful discussions we had and the pleasant times we spent together.

Last but not least, I thank those whose care, sacrifices, and commitment enabled me to become the person I am and to accomplish the little I have. They include my parents, whose sacrifices have been immeasurable and to whom this thesis is dedicated; my brother and my uncle, who complete my family; the Hewapathiranes, who provided me a home away from home in Edmonton; all the teachers I have had since my childhood; my friends and relatives, and of course, the taxpayers of Sri Lanka and Canada. I hope that this thesis will show that all the sacrifices were not in vain.

# Table of Contents

<b>1</b>	<b>Introduction</b>	<b>1</b>
1.1	Background . . . . .	1
1.1.1	Wireless Channel . . . . .	2
1.1.2	MIMO Technology . . . . .	4
1.1.3	Fundamentals . . . . .	6
1.1.4	Beamforming . . . . .	7
1.1.5	Relaying . . . . .	9
1.2	Motivation . . . . .	9
1.3	Thesis Outline & Contributions . . . . .	10
<b>2</b>	<b>GSVD Beamforming</b>	<b>12</b>
2.1	Introduction . . . . .	12
2.2	Signal Processing . . . . .	14
2.3	Characterization of Virtual Channel Gains . . . . .	17
2.4	Transmit Power Normalization . . . . .	20
2.5	Numbers of Private/Common Virtual Channels . . . . .	21
2.6	Numerical Results . . . . .	22
2.6.1	Application in Two-User MIMO Multicasting . . . . .	23
2.6.2	Application in AF Relaying . . . . .	28
2.6.3	Application in Network-Coded Two-Way Relaying . . . . .	31
2.7	Conclusion . . . . .	37
<b>3</b>	<b>Physical-Layer Multicasting</b>	<b>38</b>
3.1	Introduction . . . . .	38

3.2	Background . . . . .	40
3.2.1	Unicast vs. Multicast Virtual Channels . . . . .	40
3.2.2	Block Diagonalization . . . . .	40
3.2.3	Multicast Groups . . . . .	41
3.3	Signal Processing & System Design . . . . .	42
3.3.1	Multicast Antenna Groups (MAGs) . . . . .	43
3.3.2	Determination of MAGs . . . . .	44
3.3.3	Inter-MAG Beamforming . . . . .	48
3.3.4	Intra-MAG Beamforming . . . . .	48
3.4	Numerical Results . . . . .	50
3.5	Conclusion . . . . .	53
<b>4</b>	<b>Spatial Multipath Resolution (SMR)</b>	<b>54</b>
4.1	Introduction . . . . .	54
4.2	Signal Processing . . . . .	56
4.2.1	STBC over Multipath MIMO . . . . .	56
4.2.2	Receiver Design . . . . .	57
4.3	Multipath MIMO Channel Model . . . . .	60
4.4	Numerical Results (for STBC–SMR) . . . . .	61
4.5	Eigenmode Transmission with SMR . . . . .	65
4.6	Conclusion . . . . .	67
<b>5</b>	<b>Space Division Duplexing (SDD)</b>	<b>68</b>
5.1	Introduction . . . . .	68
5.2	Signal Processing . . . . .	70
5.2.1	Transmit vs. Receive SDD . . . . .	70
5.2.2	Eigenmode Transmission with SDD . . . . .	71
5.3	Numerical Results . . . . .	75
5.4	Conclusion . . . . .	81
<b>6</b>	<b>Performance Analysis of MIMO Channel Inversion</b>	<b>82</b>
6.1	Introduction . . . . .	82

6.2	Mathematical Framework . . . . .	84
6.2.1	Arbitrary $m \leq n$ . . . . .	85
6.2.2	Special Case: $m = 2$ . . . . .	86
6.3	Numerical Results . . . . .	87
6.3.1	Arbitrary $m \leq n$ . . . . .	87
6.3.2	Special Case: $m = 2$ . . . . .	88
6.4	Extension to Rician and Semi-Correlated Rayleigh Fading . . . . .	91
6.4.1	Rician Fading . . . . .	92
6.4.2	Min Semi-Correlated Rayleigh Fading . . . . .	94
6.5	Conclusion . . . . .	96
<b>7</b>	<b>Conclusion and Future Work</b>	<b>97</b>
	<b>Bibliography</b>	<b>100</b>
<b>A</b>	<b>Proof for Diversity Order with GSVD beamforming</b>	<b>114</b>
<b>B</b>	<b>Proofs of Theorems on MIMO Channel Inversion</b>	<b>116</b>

# List of Tables

- 2.1 Numbers of CVCs and PVCs realized through GSVD beamforming  
for antennas  $(n, m, p)$  at the source and users  $\mathcal{U}_1, \mathcal{U}_2$ , respectively . 21

# List of Figures

1.1	A basic wireless communication system . . . . .	3
1.2	A $2 \times 3$ multiple-input multiple-output (MIMO) system . . . . .	4
1.3	The basic MIMO system model . . . . .	5
2.1	A two-user MIMO multicast configuration . . . . .	13
2.2	The joint PDF of $\alpha_i$ s in Definition 2.2 for $(m, p, k) \doteq (2, 5, 2)$ . . .	18
2.3	The SERs and diversity orders of the CVCs in the $(N, M_1, M_2) \doteq (2, 3, 4)$ two-user multicast configuration . . . . .	19
2.4	The SERs of the PVCs and CVCs in $(N, M_1, M_2)$ -antenna two-user multicast configurations . . . . .	23
2.5	The SER of $CVC_1$ for $\mathcal{U}_1$ subjected to imperfect CSI in the $(N, M_1, M_2) \doteq (3, 2, 2)$ two-user multicast configuration . . . . .	25
2.6	The SERs of the PVCs and CVCs in $(N, M_1, M_2)$ -antenna asymmetric two-user multicast configurations . . . . .	26
2.7	The SERs of the PVCs and CVCs in the $(N, M_1, M_2) \doteq (4, 3, 3)$ two-user multicast configuration under asymmetric fading . . . . .	27
2.8	A MIMO relay system comprising a direct path and a relayed path .	28
2.9	The SERs of the VCs in the $(N_s, N_r, N_d) \doteq (4, 3, 5)$ MIMO AF relay configuration . . . . .	30
2.10	A network-coded MIMO two-way relay system . . . . .	31
2.11	The SERs of the VCs in the $(M, N) \doteq (4, 3)$ network-coded MIMO two-way relay configuration . . . . .	34
2.12	The hop-by-hop SERs of the VCs (for the $\mathcal{U}_1 \rightarrow \mathcal{U}_2$ direction) in the $(M, N) \doteq (4, 3)$ network-coded MIMO two-way relay configuration	35

3.1	VC-to-User mapping in physical-layer multicasting (PLM) . . . . .	39
3.2	A simple VC-to-User mapping involving three users and four mul- ticast VCs . . . . .	45
3.3	The SERs at each user in Example 3.2, assuming $N = 7$ and PLM based on $\Gamma_2$ . . . . .	50
3.4	The SERs at each user in Example 3.2, assuming $N = 6$ and PLM based on $\Gamma_2$ . . . . .	51
4.1	The basic rake receiver structure for spatial multipath resolution (SMR) . . . . .	57
4.2	Ray-scattering in accordance to the multipath MIMO channel model in Section 4.3 . . . . .	60
4.3	(a) Histogram of channel length $L$ corresponding to a $10 \times 2$ multi- path MIMO channel (b) Average relative strength of the $k^{\text{th}}$ strongest multipath component . . . . .	61
4.4	The SERs of SMR with STBC for $N_r = 10$ and Alamouti code . . .	62
4.5	The SERs of SMR with STBC for Alamouti code and the cases $N_r = 10$ and $N_r = 12$ . The channel length is constrained not to exceed 4 . . . . .	64
4.6	The SERs of partial and adaptive SMR with STBC for $N_r = 10$ and Alamouti code . . . . .	64
4.7	The SERs of $\text{VC}_k, k \in \{1, 2, 3\}$ in SMR with eigenmode transmis- sion for $N_t = 3, N_r = 10$ , and $n = 3$ . . . . .	66
5.1	A MIMO terminal using space division duplexing (SDD) . . . . .	69
5.2	Eigenmode transmission alongside MIMO SDD . . . . .	72
5.3	The SERs for $\text{VC}_1$ in either direction of $\{M_1, N_1\}_1 \leftrightarrow \{M_2, N_2\}_1$ MIMO SDD configurations . . . . .	75
5.4	The SERs for each $\text{VC}_k$ in either direction of the $\{7, 4\}_3 \leftrightarrow \{5, 3\}_2$ MIMO SDD configuration . . . . .	76
5.5	The effect of finite computational precision on the SERs for MIMO SDD eigenmode transmission . . . . .	77

5.6	The effect of finite analog-to-digital converter (ADC) resolution on the SERs for MIMO SDD eigenmode transmission . . . . .	79
5.7	The interplay of channel-estimation errors and finite ADC resolution in MIMO SDD eigenmode transmission . . . . .	80
6.1	The SERs of $N_r \times N_t$ MIMO systems—ZF vs. CI . . . . .	83
6.2	The CDF of $\Lambda$ over $\{2 \times 2, 3 \times 2, 3 \times 3\}$ MIMO systems using channel inversion (CI) . . . . .	88
6.3	Ergodic capacity (bit/s/Hz) for a $2 \times n$ MIMO system using CI . . .	89
6.4	The SER for binary phase shift keying (i.e. $\mu = \nu = 1$ ) over a $2 \times n$ MIMO system using CI . . . . .	91
6.5	The PDF of $\Lambda$ over $2 \times n$ Rician faded MIMO systems using CI . .	93
6.6	The PDF of $\Lambda$ over $2 \times n$ semi-correlated Rayleigh faded MIMO systems using CI . . . . .	95

# List of Abbreviations

<b>Abbreviation</b>	<b>Definition</b>
3GPP	3rd-generation partnership project
ADC	analog-to-digital converter
AF	amplify-and-forward
BD	block diagonalization
CDF	cumulative distribution function
CI	channel inversion
CSI	channel-state information
CVC	common virtual channel
DoF	degree of freedom
Gbps	gigabits per second
GSVD	generalized singular value decomposition
i.i.d.	independent and identically distributed
IMT	International Mobile Telecommunications
ISI	inter-symbol interference
ISM	industrial, scientific, and medical (band)
ITU	International Telecommunication Union
kbps	kilobits per second
LTE	long term evolution
MAG	multicast antenna group
Mbps	megabits per second
MG	multicast group
MGF	moment generating function
MIMO	multiple-input multiple-output

<b>Abbreviation</b>	<b>Definition</b>
OFDM	orthogonal frequency division multiplexing
PDF	probability density function
PLM	physical-layer multicasting
PVC	private virtual channel
QPSK	quadrature phase shift keying
SDD	space division duplexing
SER	symbol error rate
SMR	spatial multipath resolution
SNR	signal to noise ratio
STBC	space time block code
SVD	singular value decomposition
VC	virtual channel
XOR	(bitwise) exclusive OR (operation)
ZF	zero forcing

# List of Symbols

- Basic arithmetic, set, and calculus notations have standard definitions.

## Elementary & Special Functions

Notation	Definition
$\lceil \cdot \rceil$	ceiling function
$\lfloor \cdot \rfloor$	floor function
$\delta(\cdot)$	Kronecker delta function
$\operatorname{erf}(\cdot)$	Gauss error function [1, Sec. 7.1]
$\mathcal{G}_p^m \mathcal{G}_q^n \left( \cdot \left  \begin{matrix} a_1, \dots, a_n, a_{n+1}, \dots, a_p \\ b_1, \dots, b_m, b_{m+1}, \dots, b_q \end{matrix} \right. \right)$	Meijer $\mathcal{G}$ function [2, Sec. 9.3]
$\mathcal{I}_\nu(\cdot)$	modified Bessel function of the first kind of order $\nu$ [1, Sec. 9.6]
$\mathcal{K}_\nu(\cdot)$	modified Bessel function of the second kind of order $\nu$ [1, Sec. 9.6]
$\log(\cdot)$	natural logarithm
$\log_2(\cdot)$	logarithm to base 2
$\mathcal{Q}(\cdot)$	Gaussian $\mathcal{Q}$ -function [1, Eqn. (26.2.3)]
$\sin(\cdot)$	sine function

## Probability & Statistics

Let  $X$  be a random variable [3, Ch. 6], and  $\mathcal{A}$ , an arbitrary event.

Notation	Definition
$\mathcal{E}_X\{\cdot\}$	expected value with respect to $X$ ; $\mathcal{E}\{\cdot\}$ , if $X$ is implied
$f_X(\cdot)$	probability density function (PDF) of $X$
$F_X(\cdot)$	cumulative distribution function (CDF) of $X$
$\bar{F}_X(\cdot)$	complimentary CDF of $X$
$\mathcal{M}_X(\cdot)$	moment generating function (MGF) of $X$
$\mathcal{P}[\mathcal{A}]$	probability of $\mathcal{A}$

# Matrices

Let  $\mathbf{A} \in \mathbb{C}^{m \times n}$  denote an  $m \times n$  complex matrix [4].

Notation	Definition/ interpretation
$\mathbf{A}(i, j)$	$i^{\text{th}}$ element on the $j^{\text{th}}$ column of $\mathbf{A}$
$\ \mathbf{A}\ _F$	Frobenius norm of $\mathbf{A}$ [5, p.291]
$\{\mathbf{A}\}_{\mathcal{C}(c_a:c_b)}$	sub-matrix of $\mathbf{A}$ , formed with its columns $c_a$ through $c_b$
$\{\mathbf{A}\}_{\mathcal{C}(c)}$	shorthand for $\{\mathbf{A}\}_{\mathcal{C}(1:c)}$
$\{\mathbf{A}\}_{\mathcal{C}(\mathcal{L})}$	sub-matrix of $\mathbf{A}$ , formed with its columns whose indices are in set $\mathcal{L} \subseteq \{1, \dots, n\}$
$\{\mathbf{A}\}_{\mathcal{D}(d_a:d_b)}$	square-diagonal matrix formed with the elements in positions $d_a$ through $d_b$ along the main-diagonal of $\mathbf{A}$ .
$\{\mathbf{A}\}_{\mathcal{R}(r_a:r_b)}$	sub-matrix of $\mathbf{A}$ , formed with its rows $r_a$ through $r_b$
$\{\mathbf{A}\}_{\mathcal{R}(r)}$	shorthand for $\{\mathbf{A}\}_{\mathcal{R}(1:r)}$
$(\mathbf{A}, \mathbf{B})$	concatenation of matrices $\mathbf{A}$ and $\mathbf{B} \in \mathbb{C}^{m \times \hat{n}}$
$(\mathbf{B}_1 \dots \mathbf{B}_K)$	horizontal concatenation of matrices $\mathbf{B}_i \in \mathbb{C}^{m \times n_i}, i \in \{1, \dots, K\}$
$\begin{pmatrix} \mathbf{B}_{1,1} & \dots & \mathbf{B}_{1,n} \\ \vdots & & \vdots \\ \mathbf{B}_{m,1} & \dots & \mathbf{B}_{m,n} \end{pmatrix}$	block matrix formed by vertical/horizontal concatenation of matrices $\mathbf{B}_{i,j}$ having compatible dimensions (implicit zero matrices complete the structure)
$\mathbf{A} = \text{diag}(a_1, \dots, a_n)$	$\mathbf{A}$ is rectangular diagonal; $a_1$ through $a_n$ are the non-zero diagonal elements
$\mathbf{A}^{-1}$	inverse of $\mathbf{A}$ (for $m = n$ )
$\mathbf{A}^\dagger$	Moore-Penrose pseudo inverse of $\mathbf{A}$ [4, Sec. 3.4]
$\mathbf{A}^*$	conjugate of $\mathbf{A}$
$\mathbf{A}^H$	conjugate transpose of $\mathbf{A}$
$\mathbf{A}^T$	transpose of $\mathbf{A}$
$\text{diag}(\mathbf{A})$	elements on the main diagonal of $\mathbf{A}$
$\text{eig}(\mathbf{A})$	eigenvalues of $\mathbf{A}$ (for $m = n$ ) [4, Ch. 5]
$\mathbf{I}_n$	identity matrix of rank $n$
$\text{nullity}(\mathbf{A})$	nullity of $\mathbf{A}$ [4, p.72]
$\text{Null}(\mathbf{A})$	nullspace of $\mathbf{A}$ [4, Sec. 2.4]
$\text{Null}(\mathbf{A}^T)$	left nullspace of $\mathbf{A}$ [4, Sec. 2.4]
$\text{rank}(\mathbf{A})$	rank of $\mathbf{A}$ [5, Sec. 0.4]
$\text{trace}(\mathbf{A})$	trace of $\mathbf{A}$ (for $m = n$ ) [4, p.186]

## MIMO systems

Notation	Definition
$M \times N$ channel	multiple-input multiple-output (MIMO) channel (see Subsection 1.1.2) corresponding to $N$ transmit antennas and $M$ receive antennas
$\{M_1, \dots, M_K\} \times N$ channel	multi-user MIMO channel corresponding to an $N$ -antenna source and $K$ users having, respectively, $M_1$ through $M_K$ receive antennas (see Chapter 3)
$\{M_1, N_1\}_{s_1} \leftrightarrow \{M_2, N_2\}_{s_2}$	MIMO space division duplexing (SDD) configuration (see Chapter 5) with $(M_i, N_i)$ transmit and receive antennas at each terminal $\mathcal{U}_i$ , $i \in \{1, 2\}$ , and supporting $s_i$ virtual channels from $\mathcal{U}_1$ , and $s_2$ , from $\mathcal{U}_2$ .
$S \rightarrow D$	MIMO subsystem comprising transmit antennas of terminal $S$ and receive antennas of terminal $D$

## Miscellaneous

Notation	Definition
$ a $	absolute value of scalar $a$
$a^*$	complex conjugate of scalar $a$
$k!$	factorial of $k$ [1, Eqn. (6.1.5)]
$\binom{n}{k}$	binomial coefficient $n$ choose $k$ [1, Sec. 3.1]
$\arg \min_i (a_i)$	index $i$ corresponding to the smallest $a_i$
$\lim_{x \rightarrow a} f(x)$	the limit of function $f(x)$ as $x$ tends to $a$
$\max (a_1, a_2)$	maximum of scalars $a_1$ and $a_2$
$\min (a_1, \dots, a_n)$	minimum of all scalars $a_i$ for relevant $i$ ; also $\min_i (a_i)$
$o(x^n)$	the remainder in a Maclaurin series [2, Eqn. (0.318.2)] of a function of $x$ after the $x^n$ term
$\Re (a)$	real component of (complex) scalar $a$

# Chapter 1

## Introduction

### 1.1 Background

Led by the growth of cellular networks, wireless local/metropolitan area networks, and personal area networks, wireless communication technologies are providing ubiquitous access to information, revolutionizing virtually every aspect of our lives. For example, most consumer electronic devices, from smart phones, tablets, and notebooks to cameras, printers, and televisions, have built-in wireless connectivity. Central to these technologies is the ability to transmit data from the source wireless terminal (known as, the transmitter) in the form of a radio signal (i.e., data mapped as symbols onto radio waves) and reliably recover the data at the destination terminal (known as, the receiver) from the noisy and possibly distorted version of the signal received. Depending on the radio propagation environment, various *signal processing* techniques are utilized to satisfy the end-user requirements such as the desired minimum data rate and the tolerable maximum error rate. Bandwidth and transmit power are the major resources in wireless communication; both are expensive, and bandwidth is scarce and needs to be shared among the coexisting wireless systems. Consequently, efficient resource utilization is an important consideration with signal processing techniques.

Developing novel signal processing techniques is crucial to keep abreast with the increasing demand for faster, reliable, and seamless wireless connectivity. The ITU IMT-advanced requirements [6] for the fourth-generation cellular systems (e.g., the 3GPP LTE-advanced [7] standard), for instance, call for data rates up to 1 Gbps

for fixed/nomadic users and 100 Mbps for mobile users. Several new signal processing techniques, including multiple-input multiple-output (MIMO) [8] and orthogonal frequency division multiplexing (OFDM) [9] technologies, have been fundamental to achieving such data rates, which are an increase in orders of magnitude over the third-generation peak data rates (i.e., 2 Mbps and 384 kbps for nomadic and mobile users, respectively) a decade ago. Given the incessant demand for higher data rates [10] and improved quality-of-service, the next-generation wireless systems will require similar advancement and, hence, the development of new signal processing techniques.

A communication system has a layered architecture, perceived as a stack of ‘layers’ encompassing different functionalities. (The open systems interconnection model [11] is an example of such architecture.) The *physical layer* lies at the bottom of this stack and defines the system’s interaction with the physical communication medium, for example, in terms of modulation, channel coding, and beamforming techniques. Since the interaction between the layers dictates how the system functions, the physical-layer techniques and other intermediate-layer techniques are designed and optimized to suit the application layer, which resides at the top of this stack and defines the end-user experience of the services.

This doctoral thesis focuses on developing novel signal processing techniques for the physical layer of MIMO systems, which are wireless communication systems with terminals supporting multiple transmit and receive antennas. The remainder of this section explains the technical background; the following sections present motivation, thesis outline, and the contributions of this thesis.

### **1.1.1 Wireless Channel**

A wireless communication system comprises wireless terminals and the wireless channel [12, Ch. 2] — or simply, the *channel* (Fig. 1.1) — the radio wave propagation medium existing between them. The channel and the transceivers (i.e., transmitters and receivers) attenuate and/or amplify the signal, the cumulative effect of which is manifested as a complex channel gain. Moreover, various phenomena related to the wireless medium and the radio transceiver circuitry corrupt the received

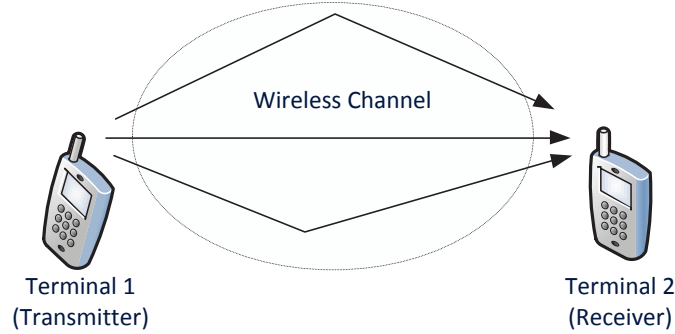


Figure 1.1: A basic wireless communication system.

signal by introducing noise. Therefore, the received signal  $\mathbf{y}$  corresponding to a transmitted signal  $\mathbf{x}$  may be mathematically modeled as

$$\mathbf{y} = h \cdot \mathbf{x} + \mathbf{n}, \quad (1.1)$$

where  $h$  and  $\mathbf{n}$ , respectively, denote the channel gain and the additive noise. Here,  $\mathbf{x}$  represents the data mapped onto symbols by using a modulation scheme [13, Ch. 5]. The additive noise  $\mathbf{n}$  arises mainly due to the thermal agitation of electrons; it is uniformly distributed across the entire bandwidth and hence referred to as white noise, and thus denoted as additive white Gaussian noise [14, Sec. 2.2]. The gain  $h$  reflects the channel state. The receiver uses the channel-state information (CSI), an estimate of  $h$  gained through the channel-estimation process, in signal detection, i.e., to determine  $\mathbf{x}$  from  $\mathbf{y}$  within a level of reliability dictated by the noise statistics and quantified in terms of the symbol error rate (SER), or how often the received symbols get detected incorrectly. The average SER<sup>1</sup> of a wireless system typically improves with the signal to noise ratio (SNR) [12, Eqn. (3.9)], which is the ratio of the average signal power to the average noise power. The rate of improvement depends on the system and the channel, and relates to the diversity order (see Subsection 1.1.3). Moreover, the channel has a maximum SNR-dependent data rate achievable with an arbitrarily small SER, known as the channel capacity [12, Ch. 5]. Wireless systems rarely operate in isolation; therefore, interference caused by other wireless systems as well the electromagnetic interference caused by various external sources gets added to  $\mathbf{y}$  in (1.1). In many wireless systems, including the

<sup>1</sup>The qualifier ‘average’ is implied where it is subsequently omitted for brevity.

cellular networks, such interference has a more detrimental effect on the systems' performance than noise.

The channel state itself is random. The random, small-scale fluctuation of the channel gain, due to reflection and scattering caused by the obstacles in the radio propagation environment, is known as fading [12, Sec. 2.1]. Fading is flat (or, frequency flat), if all frequency components of the signal are affected alike so as not to significantly distort the transmitted symbols. The opposite, the frequency selective fading condition, results from delayed reception of the signal over multiple signal propagation paths and affects the frequency components differently, causing the symbols to spread in time. Because of spreading, each symbol interferes with the reception of subsequent symbols, an effect known as the inter-symbol interference (ISI), making symbol-by-symbol signal detection impossible. Equalization [14, Sec. 10.2] and OFDM are among the techniques used to mitigate the ISI.

Channel estimation, which consumes additional bandwidth and transmit power, is typically performed once per each block of symbols; longer block lengths are desirable provided that the variation of the channel within each block is insignificant, given the amount of fading. The block fading assumptions used in performance analysis thus regard the channel as not varying within a block of symbols, simplifying the analysis and simulation of wireless systems.

### 1.1.2 MIMO Technology

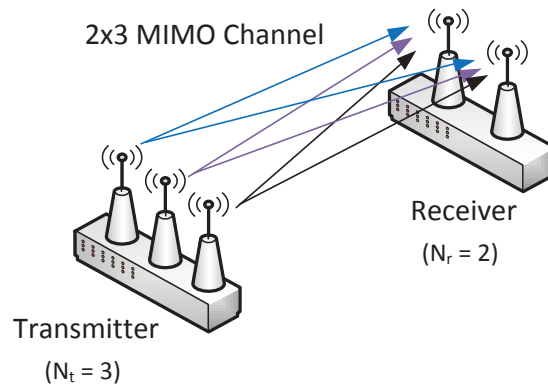


Figure 1.2: A  $2 \times 3$  MIMO system.

Conventionally, each transceiver is equipped with a single antenna. The corresponding channel is designated as single-input single-output. A *multiple-input multiple-output* (MIMO) channel (Fig. 1.2) arises when each transceiver supports synchronous data transmission/reception over multiple antennas [8, 15]. It can be represented as a matrix  $\mathbf{H} \in \mathbb{C}^{N_r \times N_t}$  of complex numbers, where  $N_t$  and  $N_r$  denote the numbers of transmitter and receiver antennas, respectively. The element  $h_{i,j} = \mathbf{H}(i, j)$  represents the channel gain between the  $j^{\text{th}}$  transmitter antenna,  $1 \leq j \leq N_t$ , and the  $i^{\text{th}}$  receiver antenna,  $1 \leq i \leq N_r$ . The  $h_{i,j}$ s are not necessarily independent; however, they fluctuate randomly, because of fading. Therefore,  $\mathbf{H}$  is modeled as a random matrix and analyzed by using random matrix theory [16].

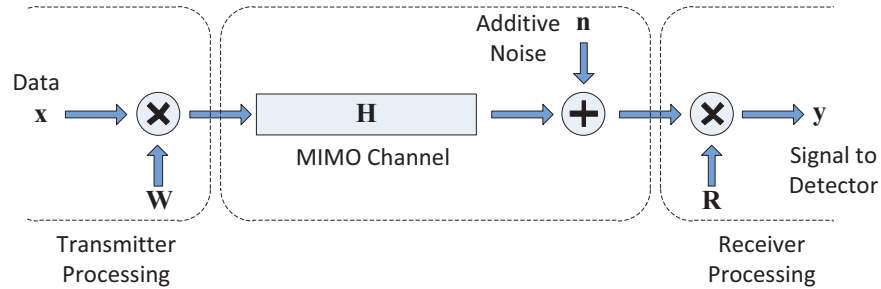


Figure 1.3: The basic MIMO system model.

Under flat fading, the channel output is modeled (Fig. 1.3) as dependent only on its present input and the state  $\mathbf{H}$ . Thus, for a transmitted signal  $\mathbf{x} \in \mathbb{C}^{n \times 1}$ , we get a signal  $\mathbf{y} \in \mathbb{C}^{n \times 1}$  of the following form as the detector input:

$$\mathbf{y} = \mathbf{R}(\mathbf{H}\mathbf{W}\mathbf{x} + \mathbf{n}). \quad (1.2)$$

$\mathbf{n} \in \mathbb{C}^{N_r \times 1}$  represents the additive noise. Signal processing is typically assumed to be linear, and, therefore, the matrices  $\mathbf{W} \in \mathbb{C}^{N_t \times n}$  and  $\mathbf{R} \in \mathbb{C}^{n \times N_r}$  represent the transmitter precoding and receiver reconstruction operations, respectively. The choice of  $\mathbf{x}$ ,  $\mathbf{W}$ , and  $\mathbf{R}$  is central to many MIMO signal processing techniques (see Subsection 1.1.4).

However with frequency-selective fading, (1.2) becomes a discrete convolution, since the corresponding channel output depends on both the present and past inputs. Chapter 4 investigates such a MIMO system.

### 1.1.3 Fundamentals

#### (DoFs, Virtual Channels, Diversity, Multiplexing, and Multicasting)

Each independent data stream that a wireless terminal may transmit and/or receive corresponds to a single *degree of freedom* (DoF) [17]. The spatial DoFs thus dictate the maximum number of data streams that may be accommodated in the space dimension alone. Depending on the communication system, the DoFs may exist over one or more orthogonal dimensions, such as time, frequency, space, and polarization. The total number of DoFs in such cases is the product of those along individual dimensions.

With transmitter and receiver signal processing techniques that may be broadly categorized as channelization schemes, *virtual channels* (VCs), i.e., multiple logical channels, each conveying an independent data stream, can be realized over the physical wireless channel. Accommodating multiple data streams over a channel is known as *multiplexing*, whose extent is quantified by the multiplexing gain [18] that is information theoretically defined as

$$\lim_{\rho \rightarrow \infty} \frac{R(\rho)}{\log(\rho)}. \quad (1.3)$$

$R(\rho)$  in (1.3) is the data rate achievable with a SNR  $\rho$ . For instance, zero forcing (ZF) [19] and space time block codes (STBCs) [20] are two channelization schemes for space-division multiplexing (i.e., for multiplexing in space dimension). The multiplexing gain is limited by the DoFs at each terminal; in space-division multiplexing, the rank of the *effective* MIMO channel the terminal has with the other terminals limits this gain. The rank is typically the minimum of the numbers of transmitter and receiver antennas; it is lower in rank-deficient channels (e.g., key-hole channels [21]). The end-user requirements could restrict further the utilization of the available DoFs for multiplexing.

Noise, interference, and fading are responsible for the symbol errors occurring in wireless communication (see Subsection 1.1.1). The detrimental effects of fading can be alleviated by sending the same information over multiple independently faded paths so that the reliability of reception improves. This approach is known as *diversity* and may be implemented over one or more of the aforementioned dimen-

sions. The diversity order (or diversity gain) quantifies the number of independently faded replicas of a transmitted symbol the destination receives. It may be technically defined [22, Eqn. (3)] as

$$\lim_{\rho \rightarrow \infty} -\frac{\log(P_e(\rho))}{\log(\rho)}, \quad (1.4)$$

where  $P_e(\rho)$  is the SER corresponding to a SNR  $\rho$ . Higher diversity orders are generally desired. A zero diversity order implies that the SER does not improve with the SNR; i.e., interference is dominant, not noise. Depending on the channelization technique, each spatially multiplexed data stream between two terminals may experience the same or different diversity gains. Moreover, a diversity–multiplexing trade-off [22] exists in many communication systems.

*Multicasting* [23] is transmitting the same information to a group of receivers known as a multicast group (MG). Subjected to the DoFs at the participating terminals, more than one concurrent multicast communication, having possibly overlapping sets of receivers, can be facilitated. Unicasting involves having one receiver in a MG, while broadcasting corresponds to a MG constituting all the receivers. With the ever increasing end-user demand for wireless multimedia content, multicasting is becoming a core capability of wireless networks. For instance, the IEEE 802.11-2012 standard [24], the latest revision of Wi-Fi, supports broadcast/multicast and unicast data delivery. The phrase ‘broadcast channel’ [25] is used in a loose sense to designate a single source terminal unicasting different messages to multiple destinations. There, the emphasis is on the broadcast nature of the underlying physical wireless channel and not on the unicast nature of the individual VCs.

### 1.1.4 Beamforming

Beamforming techniques [26] are channelization schemes that typically use linear signal processing at the transceivers, relying on the availability of the CSI to accommodate ideally non-interfering VCs in the space dimension. Each VC being single-input single-output, the modulation, coding, and resource allocation techniques for single-antenna systems can be applied unaltered on the VCs, thus rendering beamforming techniques attractive. Beamforming may be achieved through transmitter

processing, receiver processing, or joint transmitter–receiver processing. Given the MIMO channel  $\mathbf{H}$  in (1.2), beamforming involves choosing the transmit precoding and receiver reconstruction matrices  $\mathbf{W}$  and  $\mathbf{R}$ , also known as the transmit and receiver beamforming matrices, such that the product  $\mathbf{R}\mathbf{H}\mathbf{W}$  has the desired diagonal structure. Eigenmode transmission [8] and ZF [19] are two examples of beamforming techniques; eigenmode transmission uses the singular value decomposition (SVD) to jointly compute  $\mathbf{R}$  and  $\mathbf{W}$ , whereas ZF uses the pseudo-inverse of  $\mathbf{H}$  as one of them (and an identity matrix as the other).

Most beamforming techniques require CSI at the transmitter, or equivalently, feeding back the transmit beamforming matrices computed at the receiver to the transmitter. Despite the resulting complexity, such joint transmitter–receiver processing allows optimal performances. For example, eigenmode transmission achieves the MIMO channel capacity [8, Sec 3.1] by aligning the VCs along the spatial directions corresponding to the eigenvectors of a MIMO channel.

Multi-user beamforming is required where more than two terminals are involved, as with a source terminal, e.g., a base station, communicating with multiple user terminals. ZF can be used for beamforming in the broadcast channels as well. Also known as multi-user MIMO decomposition [27], block diagonalization (BD) [28] is a more effective generalization of ZF for multi-antenna receivers. The source generally does not have sufficient DoFs to accommodate all the users. As a result, additional consideration for user-selection, antenna-selection, and scheduling [29] is required with multi-user beamforming.

Some linear beamforming techniques accommodate a certain level of interference between the VCs to, for example, minimize the overall SER [30] or optimize other criteria [31]. Moreover, non-linear and iterative beamforming/precoding techniques that yield optimal performances with respect to various criteria also exist [28, 32–34]. However, the focus of this research is on linear and non-iterative beamforming techniques that facilitate interference-free channelization.

### 1.1.5 Relaying

Since wireless communication is inherently of a broadcast nature, terminals other than the intended destination can receive and detect the signals; such terminals may act as relays [35], improving the quality-of-service of wireless communications by forwarding thus received signals. Relaying encompasses conventional infrastructure-based relays as well as the emerging cooperative relays [36], and provides benefits including spatial diversity, increased coverage, and transmit-power saving. Relay processing algorithms include amplify-and-forward (AF), decode-and-forward, and code-and-forward [37] techniques. AF relays forward the received signal after amplifying and possibly beamforming, while the decode-and-forward relays forward data regenerated after signal detection and error correction. Code-and-forward relays do further processing after regeneration, employing coding techniques to, for example, improve the resource utilization.

## 1.2 Motivation

Conventional wireless terminals used to have no more than one antenna. Even where multiple receiver antennas were used to improve the diversity, as in diversity combining [13, Ch. 7], signal processing (e.g., signal detection) was more or less single-input single-output. However, with the advancement of electronics, synchronous transmission and reception via multiple antennas has become possible even in hand-held terminals, and MIMO systems have emerged. Exploiting the spatial DoFs, MIMO systems may support data rates and a quality-of-service unmatched by single-antenna systems using comparable resources. Hence, MIMO technology is becoming ubiquitous, with the latest LTE (e.g., 3GPP TS 36.201 [38]), Wi-Fi (IEEE 802.11-2012 [24]), and WiMAX (IEEE 802.16e [39]) standards as well as the emerging 60 GHz systems (e.g., IEEE 802.15.3c [40]) embracing it. Given the higher achievable data rates, MIMO technologies are also an essential component of the evolved multimedia broadcast multicast services (3GPP TS 36.300 [41]) of the LTE and LTE-advanced standards [42].

The statistical characterization of the wireless channel has certain similarities in

the space, time, and frequency dimensions. For instance, the notions of coherence distance, coherence time, and coherence bandwidth [12, Ch. 2.1] indicate that spatial DoFs have subtle similarities with their temporal and frequency counterparts. Currently, the diversity and multiplexing benefits of MIMO are being exploited to achieve higher data rates without compromising the quality-of-service. Many other possibilities (including multicasting, duplexing, and multipath resolution), which the aforementioned similarities imply, remain unexplored. The main reason for their low appeal for the research community and the consequent lack of related work in the research literature was that a terminal could possess only few spatial DoFs, given the difficulties of physically accommodating a large number of antennas at a terminal and supporting the increased signal-processing requirements. However, the advancement of electronics and the gradual shift towards higher frequency bands are increasing the availability of spatial DoFs. For instance, reference [43] describes a 16-antenna in-package design for 60 GHz systems, embodying all the antennas and the complete transceiver circuitry on a  $44 \text{ mm}^2$  semiconductor wafer. WiGig alliance [44] is already promoting the use of the unlicensed 60 GHz industrial, scientific, and medical (ISM) band for high-speed wireless communication alongside the other ISM bands. This emerging trend makes the aforementioned non-conventional uses of spatial DoFs viable. The need to develop new signal processing techniques to facilitate them motivated this research.

### 1.3 Thesis Outline & Contributions

Chapters 2–6 of this thesis deal with either unexplored or sparingly studied issues in spatial signal processing, establishing a background/framework for future research. Chapter 7 presents the conclusions; the bibliography and the appendices follow.

- Chapter 2 introduces *GSVD beamforming*, which the author has proposed for two-user MIMO downlink channels [45, 46], and investigates its characteristics. The SER performance of applications in multicasting, AF relaying, and physical-layer network-coded two-way relaying is examined via simulation to gain further insights. Distinguishing between the private and common VCs and exactly char-

acterizing the VC gains of certain configurations are also novel.

- In Chapter 3, a beamforming scheme [47] for *physical-layer multicasting* (PLM) is presented. By employing a divide-and-conquer strategy based on the novel notion of multicast antenna groups (MAGs), the scheme can implement, through non-iterative beamforming, all the point-to-point and point-to-multipoint VCs corresponding to an arbitrary VC-to-User mapping (provided sufficient DoFs are present at the terminals). This ability makes the scheme unique among non-iterative PLM techniques; its feasibility is demonstrated through SER simulation.
- Chapter 4 is on *spatial multipath resolution* (SMR), a unique use of spatial DoFs to combat multipath fading, proposed and explored in this research [48,49]. SMR uses the space dimension to extract multipath components of the received signal; they are appropriately delayed and combined to flatten the effective MIMO channel. The benefits and drawbacks of SMR are investigated through SER simulation for STBC and beamforming applications. Moreover, the benefits of partial and adaptive SMR are shown with respect to the STBC application.
- Although presently impeded by practical hardware limitations, *space division duplexing* (SDD) is recognized as a technology with the potential to double the spectral efficiency of wireless systems. Recent experimental evidence [50] demonstrating the ability of SDD to achieve a duplex separation of over 45 dB has brought it back to the limelight. Chapter 5 discusses implementing eigenmode transmission on top of SDD as investigated in [51] and provides useful insights about the corresponding SER performance. For instance, the role of low analog-to-digital converter (ADC) resolution behind the limited achievable duplex separations is identified.
- Chapter 6 investigates the feasibility of using the channel inversion (CI) power allocation scheme on top of eigenmode transmission. A mathematical framework for performance analysis of MIMO CI is developed; new closed-form results characterizing the received SNR and the SER are derived during this process [52].

~

# Chapter 2

## GSVD Beamforming

This chapter introduces the fundamentals of GSVD beamforming, a non-iterative beamforming technique proposed in this research for two-user multicast channels, providing detailed insights into its performance and highlighting its potential applications. GSVD beamforming, given its ability to facilitate both common and private virtual channels (VCs), may be applied in multiple-input multiple-output (MIMO) relaying and physical-layer multicasting.

### 2.1 Introduction

Beamforming techniques (see Subsection 1.1.4) for the single-user MIMO channel are well-characterized. For instance, eigenmode transmission achieves the MIMO capacity [8, Sec 3.1] by aligning the VCs along spatial directions corresponding to the eigenvectors of the channel. However, beamforming techniques for multi-user MIMO multicast channels, where a single source (e.g., a base station) spatially multiplexes transmissions to multiple users/destinations, are not as well developed. In fact, before GSVD beamforming, only iterative beamforming techniques for facilitating point-to-multipoint VCs (for multicast data) were mentioned in the literature. Block diagonalization (BD) [28], the best known non-iterative multi-user beamforming technique, for instance, produces only point-to-point VCs; it also requires that the source has more antennas than those of all the users combined, even if implementing a mere fraction of the realizable VCs. Thus, developing novel multi-user beamforming techniques is of great interest, especially for meeting the

demands of multicasting and relaying applications. Since each user brings in a distinct channel matrix, joint matrix decomposition is the key to such techniques.

GSVD beamforming, proposed by the author in [45,46] is based on generalized singular value decomposition (GSVD) [53], a joint matrix decomposition technique from linear algebra. Although not as popular as the singular value decomposition (SVD), the GSVD has been used in different wireless applications, including multi-user MIMO transmission [31, 54], MIMO secrecy communication [55, 56], and MIMO relaying [57], but, before the studies presented in [45,46], GSVD had not been exploited for beamforming, despite being a natural generalization of the SVD for two matrices and mentioned [55, p.1] in a slightly different context, as potentially useful for beamforming.

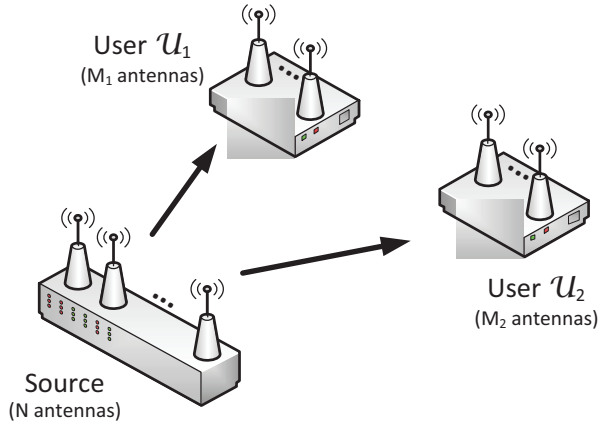


Figure 2.1: A two-user MIMO multicast configuration.

Although restricted to two-user MIMO multicast channels (Fig. 2.1), GSVD beamforming is a non-iterative multi-user beamforming alternative to BD. Unlike BD, it produces common virtual channels (CVCs), which are point-to-two point VCs from the source to  $\mathcal{U}_1$  and  $\mathcal{U}_2$ , in addition to private virtual channels (PVCs), i.e., the conventional point-to-point VCs from source to  $\mathcal{U}_1$  or  $\mathcal{U}_2$ .

GSVD beamforming places no restriction on the number of antennas at any of the terminals. However, the numbers of CVCs and PVCs it produces depend on the spatial degrees of freedom (DoFs) at the terminals. In fact, the numbers maximally exploit the DoFs at all three terminals for multiplexing. For an  $N$ -antenna source catering to user terminals  $\mathcal{U}_1$  and  $\mathcal{U}_2$  having  $M_1$  and  $M_2$  antennas, respectively,

GSVD beamforming yields  $\min(M_1, N) + \min(M_2, N) - \min(M_1 + M_2, N)$  CVCs and  $\min(M_1 + M_2, N) - \min(M_{(3-i)}, N)$  PVCs for each  $\mathcal{U}_i, i \in \{1, 2\}$  under rich scattering. Moreover, GSVD beamforming can be interpreted as a generalization of zero forcing (ZF), in the sense that the MIMO channel between the source and the user terminals is effectively inverted<sup>1</sup> irrespective of the numbers of antennas at the terminals. These facts make GSVD beamforming worth investigating.

**The chapter is organized as follows:** Section 2.2 introduces the GSVD, highlighting how GSVD beamforming implements the VCs. Section 2.3 characterizes the VC gains. It also derives, for systems with only CVCs, the exact joint probability density function (PDF) of the gains under independent and identically distributed (i.i.d.) Rayleigh fading. In Sections 2.4 and 2.5, transmit power normalization and the dependence of the numbers of PVCs/CVCs on the spatial DoFs are examined, respectively. The numerical results for the symbol error rate (SER), including those for elementary multicasting, amplify-and-forward (AF) relaying, and two-way relaying applications, are presented in Section 2.6. The conclusion follows (Section 2.7); the proof of Theorem 2.1 is presented in Appendix A.

## 2.2 Signal Processing

In the literature, the GSVD is found in two forms: the original definition by Van Loan [53, Thm. 2] (Definition 2.1) and a generalization by Paige and Saunders [58] (Definition 2.2). Each form is given below, and its characteristics' relevance to GSVD beamforming is highlighted.

**Definition 2.1 [Van Loan form]** Consider matrices  $\mathbf{H}_1 \in \mathbb{C}^{m \times n}$  with  $m \geq n$  and  $\mathbf{H}_2 \in \mathbb{C}^{p \times n}$ , which have the same number  $n$  of columns. Let  $q = \min(p, n)$ .

$\mathbf{H}_1$  and  $\mathbf{H}_2$  can be jointly decomposed as

$$\mathbf{H}_1 = \mathbf{U}\mathbf{\Sigma}\mathbf{Q} \text{ and } \mathbf{H}_2 = \mathbf{V}\mathbf{\Lambda}\mathbf{Q}, \quad (2.1)$$

where

i.)  $\mathbf{U} \in \mathbb{C}^{m \times m}$  and  $\mathbf{V} \in \mathbb{C}^{p \times p}$  are unitary,

---

<sup>1</sup> In fact, GSVD beamforming reduces to transmit ZF when the source has more antennas than the two users combined.

ii.)  $\mathbf{Q} \in \mathbb{C}^{n \times n}$  is non-singular, and

iii.)  $\mathbf{\Sigma} = \text{diag}(\sigma_1, \dots, \sigma_n) \in \mathbb{C}^{m \times n}, \sigma_i \geq 0$  and

$\mathbf{\Lambda} = \text{diag}(\lambda_1, \dots, \lambda_q) \in \mathbb{C}^{p \times n}, \lambda_i \geq 0$ .

•

Suppose that  $\mathbf{H}_1$  and  $\mathbf{H}_2$  in (2.1) represent the MIMO channels  $\mathcal{S} \rightarrow \mathcal{U}_1$  and  $\mathcal{S} \rightarrow \mathcal{U}_2$ , from a source  $\mathcal{S}$  to users  $\mathcal{U}_1$  and  $\mathcal{U}_2$ . Assume block fading and perfect channel-state information (CSI) on  $\mathbf{H}_1$  and  $\mathbf{H}_2$  at all  $\mathcal{S}, \mathcal{U}_1$ , and  $\mathcal{U}_2$ . With a transmit precoding matrix  $\rho\mathbf{Q}^{-1}$  and receiver reconstruction matrices  $\mathbf{U}^H/\rho$  and  $\mathbf{V}^H/\rho$ , we get  $q$  non-interfering broadcast (common) VCs, each catering to both the users. The factor  $\mathbf{Q}$  in (2.1) facilitates joint transmit precoding, while the factors  $\mathbf{U}$  and  $\mathbf{V}$  enable receiver reconstruction without noise enhancement. The diagonal elements of  $\mathbf{\Sigma}$  and  $\mathbf{\Lambda}$  represent the gains of those VCs. Since  $\mathbf{Q}$  is non-unitary, precoding causes the instantaneous transmit power to fluctuate; this result is a drawback, and the transmit signal needs to be normalized to maintain the desired level of average transmit power. (The coefficient  $\rho$  represents transmit power normalization.) Thus, GSVD beamforming is applicable for two-user channels. Since this three-terminal configuration appears in various MIMO subsystems, GSVD beamforming has the potential to be a useful tool.

**Definition 2.2 [Paige and Saunders form]** Consider matrices  $\mathbf{H}_1 \in \mathbb{C}^{m \times n}$  and  $\mathbf{H}_2 \in \mathbb{C}^{p \times n}$ , which have the same number  $n$  of columns. Let  $\mathbf{H}_0 = (\mathbf{H}_1^T, \mathbf{H}_2^T)^T$ ,  $k = \text{rank}(\mathbf{H}_0)$ ,  $r = k - \text{rank}(\mathbf{H}_2)$ , and  $s = \text{rank}(\mathbf{H}_1) + \text{rank}(\mathbf{H}_2) - k$ . Unitary matrices  $\mathbf{U} \in \mathbb{C}^{m \times m}$ ,  $\mathbf{V} \in \mathbb{C}^{p \times p}$ ,  $\mathbf{W} \in \mathbb{C}^{k \times k}$ , and  $\mathbf{Q} \in \mathbb{C}^{n \times n}$  can be found such that

$$\begin{aligned} \mathbf{H}_1 &= \mathbf{U} \cdot \mathbf{\Sigma}_1 \cdot (\mathbf{W}^H \mathbf{R}, \mathbf{0}) \mathbf{Q}^H \text{ and} \\ \mathbf{H}_2 &= \mathbf{V} \cdot \mathbf{\Sigma}_2 \cdot (\mathbf{W}^H \mathbf{R}, \mathbf{0}) \mathbf{Q}^H, \end{aligned} \quad (2.2)$$

where

i.)  $\mathbf{\Sigma}_1 \in \mathbb{C}^{m \times k}$ ,  $\mathbf{\Sigma}_2 \in \mathbb{C}^{p \times k}$  have block-diagonal structures:

$$\mathbf{\Sigma}_1 \triangleq \begin{pmatrix} \tilde{\mathbf{I}}_1 & & \\ & \mathbf{S}_1 & \\ & & \mathbf{0}_1 \end{pmatrix} \text{ and } \mathbf{\Sigma}_2 \triangleq \begin{pmatrix} \mathbf{0}_2 & & \\ & \mathbf{S}_2 & \\ & & \tilde{\mathbf{I}}_2 \end{pmatrix}, \quad (2.3)$$

- ii.)  $\mathbf{R} \in \mathbb{C}^{k \times k}$  is invertible and has the same singular values as the nonzero singular values of  $\mathbf{H}_0$ ,
- iii.)  $\mathbf{0} \in \mathbb{C}^{k \times (n-k)}$  is a zero matrix,
- iv.)  $\tilde{\mathbf{I}}_1 \in \mathbb{C}^{r \times r}$  and  $\tilde{\mathbf{I}}_2 \in \mathbb{C}^{(k-r-s) \times (k-r-s)}$  are identity matrices,
- v.)  $\mathbf{0}_1 \in \mathbb{C}^{(m-r-s) \times (k-r-s)}$  and  $\mathbf{0}_2 \in \mathbb{C}^{(p-k+r) \times r}$  are zero matrices possibly having no rows or no columns, and
- vi.)  $\mathbf{S}_1 = \text{diag}(\alpha_1, \dots, \alpha_s)$  and  $\mathbf{S}_2 = \text{diag}(\beta_1, \dots, \beta_s)$  such that  $1 > \alpha_1 \geq \dots \geq \alpha_s > 0$  and  $\alpha_i^2 + \beta_i^2 = 1$  for  $i \in \{1, \dots, s\}$ .

•

If matrices  $\mathbf{H}_1$  and  $\mathbf{H}_2$  represent the wireless channels corresponding to  $\mathcal{S} \rightarrow \mathcal{U}_1$  and  $\mathcal{S} \rightarrow \mathcal{U}_2$  as before, the beamforming matrices  $\rho \{\mathbf{Q}\}_{\mathcal{C}(1:k)} \mathbf{R}^{-1} \mathbf{W}$  at the source and  $\mathbf{U}^H / \rho$ ,  $\mathbf{V}^H / \rho$  at the respective users  $\mathcal{U}_1$ ,  $\mathcal{U}_2$  reduce the effective channels between the source and the users to  $\Sigma_1$  and  $\Sigma_2$ , respectively.

Each column of  $\Sigma_1$  (and  $\Sigma_2$ ) corresponds to a VC from the source.

- The sets of columns  $\{1, \dots, r\}$  and  $\{r+s+1, \dots, k\}$ , if non-empty, produce, respectively,  $r$  and  $(k-r-s)$  PVCs for  $\mathcal{U}_1$  and  $\mathcal{U}_2$ , each PVC catering to just one user and having a unit gain.
- The columns  $\{r+1, \dots, r+s\}$  corresponding to  $\mathbf{S}_1$  (and  $\mathbf{S}_2$ ) yield  $s$  point-to-two point CVCs. The corresponding amplitude gains experienced by  $\mathcal{U}_1$  are given by  $\alpha_i$  for  $i \in \{1, \dots, s\}$ . Likewise, the  $\beta_i$ s represent the gains experienced by  $\mathcal{U}_2$ .

Any subset of VCs may be selected by appropriately leaving out certain columns from the transmit beamforming matrix and the corresponding rows from the receiver beamforming matrices. When  $\text{rank}(\mathbf{H}_0) = \text{rank}(\mathbf{H}_1) + \text{rank}(\mathbf{H}_2)$ ,  $s$  becomes zero, and the scheme reduces to transmit ZF. This process is the essence of GSVD beamforming as a tool for multiplexing private and/or common data streams catering to two users.

## 2.3 Characterization of Virtual Channel Gains

As outlined in Section 2.2, the GSVD of channel matrices  $\mathbf{H}_1 \in \mathbb{C}^{m \times n}$  and  $\mathbf{H}_2 \in \mathbb{C}^{p \times n}$ , corresponding to users  $\mathcal{U}_1$  and  $\mathcal{U}_2$ , is of form  $\mathbf{H}_1 = \mathbf{U}\Sigma_1(\mathbf{W}^H\mathbf{R}, \mathbf{0})\mathbf{Q}^H$  and  $\mathbf{H}_2 = \mathbf{V}\Sigma_2(\mathbf{W}^H\mathbf{R}, \mathbf{0})\mathbf{Q}^H$ . All PVCs have unit gains. The gain experienced for the  $i^{\text{th}}$  CVC: CVC $_i$  by  $\mathcal{U}_1$  is given by  $\alpha_i \in \text{diag}(\Sigma_1)$ ,  $\alpha_i \in (0, 1)$ , a non-trivial diagonal element of  $\Sigma_1$  for  $i \in \{1, \dots, s\}$ . Since  $\beta_i = \sqrt{1 - \alpha_i^2}$ , each  $\alpha_i$  also characterizes the gain experienced by  $\mathcal{U}_2$  for CVC $_i$ .

Let  $\mathbf{P} \in \mathbb{C}^{(m+p) \times (m+p)}$  be the matrix formed with the left singular vectors of  $\mathbf{H}_0 = (\mathbf{H}_1^T, \mathbf{H}_2^T)^T$  and  $k = \text{rank}(\mathbf{H}_0)$ . The  $\alpha_i$ s are non-trivial singular values of the  $m \times k$  submatrix  $\mathbf{Q} = \left\{ \{\mathbf{P}\}_{\mathcal{C}(1:k)} \right\}_{\mathcal{R}(1:m)}$ , the trivial ones being 0 or 1 [58, Eqn. (2.7)]; thus, we have  $\{\alpha_i | \alpha_i^2 \in \text{eig}(\mathbf{Q}^H\mathbf{Q}) - \{0, 1\}\}$ . The eigenvalue distribution of  $\mathbf{Q}^H\mathbf{Q}$  is not known in general. However, it can be found under certain rank restrictions when  $\mathbf{P}$  is a Haar distributed random unitary matrix [16, Sec. 2.1.4]. This scenario corresponds to  $\mathbf{H}_1$  and  $\mathbf{H}_2$  undergoing i.i.d. Rayleigh fading, because the singular vectors of a complex Gaussian matrix produce a Haar distributed random unitary matrix when concatenated. The eigenvalue distribution depends only on the ranks of  $\mathbf{H}_1$ ,  $\mathbf{H}_2$ , and  $\mathbf{H}_0$ , or, in other words, on the spatial DoFs available at  $\mathcal{U}_1$ ,  $\mathcal{U}_2$ , and the source. This observation is not surprising, since the factor  $\mathbf{R}^{-1}\mathbf{W}$  of the transmit precoding matrix effectively inverts  $\mathbf{H}_0$ , the MIMO channel the source has with the users. This inversion is also why GSVD beamforming reduces to transmit ZF where the source has more antennas than the users combined.

The eigenvalue distribution of  $v \times v$  (square) truncations of  $(u + v) \times (u + v)$  Haar distributed unitary matrices has been examined in the literature [59, 60] for the case of  $v < u$ ; however, the results are not general enough to characterize GSVD beamforming. The eigenvalue distribution of the  $\beta$ -Jacobi ensemble [61, Ch. 5] is more relevant because whenever  $m \geq k$  and  $p \geq k$ , the squared  $\alpha_i$ s follow the same joint distribution as the eigenvalues of the  $\beta$ -Jacobi ensemble [62, Prop. 1.2] for  $\beta = 2$ . Applying the variable transformation  $\lambda_i = \alpha_i^2$  on the joint PDF [63, Eqn. (5)] of the ordered eigenvalues  $\lambda_i$ s of the  $\beta$ -Jacobi ensemble (for  $\beta = 2$ ), we get Proposition 2.1. Note that the condition  $\min(m, p) \geq k$  restricts it to configurations supporting only CVCs (with  $k = s$ ).

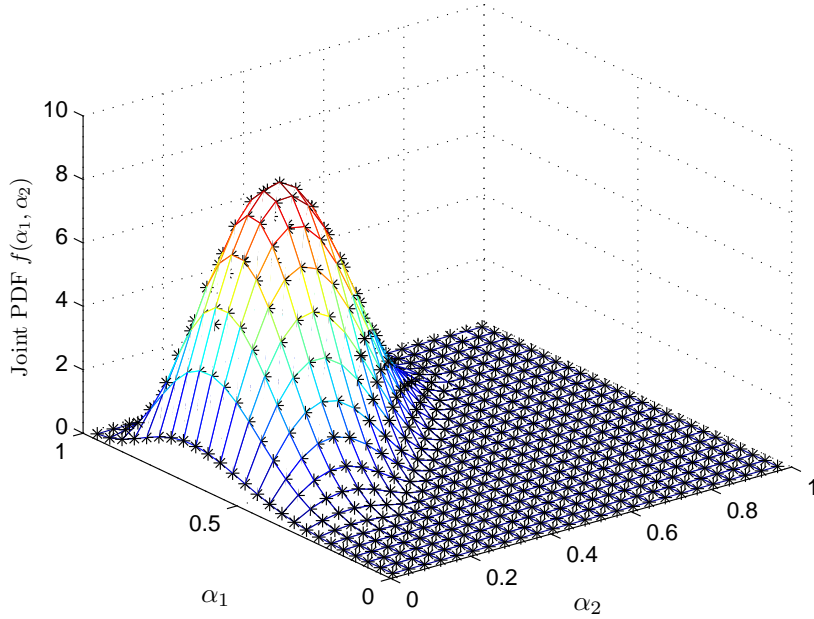


Figure 2.2: The joint PDF of  $\alpha_i$ s in Definition 2.2 for  $(m, p, k) \doteq (2, 5, 2)$ —analytic from (2.4) vs. simulated (\*).

**Proposition 2.1** Where  $\min(m, p) \geq k$ , the joint PDF of the ordered  $\alpha_i$ s',  $\alpha_i \in \text{diag}(\Sigma_1)$  for  $\Sigma_1$  in (2.3), is given by

$$f_{\alpha}(\alpha_1, \dots, \alpha_k) = c_{m,p,k} \prod_{i=1}^k \alpha_i^{2(m-k)+1} (1 - \alpha_i^2)^{p-k} \cdot \prod_{1 \leq i < j \leq k} (\alpha_i^2 - \alpha_j^2)^2, \quad (2.4)$$

for  $1 > \alpha_1 > \dots > \alpha_k > 0$ , where

$$c_{m,p,k} = k! \cdot 2^k \prod_{i=1}^k \frac{(m+p-i)!}{i! (m-i)! (p-i)!}. \quad (2.5)$$

The joint PDF of the unordered  $\alpha_i$ s has the same expression as (2.4) except for the factor  $k!$  in (2.5).

Fig. 2.2 compares, for the case  $(m, p, k) \doteq (2, 5, 2)$ , the joint PDF of  $\alpha_1$  and  $\alpha_2$  obtained analytically by using Proposition 2.1 against the  $10^8$ -point Monte Carlo simulation results. The figure reveals the exact agreement of the analytic and simulation results, which also conform with the fact that  $\alpha_i \in (0, 1)$ . Proposition 2.1 can be used for performance analysis of configurations supporting only CVCs; Theorem 2.1 on the diversity orders exemplifies this proposition's usefulness.

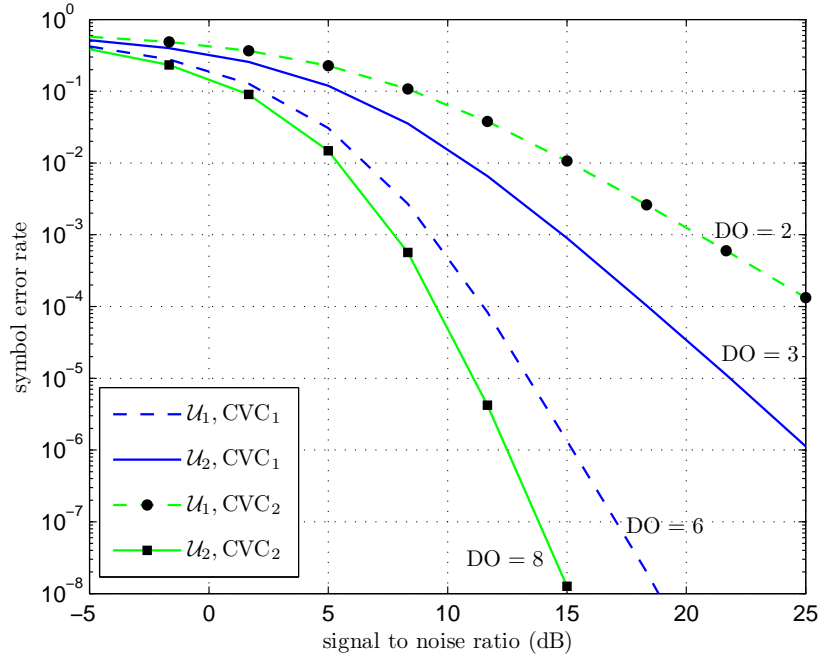


Figure 2.3: The SERs and diversity orders of the CVCs in the  $(N, M_1, M_2) \doteq (2, 3, 4)$  two-user multicast configuration. The gradients of the SER curves at high SNR correspond to diversity orders  $\text{DO} = \{2, 3, 6, 8\}$ . QPSK modulation is used.

**Theorem 2.1** *Diversity Order for the Case:  $\min(m, p) \geq k$*

Consider GSVD beamforming over MIMO channels  $\mathbf{H}_1 \in \mathbb{C}^{m \times n}$  and  $\mathbf{H}_2 \in \mathbb{C}^{p \times n}$ , corresponding to users  $\mathcal{U}_1$  and  $\mathcal{U}_2$  undergoing i.i.d. Rayleigh fading. Suppose  $\text{rank}((\mathbf{H}_1^T, \mathbf{H}_2^T)) = k \leq \min(m, p)$ . Then the diversity order of  $\text{CVC}_r$  for  $\mathcal{U}_1$  is given by  $(m - r + 1)(k - r + 1)$  for  $r \in \{1, \dots, k\}$ .

**Proof:** See Appendix A. ■

The diversity orders  $(m - r + 1)(k - r + 1)$  for  $\text{CVC}_r, r \in \{1, \dots, k\}$  are intuitive, since the  $\alpha_r$ s are the sorted singular values of an  $m \times k$  matrix. In fact, the diversity orders are the same as those corresponding to eigenmode transmission between the source and  $\mathcal{U}_1$  (or  $\mathcal{U}_2$ ) alone. For  $r > k$ , they exceed  $(m - k + 1)$ , which is the diversity order of the CVCs that ZF reception provides. For an  $(N, M_1, M_2) \doteq (2, 3, 4)$ -antenna two-user multicast configuration involving users  $\mathcal{U}_1, \mathcal{U}_2$  and corresponding to  $k = 2, m = 4$ , and  $p = 4$ , Fig. 2.3 verifies that GSVD beamforming yields a diversity order of  $(3 - r + 1) \times (2 - r + 1)$  for each  $\text{CVC}_r, r \in \{1, 2\}$  of  $\mathcal{U}_1$ .

Likewise, a diversity order  $(4 - (3 - r) + 1) \times (2 - (3 - r) + 1)$  is observed for each  $\text{CVC}_r$  of  $\mathcal{U}_2$ .  $10^8$ -point Monte Carlo simulation with 100 quadrature phase shift keying (QPSK) modulated symbols per VC per channel realization is used to obtain the SER curves.

Numerical analysis based on (2.4) is inherently simpler given the finite range  $(0, 1)$  of  $\alpha_i, i \in \{1, \dots, k\}$ . Because standard integral expressions used in wireless performance analysis typically assume a  $[0, \infty)$  range, the finite range could, however, complicate most exact analyses.

## 2.4 Transmit Power Normalization

The numbers of PVCs and CVCs realizable for a given system depend on the spatial DoFs at all the terminals. Suppose the transmitted data vector  $\mathbf{x} \in \mathbb{C}^{|\mathcal{L}| \times 1}$  is mapped to an arbitrary combination of  $|\mathcal{L}|$  private/common VCs; the columns of  $\mathbf{\Sigma}_1$  and  $\mathbf{\Sigma}_2$  whose indices are in  $\mathcal{L}$  represent the VC gains. Such mapping can be realized with a transmit beamforming matrix  $\rho \{\mathbf{Q}\}_{\mathcal{C}(1:k)} \mathbf{R}^{-1} \{\mathbf{W}\}_{\mathcal{C}(\mathcal{L})}$ , where  $\rho$  is the transmit power normalization coefficient ensuring a desired average total transmit power  $P$ . Thus, we have

$$P = \rho^2 \mathcal{E} \left\{ \left\| \{\mathbf{Q}\}_{\mathcal{C}(1:k)} \mathbf{R}^{-1} \{\mathbf{W}\}_{\mathcal{C}(\mathcal{L})} \mathbf{x} \right\|_F^2 \right\}. \quad (2.6)$$

Generally,  $\rho$  needs to be computed numerically. Nevertheless, further insights can be gained as follows for special cases.

Assume uncorrelated data and equal energy modulation. Without a loss of generality, we may set  $\mathcal{E}_{\mathbf{x}} \{\mathbf{x}\mathbf{x}^H\} = \mathbf{I}$  to obtain

$$\begin{aligned} P &= \rho^2 \mathcal{E} \left\{ \text{trace} \left( \{\mathbf{W}\}_{\mathcal{C}(\mathcal{L})}^H \mathbf{R}^{-1} \{\mathbf{Q}^H\}_{\mathcal{R}(1:k)} \cdot \{\mathbf{Q}\}_{\mathcal{C}(1:k)} \mathbf{R}^{-1} \{\mathbf{W}\}_{\mathcal{C}(\mathcal{L})} \right) \right\} \\ &= \rho^2 \mathcal{E} \left\{ \text{trace} \left( \mathbf{R}^{-2} \{\mathbf{W}\}_{\mathcal{C}(\mathcal{L})} \{\mathbf{W}\}_{\mathcal{C}(\mathcal{L})}^H \right) \right\}. \end{aligned} \quad (2.7)$$

The product  $\{\mathbf{W}\}_{\mathcal{C}(\mathcal{L})} \{\mathbf{W}\}_{\mathcal{C}(\mathcal{L})}^H$  is an identity matrix when  $\mathcal{L} \equiv \{1, \dots, k\}$ , i.e., when all the VCs are in use. For that case only, and using the fact that the squared singular values of  $\mathbf{R}$  are the non-zero eigenvalues of  $\mathbf{H}_0 \mathbf{H}_0^H$  product, we get a

configuration	# CVCs	# PVCs	
	$S \rightarrow \mathcal{U}_1, \mathcal{U}_2$	$S \rightarrow \mathcal{U}_1$	$S \rightarrow \mathcal{U}_2$
$m > n, p \leq n$	$p$	$n - p$	0
$m \leq n, p > n$	$m$	0	$n - m$
$m \geq n, p \geq n$	$n$	0	0
$m < n, p < n, (m + p) > n$	$m + p - n$	$n - p$	$n - m$
$n \geq (m + p)$	0	$m$	$p$

Table 2.1: Numbers of CVCs and PVCs realized through GSVD beamforming for antennas  $(n, m, p)$  at the source and users  $\mathcal{U}_1, \mathcal{U}_2$ , respectively.

simplified expression:

$$\rho = \sqrt{\frac{P}{\mathcal{E}\{\text{trace}(\mathbf{R}^{-2})\}}} = \sqrt{\frac{P}{\mathcal{E}\left\{\sum_{i=1}^k \lambda_i^{-1}\right\}}}, \quad (2.8)$$

where  $\lambda_i \in \text{eig}(\mathbf{H}_0 \mathbf{H}_0^H)$  for  $i \in \{1, \dots, k\}$ . By using [16, Lemma 2.10], Eqn. (2.8) may be further simplified; e.g.,  $\rho = \sqrt{\frac{P|m+p-n|}{\min(m+p,n)}}$  for i.i.d. Rayleigh fading.

## 2.5 Numbers of Private/Common Virtual Channels

As outlined in Section 2.2, GSVD beamforming on the channels  $\mathbf{H}_1 \in \mathbb{C}^{m \times n}$  and  $\mathbf{H}_2 \in \mathbb{C}^{p \times n}$  corresponding to users  $\mathcal{U}_1$  and  $\mathcal{U}_2$  yields  $s$  CVCs,  $r$  PVCs for  $\mathcal{U}_1$ , and  $(k - r - s)$  PVCs for  $\mathcal{U}_2$ . The numbers of VCs add up to  $k = \text{rank}(\mathbf{H}_0)$ , indicating full-utilization of the spatial DoFs at the source for multiplexing.

The numbers  $k = \text{rank}(\mathbf{H}_0)$ ,  $r = k - \text{rank}(\mathbf{H}_2)$ , and  $s = \text{rank}(\mathbf{H}_1) + \text{rank}(\mathbf{H}_2) - k$  are governed by the MIMO channel ranks. Where the channels are not rank-deficient as with rich scattering,  $k = \min(m + p, n)$ ,  $r = k - \min(p, n)$ , and  $s = \min(m, n) + \min(p, n) - k$  depend on the number of antennas at the three terminals. Consequently, the numbers of VCs depend on the antenna configuration (see Table 2.1). The ensuing lack of flexibility can be circumvented by using additional transmit and/or receiver processing<sup>2</sup> for rank reduction, i.e., by reducing the *effective* number of antennas, as highlighted in Example 2.1.

<sup>2</sup> Antenna selection is a less attractive alternative.

**Example 2.1** Let  $\tilde{m} = n_c + n_{p_1} \leq m$ ,  $\tilde{p} = n_c + n_{p_2} \leq p$ , and  $\tilde{n} = n_c + n_{p_1} + n_{p_2} \leq n$  be the effective numbers of antennas required, respectively, at users  $\mathcal{U}_1, \mathcal{U}_2$  and the source, to realize the desired numbers of VCs:  $n_c$  CVCs and  $n_{p_1}, n_{p_2}$  PVCs catering to  $\mathcal{U}_1, \mathcal{U}_2$ . These numbers are achievable as follows, provided  $k = \text{rank}(\mathbf{H}_0) \geq \tilde{n}$ .

Suppose  $\mathbf{H}_1 = \mathbf{U}_1 \mathbf{\Lambda}_1 \mathbf{V}_1^H$ ,  $\mathbf{H}_2 = \mathbf{U}_2 \mathbf{\Lambda}_2 \mathbf{V}_2^H$ , and  $\mathbf{H}_0 = (\mathbf{H}_1^T, \mathbf{H}_2^T)^T = \mathbf{U}_0 \mathbf{\Lambda}_0 \mathbf{V}_0^H$  are the SVDs. Define  $\mathbf{X}_1 = \{\mathbf{U}_1^H\}_{\mathcal{R}(1:\tilde{m})}$ ,  $\mathbf{X}_2 = \{\mathbf{U}_2^H\}_{\mathcal{R}(1:\tilde{p})}$ , and  $\mathbf{X}_0 = \{\mathbf{V}_0\}_{\mathcal{C}(1:\tilde{n})}$ . Then, compute the GSVD as follows:

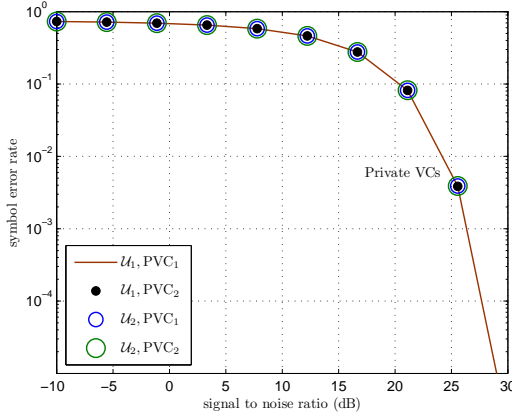
$$\begin{aligned} \mathbf{X}_1 \mathbf{H}_1 \mathbf{X}_0 &= \mathbf{U} \cdot \Sigma_1 \cdot (\mathbf{W}^H \mathbf{R}, \mathbf{0}) \mathbf{Q}^H \text{ and} \\ \mathbf{X}_2 \mathbf{H}_2 \mathbf{X}_0 &= \mathbf{V} \cdot \Sigma_2 \cdot (\mathbf{W}^H \mathbf{R}, \mathbf{0}) \mathbf{Q}^H. \end{aligned} \quad (2.9)$$

The beamforming matrices  $\rho \mathbf{X}_0 \{\mathbf{Q}\}_{\mathcal{C}(1:k)} \mathbf{R}^{-1} \mathbf{W}$  at the source, and  $\mathbf{U}^H \mathbf{X}_1 / \rho$  and  $\mathbf{V}^H \mathbf{X}_2 / \rho$ , respectively, at users  $\mathcal{U}_1$  and  $\mathcal{U}_2$ , yield the desired numbers of VCs. Note that the products  $\mathbf{X}_1 \mathbf{H}_1 \mathbf{X}_0$  and  $\mathbf{X}_2 \mathbf{H}_2 \mathbf{X}_0$  in (2.9), acting as the effective matrices for the GSVD, are of reduced dimensions when compared to the original matrices  $\mathbf{H}_1$  and  $\mathbf{H}_2$ . •

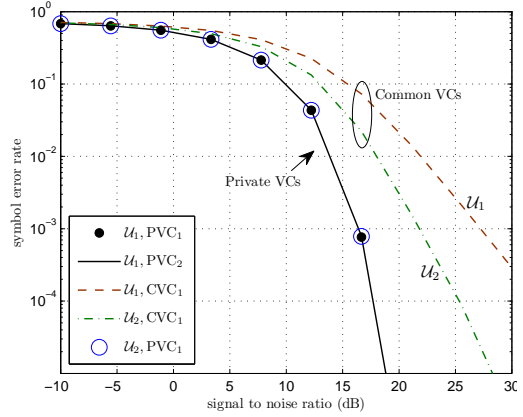
## 2.6 Numerical Results

This section uses Monte Carlo simulation of the SER to gain insights into GSVD beamforming. A two-user MIMO multicast configuration is considered first; a simple AF relay configuration is investigated next; and a network coded two-way relay configuration thereafter.

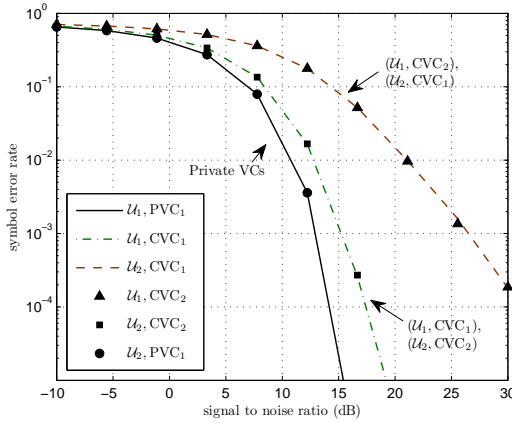
Assumptions: Block fading is assumed; 100 uncoded QPSK modulated symbols are simulated per VC per channel realization. The SER curves are obtained by averaging over  $10^5$  channel realizations. The average total transmit power is held at 1, and the noise variance is adjusted to reflect the signal to noise ratio (SNR).



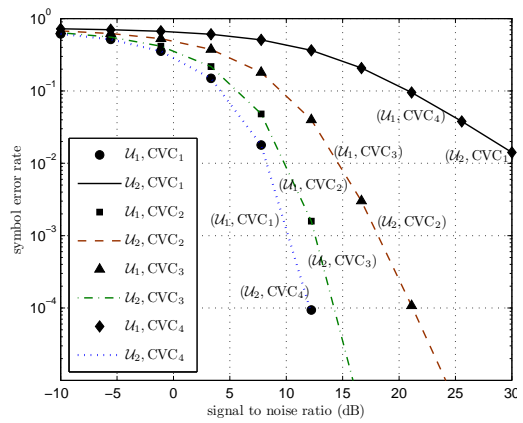
(a)  $(N, M_1, M_2) \doteq (4, 2, 2)$



(b)  $(N, M_1, M_2) \doteq (4, 3, 2)$



(c)  $(N, M_1, M_2) \doteq (4, 3, 3)$



(d)  $(N, M_1, M_2) \doteq (4, 4, 4)$

Figure 2.4: The SERs of the PVCs and CVCs in  $(N, M_1, M_2)$ -antenna two-user multicast configurations. QPSK modulation is used.

## 2.6.1 Application in Two-User MIMO Multicasting

Consider a simple two-user MIMO broadcast/multicast configuration (Fig. 2.1) corresponding to a source  $\mathcal{S}$  catering to the users  $\mathcal{U}_1$  and  $\mathcal{U}_2$ . Being the simplest possible GSVD beamforming application, this system is ideal for gaining insights into PVC/CVC performance and the effect of channel-estimation errors and channel fading on it.

Figs. 2.4a–2.4d depict the SER curves for different antenna configurations. It is assumed that i.i.d. Rayleigh fading affects both the users.

- Fig. 2.4a corresponds to the  $(N, M_1, M_2) \doteq (4, 2, 2)$  configuration, where the source has four spatial DoFs, i.e., just as many as the two users' combined. As speculated in Section 2.3, GSVD beamforming yields identical PVCs as with transmit ZF. (In the other three cases, corresponding to Figs. 2.4b–2.4d, the source does not have sufficient antennas to perform ZF.)
- Fig. 2.4b corresponds to the  $(N, M_1, M_2) \doteq (4, 3, 2)$  scenario. The single CVC utilizes one of the DoFs at the source; the remaining DoFs facilitate the PVCs. Clearly, this CVC and PVC allocation yields the highest multiplexing gain, as always is the case with GSVD beamforming.

As speculated in Section 2.2, the PVCs show identical SER performance, while the CVC performs worse. Notably, the two users experience different SER performance with respect to the same CVC. This observation indicates that coding techniques for the single-antenna broadcast channel [25] can be employed to exploit the capacity of a CVC.

- The  $(N, M_1, M_2) \doteq (4, 3, 3)$  antenna configuration, whose SER performance is shown in Fig. 2.4c, is even more interesting, for each of the two CVCs imparts different SERs upon its end users. The statistical symmetry in the  $\mathcal{S} \rightarrow \mathcal{U}_1$  and  $\mathcal{S} \rightarrow \mathcal{U}_2$  MIMO channels (i.e.,  $M_1 = M_2$  and the channels are i.i.d. Rayleigh fading) makes the SER experienced by  $\mathcal{U}_1$  for CVC<sub>1</sub> identical to that experienced by  $\mathcal{U}_2$  for CVC<sub>2</sub>. Similar observations can be made regarding  $\mathcal{U}_2$ 's experience for CVC<sub>1</sub> and  $\mathcal{U}_1$ 's for CVC<sub>2</sub>. The SER degrades from CVC<sub>1</sub> to CVC<sub>2</sub> for  $\mathcal{U}_1$ , while it improves for  $\mathcal{U}_2$ ; this observation is consistent with the fact that, in GSVD, the coefficients  $\alpha_i$ s appear in descending order, while the  $\beta_i = \sqrt{1 - \alpha_i^2}$ ,  $i \in \{1, \dots, s\}$  ascend.
- Fig. 2.4d corresponds to the case of  $N = M_1 = M_2 = 4$ . GSVD beamforming yields four CVCs. The symmetry dictates that the SER performance for  $\mathcal{U}_1$ 's CVC <sub>$k$</sub>  is identical to that of  $\mathcal{U}_2$ 's CVC <sub>$(5-k)$</sub>  for  $k \in \{1, \dots, 4\}$ . Again, for  $\mathcal{U}_1$ , the performance degrades from CVC<sub>1</sub> to CVC<sub>4</sub>.

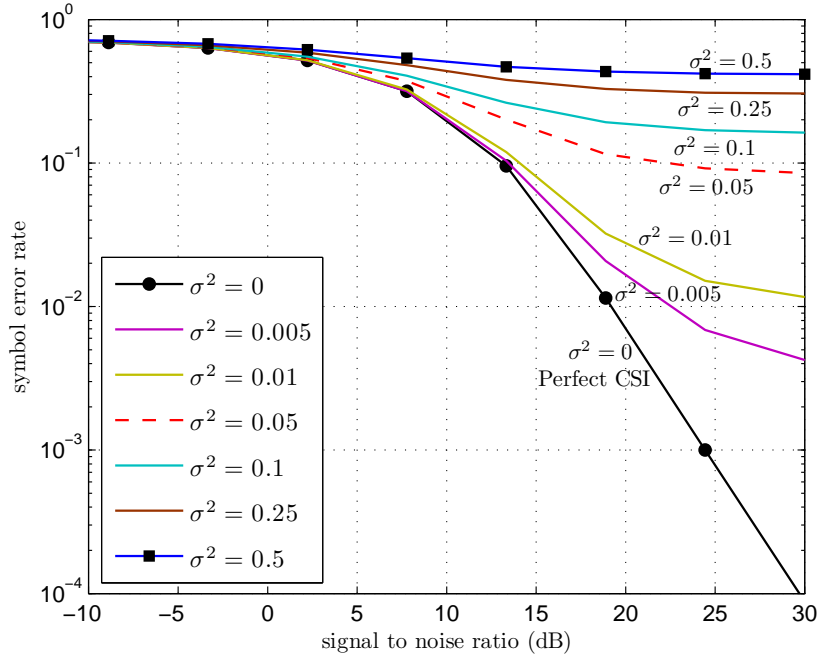
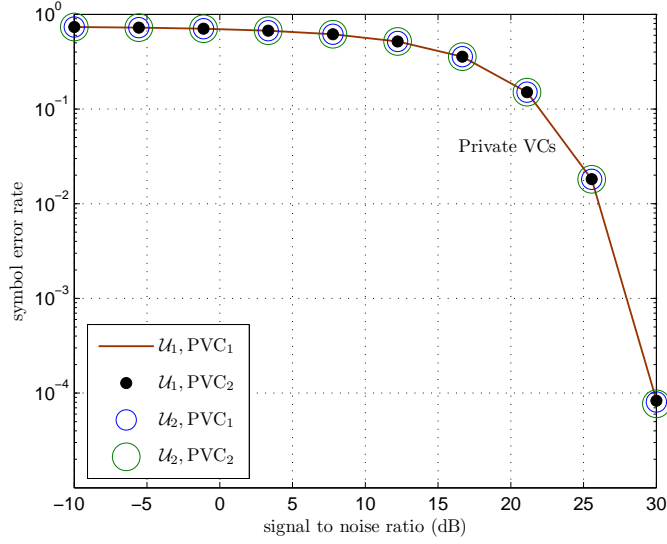


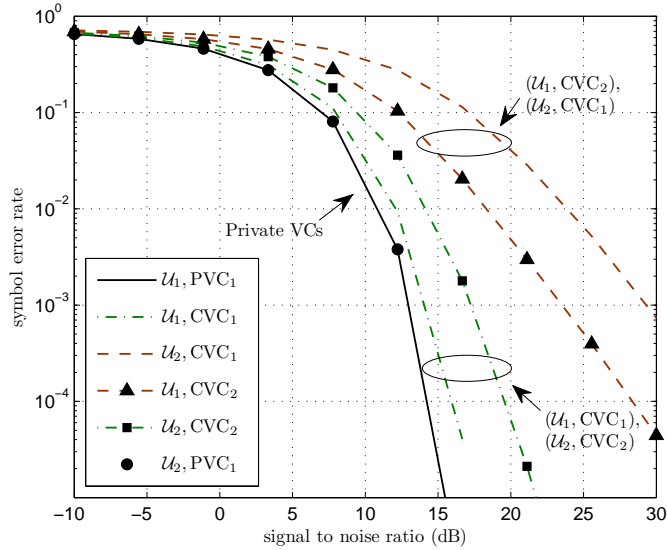
Figure 2.5: The SER of  $\text{CVC}_1$  for  $\mathcal{U}_1$  subjected to imperfect CSI in the  $(N, M_1, M_2) \doteq (3, 2, 2)$  two-user multicast configuration. QPSK modulation and complex Gaussian channel-estimation errors with  $\sigma^2$  variance are assumed.

Note that the SER curves exhibit no error-floors; i.e., inter-channel interference gets eliminated perfectly for both the users. This achievement is impossible with traditional non-iterative beamforming schemes (except with the configuration shown in Fig. 2.4d).

Figs. 2.4a–2.4d assume the availability of perfect CSI. What would happen with imperfect CSI? Fig. 2.5 shows the effect of channel-estimation errors on the SER, if we consider  $\text{CVC}_1$  of  $\mathcal{U}_1$  in the  $(N, M_1, M_2) \doteq (3, 2, 2)$  configuration and assume i.i.d. Rayleigh fading. For each channel matrix  $\mathbf{H}_i, i \in \{1, 2\}$ , the channel-estimation error  $\sigma \Delta \mathbf{H}_i$  is assumed to be complex Gaussian with zero mean and  $\sigma^2$  variance, such that the channel estimate  $\hat{\mathbf{H}}_i = \mathbf{H}_i + \sigma \Delta \mathbf{H}_i$  is used for computing the beamforming matrices. As expected, with increasing  $\sigma^2$ , the performance degrades rapidly, producing error-floors. For instance, a 10 dB degradation occurs for  $\sigma^2 = 0.01$ , even at the relatively high  $10^{-2}$  SER level. Such degradation should be expected given the presence of multiple spatially separated VCs; however, it emphasizes the crucial role of channel estimation with GSVD beamforming.



(a)  $(N, M_1, M_2) \doteq (4, 2, 2)$



(b)  $(N, M_1, M_2) \doteq (4, 3, 3)$

Figure 2.6: The SERs of the PVCs and CVCs in  $(N, M_1, M_2)$ -antenna asymmetric two-user multicast configurations. The  $\mathcal{S} \rightarrow \mathcal{U}_1$  channel is 3 dB stronger than the  $\mathcal{S} \rightarrow \mathcal{U}_2$  channel. QPSK modulation is used.

Figs. 2.6a and 2.6b show the SER performance for asymmetric configurations, in which  $\mathcal{U}_1$  experiences, on average, a 3 dB stronger channel than  $\mathcal{U}_2$ . Rayleigh fading is assumed here as well. As in Fig. 2.4a, GSVD beamforming produces four identical PVCs for the case depicted in Fig. 2.6a. The relative merits of the SER curves of Fig. 2.6b, however, differ from those in the corresponding symmetric case

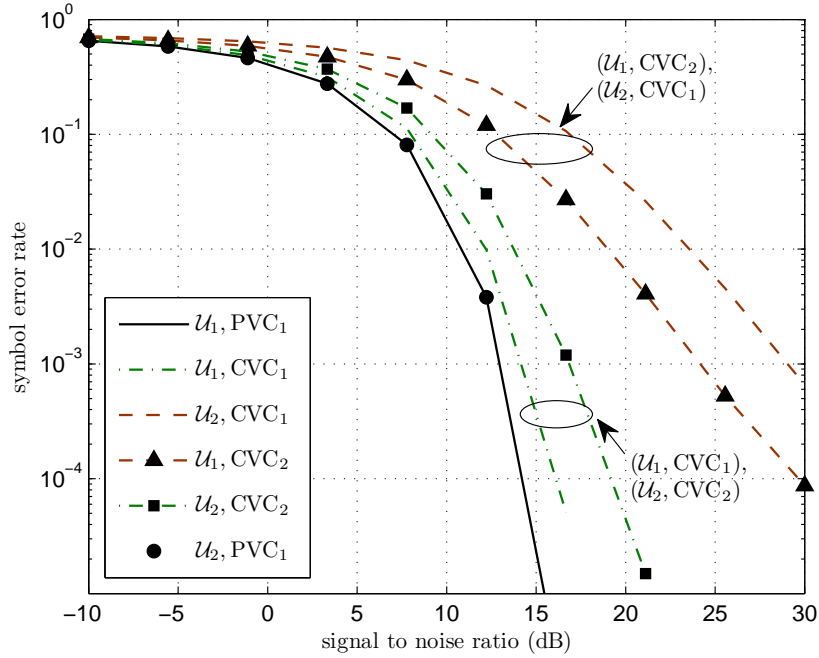


Figure 2.7: The SERs of the PVCs and CVCs in the  $(N, M_1, M_2) \doteq (4, 3, 3)$  two-user multicast configuration under asymmetric fading. The  $\mathcal{S} \rightarrow \mathcal{U}_1$  and  $\mathcal{S} \rightarrow \mathcal{U}_2$  channels undergo Rician fading and Rayleigh fading, respectively. QPSK modulation is used.

depicted in Fig. 2.4c; because  $\mathcal{U}_1$  has a stronger channel, the symmetry observable in Fig. 2.4c no longer holds for Fig. 2.6b. Even here, the PVCs deliver the best error rates, as expected.

The MIMO channels corresponding to Fig. 2.7 are asymmetric because only  $\mathcal{U}_1$ 's channel has a specular component. More specifically, the  $\mathcal{S} \rightarrow \mathcal{U}_1$  channel undergoes Rician fading, with a Rice factor of 1 and a non-centrality matrix having (arbitrarily chosen) eigenvalues  $\{8.83, 2.39\}$ ; the  $\mathcal{S} \rightarrow \mathcal{U}_2$  channel undergoes i.i.d. Rayleigh fading statistically identical to the scatter component of the  $\mathcal{S} \rightarrow \mathcal{U}_1$  channel. The symmetry observed in Fig. 2.4c with respect to the CVC SER performance is no longer present in this scenario. The line-of-sight component of the  $\mathcal{S} \rightarrow \mathcal{U}_1$  channel is seen to improve the SERs  $\mathcal{U}_1$  experiences for the CVCs. Nevertheless, the SER performance of the PVCs is identical for both the users, confirming that GSVD, irrespective of the fading distribution, yields PVCs having an identical (and constant) gain.

## 2.6.2 Application in AF Relaying

This section evaluates the SER performance of GSVD beamforming in a MIMO AF relay configuration (Fig. 2.8) comprising a source  $S$ , a relay  $R$ , and a destination  $D$ , comparing this performance with that of eigenmode transmission (i.e., SVD beamforming).

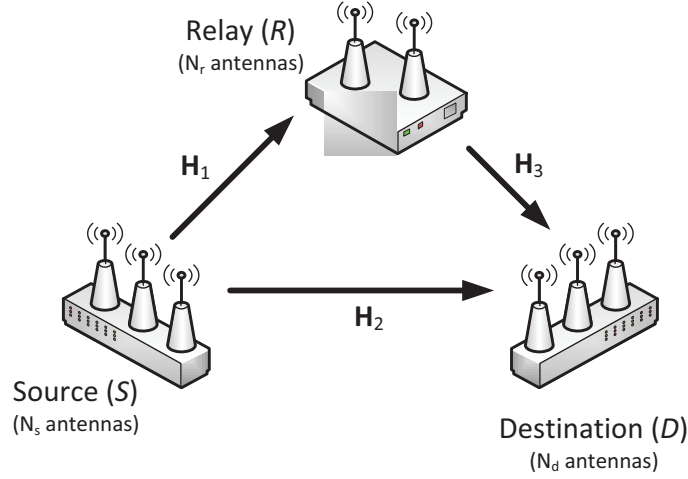


Figure 2.8: A MIMO relay system comprising a direct path and a relayed path.

The channelization scheme involves two time slots. The source precodes and transmits a symbol vector  $\mathbf{x}$  in the first time slot; the relay amplifies and forwards what it receives in the second time slot. The  $S \rightarrow R$ ,  $S \rightarrow D$ , and  $R \rightarrow D$  MIMO channels are  $\mathbf{H}_1$ ,  $\mathbf{H}_2$ , and  $\mathbf{H}_3$ ; the corresponding outputs are  $\mathbf{y}_1$ ,  $\mathbf{y}_2$ , and  $\mathbf{y}_3$ , and the additive white Gaussian noise vectors are  $\mathbf{n}_1$ ,  $\mathbf{n}_2$ , and  $\mathbf{n}_3$ . AF relay processing being linear, the relay gains are represented by a matrix  $\mathbf{F}$ . Thus, we get

$$\text{for Time Slot 1: } \mathbf{y}_1 = \mathbf{H}_1 \mathbf{W} \mathbf{x} + \mathbf{n}_1, \mathbf{y}_2 = \mathbf{H}_2 \mathbf{W} \mathbf{x} + \mathbf{n}_2, \text{ and } \quad (2.10a)$$

$$\text{for Time Slot 2: } \mathbf{y}_3 = \mathbf{H}_3 \mathbf{F} \mathbf{y}_1 + \mathbf{n}_3, \quad (2.10b)$$

where  $\mathbf{W}$  represents transmit precoding. With a receiver reconstruction matrix  $\mathbf{R}_i$  for each  $i^{\text{th}}$  time slot for  $i \in \{1, 2\}$ , we get  $\hat{\mathbf{y}} = \mathbf{R}_1 \mathbf{y}_2 + \mathbf{R}_2 \mathbf{y}_3$  at the detector input.

Suppose  $n \leq \min_i (\text{rank}(\mathbf{H}_i))$  VCs,  $\text{VC}_k$  for  $k \in \{1, \dots, n\}$ , are to be realized. Let  $N_d > N_s$  (or  $N_r > N_s$ ) so that the Van Loan form of GSVD (Definition 2.1) holds, producing  $n \leq \min(N_s, N_r, N_d)$  VCs. Applying the GSVD on the channel

matrices  $\mathbf{H}_1$  and  $\mathbf{H}_2$ , we get  $\mathbf{H}_1 = \mathbf{U}_1 \mathbf{\Sigma}_1 \mathbf{Q}$  and  $\mathbf{H}_2 = \mathbf{U}_2 \mathbf{\Sigma}_2 \mathbf{Q}$ ; the SVD yields  $\mathbf{H}_3 = \mathbf{V} \mathbf{\Lambda} \mathbf{R}^H$ . Choose  $\mathbf{W} = \alpha \{\mathbf{Q}^{-1}\}_{\mathcal{C}(n)}$ ,  $\mathbf{F} = \mathbf{R} \mathbf{U}_1^H$ ,  $\mathbf{R}_1 = \{\mathbf{U}_2^H\}_{\mathcal{R}(n)}$ , and  $\mathbf{R}_2 = \{\mathbf{V}^H\}_{\mathcal{R}(n)}$ , where  $\alpha$  is the transmit power normalization coefficient. Then we get

$$\hat{\mathbf{y}} = \left\{ \alpha \{(\mathbf{\Lambda} \mathbf{\Sigma}_1 + \mathbf{\Sigma}_2)\}_{\mathcal{C}(n)} \mathbf{x} + \mathbf{\Lambda} \tilde{\mathbf{n}}_1 + \tilde{\mathbf{n}}_2 + \tilde{\mathbf{n}}_3 \right\}_{\mathcal{R}(n)}, \quad (2.11)$$

where each  $\tilde{\mathbf{n}}_i$  has the same distribution as  $\mathbf{n}_i$  for  $i \in \{1, 2, 3\}$ .

SVD beamforming is also possible as follows for this system, since AF relaying is used and the system has a single source–destination pair. Define  $\mathbf{y} = (\mathbf{y}_2^T, \mathbf{y}_3^T)^T$ . Then we have

$$\mathbf{y} = \underbrace{\begin{pmatrix} \mathbf{H}_3 \mathbf{F} \mathbf{H}_1 \\ \mathbf{H}_2 \end{pmatrix}}_{\hat{\mathbf{H}}} \mathbf{W} \mathbf{x} + \begin{pmatrix} \mathbf{H}_3 \mathbf{F} \mathbf{n}_1 \\ \mathbf{0} \end{pmatrix} + \begin{pmatrix} \mathbf{n}_3 \\ \mathbf{n}_2 \end{pmatrix}. \quad (2.12)$$

The effective channel  $\hat{\mathbf{H}}$  in (2.12) can be diagonalized by choosing the transmit and receiver beamforming matrices  $\mathbf{W} = \{\hat{\mathbf{V}}\}_{\mathcal{C}(n)}$  and  $\mathbf{R} = \{\hat{\mathbf{U}}^H\}_{\mathcal{R}(n)}$ , where  $\hat{\mathbf{H}} = \hat{\mathbf{U}} \hat{\mathbf{\Sigma}} \hat{\mathbf{V}}^H$  is the SVD. However, the choice of  $\mathbf{F}$  is not straightforward with this approach.

- An apparent choice is selecting  $\mathbf{F}$  to invert  $\mathbf{H}_3$ . This alternative is as same as performing transmit ZF at the relay.
- Another is having  $\mathbf{F} = \mathbf{V}_3 \mathbf{U}_1^H$ , where  $\mathbf{H}_i = \mathbf{U}_i \mathbf{\Sigma}_i \mathbf{V}_i^H$  for  $i \in \{1, 3\}$  are SVDs. Its optimality, reasoned out for slightly different configurations in [64, Eqn. (22)] and [65, Eqn. (7)], may be appreciated intuitively: using the spatial directions corresponding to the eigenvectors of the input and output channels appears to be the best choice the relay has, if  $\mathbf{F}$  and the beamforming matrices  $\mathbf{W}$ ,  $\mathbf{R}$  are not jointly computed.

Fig. 2.9 shows the SERs of the three CVCs in the  $(N_s, N_r, N_d) \doteq (4, 3, 5)$  relay configuration for both GSVD beamforming and SVD beamforming. The latter form of  $\mathbf{F}$  (stated above) is assumed with SVD beamforming.  $10^7$ -point Monte Carlo simulation based on (2.11) and (2.12) is employed, and QPSK modulation is assumed; the constant  $\alpha$  is computed through simulation to ensure  $\mathcal{E}\{\|\mathbf{W} \mathbf{x}\|_F^2\} = 1$ .

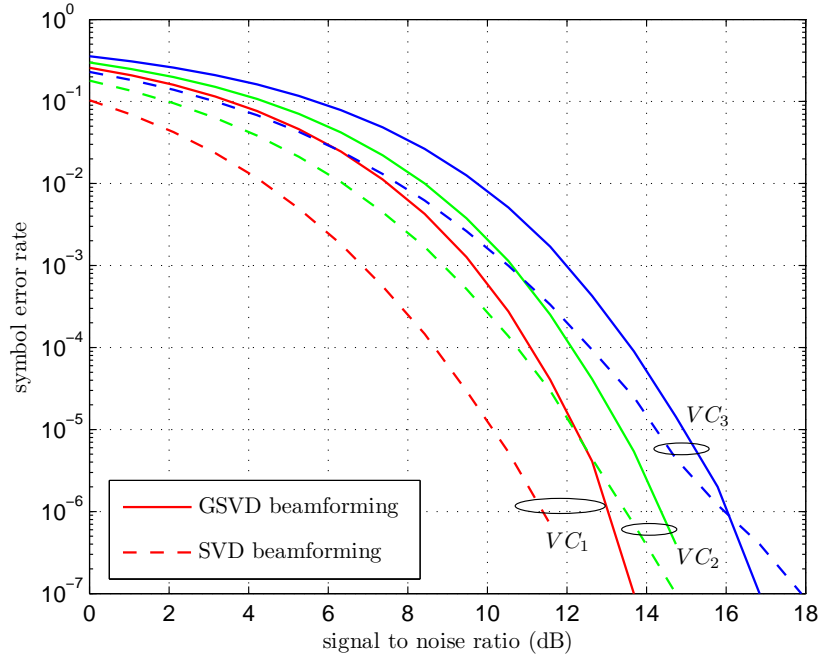


Figure 2.9: The SERs of the VCs in the  $(N_s, N_r, N_d) \doteq (4, 3, 5)$  MIMO AF relay configuration — GSVD beamforming vs. SVD beamforming. QPSK modulation is used.

As expected,  $VC_1$  performs better than  $VC_2$  or  $VC_3$ . GSVD beamforming achieves within 3 dB of SVD beamforming for moderate SNR; interestingly, GSVD beamforming appears to have higher diversity orders.

Since GSVD beamforming decouples the VCs perfectly at both the relay and the destination, independent signal detection of each VC is possible at the relay as well. Such detection is generally impossible with SVD beamforming. Thus, GSVD beamforming is preferred with decode-and-forward and code-and-forward relay processing schemes. Moreover, having no inter-VC interference, the instantaneous SNR  $\gamma_i$  for each  $VC_i$  with GSVD beamforming (under block fading assumptions) is given by

$$\gamma_i = \frac{(\mathbf{\Lambda}(i, i) \mathbf{\Sigma}_1(i, i) + \mathbf{\Sigma}_2(i, i))^2}{\mathbf{\Lambda}(i, i)^2 + 2} \alpha^2 P, \quad (2.13)$$

where  $P$  is the transmit SNR. Eqn. (2.13) also enables semi-analytic Monte Carlo simulation.

### 2.6.3 Application in Network-Coded Two-Way Relaying

In this section, the SER performance of two-way relaying (Fig. 2.10) with physical-layer network coding [66] is investigated.

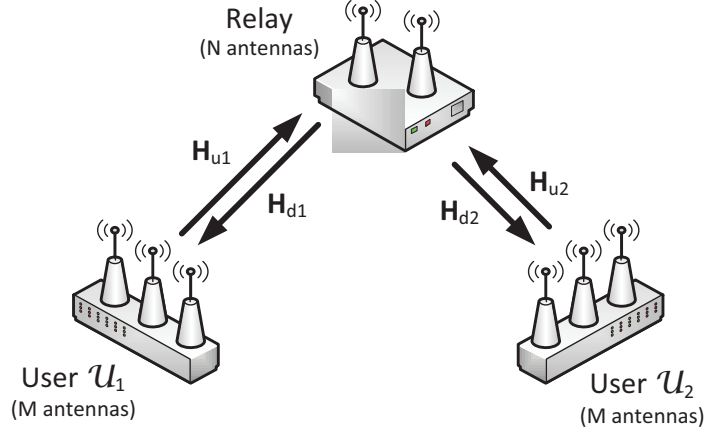


Figure 2.10: A network-coded MIMO two-way relay system.

As with AF relaying in Subsection 2.6.2, the channelization involves two time slots; they correspond to the uplink and downlink transmissions, respectively. In the uplink, the users transmit precoded data simultaneously; the relay jointly decodes the received signal (by using the corresponding superimposed constellation) such that the transmitted data effectively ‘XOR in the air’ [67], and the XORing is manifested as physical-layer network coding. In the downlink time slot, the relay regenerates the decoded data (which are now the XOR of the two users’ data, possibly with noise-introduced errors) and broadcasts to both the users; each user may extract the other user’s data by detecting the received signal and XORing away its own (transmitted) data.

Suppose that the relay has  $N$  antennas, and each user  $\mathcal{U}_i, i \in \{1, 2\}$  has  $M$  antennas;  $N$  VCs,  $\text{VC}_i$  for  $i \in \{1, \dots, N\}$ , are to be realized in each direction  $\mathcal{U}_1 \rightarrow \mathcal{U}_2$  and  $\mathcal{U}_2 \rightarrow \mathcal{U}_1$  via the relay. A constraint  $N < M$  is imposed to make ZF transmission/reception realizable at the users; it also ensures that GSVD beamforming yields only CVCs, as physical-layer network coding requires. Let  $\mathbf{H}_{u1}, \mathbf{H}_{u2} \in \mathbb{C}^{N \times M}$  denote the uplink MIMO channels from  $\mathcal{U}_1$  and  $\mathcal{U}_2$ , respectively;  $\mathbf{H}_{d1}, \mathbf{H}_{d2} \in \mathbb{C}^{M \times N}$  are the corresponding downlink MIMO channels from

the relay. If time division duplexing is used,  $\mathbf{H}_{d1} = \mathbf{H}_{u1}^T$  and  $\mathbf{H}_{d2} = \mathbf{H}_{u2}^T$  hold due to channel reciprocity.

Consider the following three channelization schemes:

- **Scheme 1:** ZF transmission is used in the uplink, while GSVD beamforming is used in the downlink.
- **Scheme 2:** ZF transmission and reception are employed, respectively, in the uplink and the downlink.
- **Scheme 3:** GSVD beamforming is used in the downlink; a multiple-access variant of GSVD beamforming implements the uplink.

Scheme 1: Here, transmit ZF is employed in the uplink. Thus, the transmit beamforming matrices at  $\mathcal{U}_1$  and  $\mathcal{U}_2$  are  $\mathbf{W}_1 = \alpha_u (\mathbf{H}_{u1})^\dagger$  and  $\mathbf{W}_2 = \alpha_u (\mathbf{H}_{u2})^\dagger$ , respectively. Receiver beamforming at the relay, represented by a matrix  $\mathbf{R} = \mathbf{I}_N / \alpha_u$ , merely involves normalization;  $\alpha_u$  is the transmit power normalization coefficient.

Since the downlink is a two-user broadcast channel, GSVD beamforming can be applied unmodified on  $\mathbf{H}_{d1}$  and  $\mathbf{H}_{d2}$ . Let  $\mathbf{H}_{d1} = \mathbf{U}_{d1} \mathbf{\Sigma}_{d1} \mathbf{V}_d$  and  $\mathbf{H}_{d2} = \mathbf{U}_{d2} \mathbf{\Sigma}_{d2} \mathbf{V}_d$  be the corresponding GSVD, where  $\mathbf{V}_d \in \mathbb{C}^{N \times N}$  represents the common factor given by the decomposition, i.e., the factor  $(\mathbf{W}^H \mathbf{R}, \mathbf{0}) \mathbf{Q}^H$  in (2.2).

The following choice of transmit beamforming matrix  $\mathbf{W}$  (for the relay) and the receiver beamforming matrices  $\mathbf{R}_1, \mathbf{R}_2$  (for  $\mathcal{U}_1$  and  $\mathcal{U}_2$ , respectively) ensures joint diagonalization of the MIMO channels:

$$\mathbf{W} = \alpha_d \cdot (\mathbf{V}_d)^{-1} \quad (2.14a)$$

$$\mathbf{R}_1 = \frac{1}{\alpha_d} \cdot \{\mathbf{U}_{d1}^H\}_{\mathcal{R}(1:N)} \quad (2.14b)$$

$$\mathbf{R}_2 = \frac{1}{\alpha_d} \cdot \{\mathbf{U}_{d2}^H\}_{\mathcal{R}(M-N+1:M)} \quad (2.14c)$$

Corresponding VC gains for  $\mathcal{U}_1, \mathcal{U}_2$  are, respectively, given by  $\text{diag}(\{\mathbf{\Sigma}_{d1}\}_{\mathcal{R}(1:N)})$  and  $\text{diag}(\{\mathbf{\Sigma}_{d2}\}_{\mathcal{R}(M-N+1:N)})$ ;  $\alpha_d$  normalizes the average relay transmit power.

Scheme 2: In this scheme, beamforming for the uplink is as in Scheme 1. However, ZF reception is employed in the downlink. Thus, the corresponding beamforming matrices are  $\mathbf{W}_1 = \beta_u (\mathbf{H}_{u1})^\dagger$ ,  $\mathbf{W}_2 = \beta_u (\mathbf{H}_{u2})^\dagger$ ,  $\mathbf{R} = \mathbf{I}_N / \beta_u$ ,  $\mathbf{W} = \beta_d \mathbf{I}_N$ ,

$\mathbf{R}_1 = (\mathbf{H}_{d1})^\dagger / \beta_d$ , and  $\mathbf{R}_2 = (\mathbf{H}_{d2})^\dagger / \beta_d$ , where  $\beta_u$  and  $\beta_d$ , respectively, normalize the average transmit power in the uplink and downlink time slots. Note that  $\mathcal{U}_1$  and  $\mathcal{U}_2$  are responsible for all the MIMO signal processing in both directions.

Scheme 3: Here, GSVD beamforming is employed in the reverse direction for the uplink, with a minor modification to ensure that the effective CVC gains are 1. Consider the GSVD of  $\mathbf{H}_{u1}^T \in \mathbb{C}^{M \times N}$  and  $\mathbf{H}_{u2}^T \in \mathbb{C}^{M \times N}$  given by  $\mathbf{H}_{u1}^T = \mathbf{U}_{u1} \boldsymbol{\Sigma}_{u1} \mathbf{V}_u$  and  $\mathbf{H}_{u2}^T = \mathbf{U}_{u2} \boldsymbol{\Sigma}_{u2} \mathbf{V}_u$ . The transmit beamforming matrices,

$$\begin{aligned} \mathbf{W}_1 &= \delta_u \cdot \left( (\mathbf{U}_{u1} \boldsymbol{\Sigma}_{u1})^\dagger \right)^T \\ &= \delta_u \cdot \left( \{\mathbf{U}_{u1}\}_{\mathcal{C}(1:N)} \right)^* \cdot \left( \{\boldsymbol{\Sigma}_{u1}\}_{\mathcal{R}(1:N)} \right)^{-1} \quad \text{and} \end{aligned} \quad (2.15a)$$

$$\begin{aligned} \mathbf{W}_2 &= \delta_u \cdot \left( (\mathbf{U}_{u2} \boldsymbol{\Sigma}_{u2})^\dagger \right)^T \\ &= \delta_u \cdot \left( \{\mathbf{U}_{u2}\}_{\mathcal{C}(M-N+1:M)} \right)^* \cdot \left( \{\boldsymbol{\Sigma}_{u2}\}_{\mathcal{R}(M-N+1:M)} \right)^{-1}, \end{aligned} \quad (2.15b)$$

respectively, for  $\mathcal{U}_1$  and  $\mathcal{U}_2$ , and the receiver beamforming matrix,

$$\mathbf{R} = \frac{1}{\delta_u} \cdot (\mathbf{V}_u^{-1})^T, \quad (2.15c)$$

for the relay jointly force each effective uplink channel to be a rank- $N$  identity matrix.  $\delta_u$  normalizes the average total user transmit power. The transmitter–receiver processing involved here can be thus interpreted as a form of simultaneous transmit and receiver ZF. Downlink beamforming is the same as with Scheme 1; therefore,  $\mathbf{W}$ ,  $\mathbf{R}_1$ , and  $\mathbf{R}_2$  are given by equations similar to (2.14a)–(2.14c).

Fig. 2.11 compares the SER performance of the above three schemes for a MIMO two-way relay system with  $(M, N) \doteq (4, 3)$ .

Assumptions: QPSK modulation with binary symbol mapping is assumed at  $\mathcal{U}_1$  and  $\mathcal{U}_2$ . The relay directly decodes the XORed symbols by using the maximum-likelihood detection rule on the corresponding superimposed constellation, and re-modulates the regenerated symbols by using QPSK. Time division duplexing, channel reciprocity, and a symmetric two-way relay configuration undergoing i.i.d. Rayleigh fading are assumed. Normalization coefficients are selected to cause the average transmit power used by each user and the relay 1/3 power units.

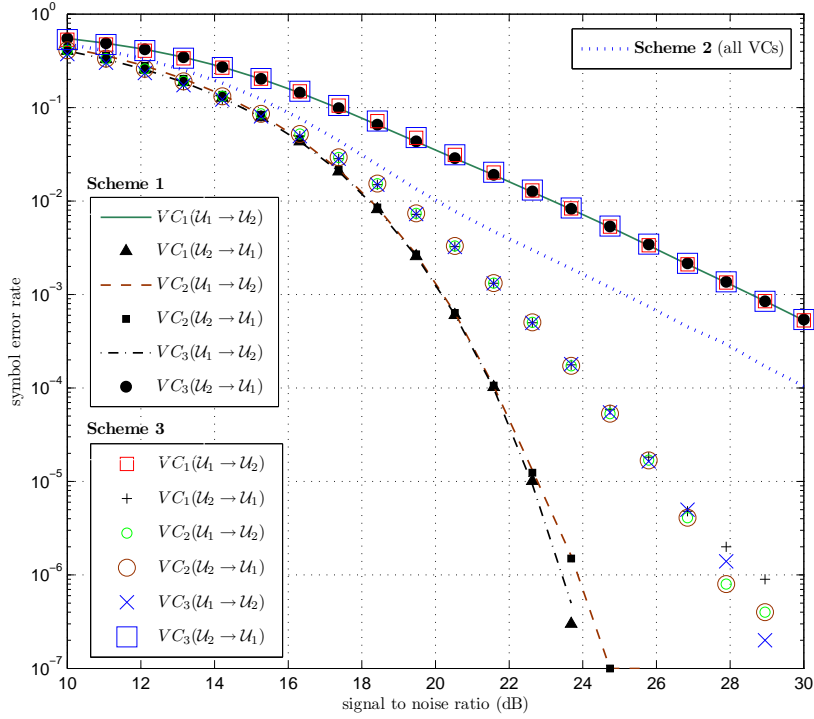


Figure 2.11: The SERs of the VCs in the  $(M, N) \doteq (4, 3)$  network-coded MIMO two-way relay configuration. QPSK modulation is used.

Each scheme produces three VCs in either direction.

- Scheme 1: Except for the weakest VC in each direction (i.e.,  $VC_1$  in the  $\mathcal{U}_1 \rightarrow \mathcal{U}_2$  direction and  $VC_3$  in the  $\mathcal{U}_2 \rightarrow \mathcal{U}_1$  direction) having diversity order 2, all other VCs exhibit the same SER performance, faring better than the VCs produced by Scheme 2. (The weakest VCs are about 4 dB worse than those.)
- Scheme 2: All the VCs exhibit the same SER performance and a diversity order 2, faring worse than all but the weakest VCs of Schemes 1 and 3.
- Scheme 3: The weakest VCs are exactly those of Scheme 1 and exhibit the same SERs as they do. All the other VCs perform identically, yet have the SERs between Scheme 1 and Scheme 3.

To summarize, Scheme 1 fares impressively when compared to Scheme 2, which is

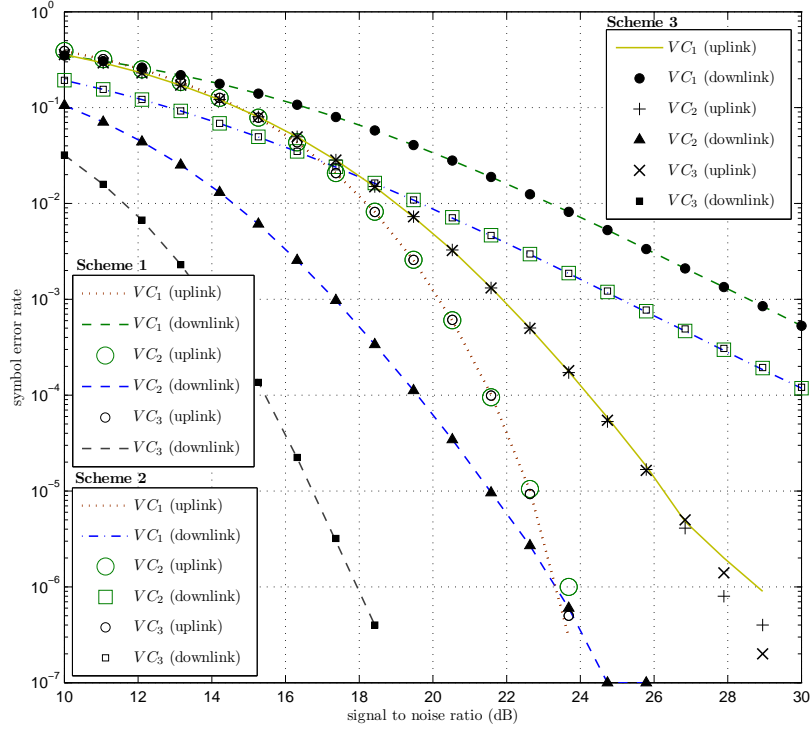


Figure 2.12: The hop-by-hop SERs of the VCs (for the  $\mathcal{U}_1 \rightarrow \mathcal{U}_2$  direction) in the  $(M, N) \doteq (4, 3)$  network-coded MIMO two-way relay configuration. QPSK modulation is used.

the transmit ZF and receiver ZF-based MIMO two-way relay network implementation typically considered in the literature. Also, GSVD beamforming appears to perform the best, when employed in the downlink, in its original form.

With physical-layer network coding, the overall SER corresponding to each VC is approximately the worst SER it experiences in either of the hops: the uplink or the downlink. Therefore, the above observations can be explained by using a hop-by-hop SER analysis. Given the lack of exact analytic results, we resort to intuitions and simulation results (Fig. 2.12) for this purpose. Because the two-way relay configuration of concern is symmetric, it is sufficient to consider a single direction (say, the  $\mathcal{U}_1 \rightarrow \mathcal{U}_2$  direction via the relay).

Since no pre-ordering of the VCs happens at the transmitter, for a given scheme, all the VCs experience the same SER in the uplink. Therefore, the performance distinctions among the VCs realized by a given scheme can be attributed to downlink

beamforming. According to Theorem 2.1, GSVD beamforming in the downlink causes each  $VC_r$  in the  $\mathcal{U}_2 \rightarrow \mathcal{U}_1$  direction and each  $VC_{(N-r+1)}$  in the  $\mathcal{U}_1 \rightarrow \mathcal{U}_2$  direction to have a diversity order  $(M - r + 1)(N - r + 1)$  for  $r \in \{1, \dots, N\}$ . Therefore, the weakest VC has a diversity order  $(M - N + 1)$  that of a ZF-based downlink. Confirming these facts, the downlink  $VC_1$  and  $VC_2$  for Schemes 1 and 3 are observed (Fig. 2.12) to have diversity orders 2 and 6, respectively. (Low Monte Carlo precision precludes curves corresponding to  $VC_3$  from showing a diversity order 12.) Moreover, the downlink VCs for Scheme 2 show the diversity order 2. Despite having the same diversity order, ZF reception can be observed to yield better SER than that of the weakest VC realized through GSVD beamforming. These performance distinctions are manifested in the overall SER of a VC (Fig. 2.11) whenever its uplink SER is better than the downlink SER.

Transmit ZF makes the uplink effectively additive Gaussian and causes VCs to have theoretically infinite diversity orders. However, as evident from Fig. 2.12, the corresponding SER is worse than all but the weakest VC of a GSVD downlink (even at the  $10^{-5}$  SER level). As a result, for Scheme 1, the downlink governs the overall SER of the weakest VC, while the uplink appears to dictate those of all other VCs. However, at even higher SNR values (and impractically low SER levels) the downlink would dominate the performance of all the VCs. Thus, theoretically, the diversity orders of Scheme 1 will be those of a GSVD downlink (with each VC performing differently). For Scheme 2, the downlink dictates the overall SER, except at low SNR values. Thus, the SER performance of Scheme 1 and Scheme 3 observed in Fig. 2.11 may be qualitatively explained by using the worst of the uplink and downlink SERs. The performance of Scheme 3 can be explained similarly. Moreover, since GSVD uplink beamforming does not completely negate fading as transmit ZF does, GSVD uplink VCs perform worse than their transmit ZF counterparts. This fact, also observed in Fig. 2.12, explains the relative performance difference in Scheme 1 and Scheme 3.

## 2.7 Conclusion

GSVD beamforming, a non-iterative two-user beamforming technique that produces point-to-two point (common) VCs in addition to the classic point-to-point (private) VCs, was proposed. As demonstrated through numerical results, applications having the corresponding two-user multicast MIMO configuration, including MIMO multicasting and relaying, can benefit significantly. This chapter also provided useful insights about the numbers of private/common VCs and transmit power normalization. Moreover, by using the results from random matrix theory to characterize the VC gains, a foundation was laid for exact performance analysis of GSVD beamforming for Rayleigh fading and MIMO configurations supporting only common VCs.

Since the GSVD does not generalize to more than two matrices, a direct extension of GSVD beamforming for three or more users cannot be foreseen. Such extension will have to exploit a more general joint matrix decomposition technique.

### **Future directions:**

- As illustrated with Theorem 2.1, the framework based on Proposition 2.1 can be used to quantify the performance of certain GSVD beamforming configurations. Obtaining such numerical (and perhaps, exact analytic) performance results are among the future possibilities. Generalizing Proposition 2.1 to eliminate the condition  $\min(m, p) \geq k$  is a more challenging possibility; such a generalization would also contribute to random matrix theory.
- The capacity of the two-user MIMO downlink under GSVD beamforming is also worth investigating. Such a result, along with the SER performance, would be useful for determining how GSVD beamforming ranks against the other channelization schemes in a particular situation.
- GSVD beamforming assumes perfect CSI; developing ‘robust’ counterparts that achieve acceptable SER performance under imperfect CSI has a greater practical significance.

~

# Chapter 3

## Physical-Layer Multicasting

This chapter outlines a non-iterative beamforming scheme for physical-layer multicasting (PLM) proposed and investigated in this research [47]. The proposed scheme follows a divide-and-conquer strategy that reduces an arbitrary virtual channel (VC)-to-User mapping into a set of manageable non-overlapping sub-mappings, each represented by a *multicast antenna group* (MAG). A two-phased beamforming scheme comprising *inter-MAG* beamforming and *intra-MAG* beamforming phases is then employed to systematically realize all the VCs.

### 3.1 Introduction

Multicasting [23], or the ability to send the same information to multiple users forming a multicast group (MG), is crucial for multimedia applications such as video streaming. Typically, multicasting happens at higher layers in the network architecture [11], e.g., at the network layer as in IP multicasting [68], or at the medium access control layer as in the IEEE 802.11-2012 standard [24], on top of multiple unicast physical channels. However, when all the users share a common physical medium as in a wireless network (e.g., content delivery over a wireless home media network), multicasting at the physical layer, also known as PLM [69], appears intuitive and attractive because of PLM's potential for facilitating a multicast data stream by using a single spatial degree of freedom (DoF) at each participating user-terminal. Multicasting at higher layers, by contrast, requires the repetition of the same data over multiple VCs (see Subsection 1.1.4) in the physical layer and thus

uses more spatial DoFs and transmit power.

Since wireless channels are of a broadcast nature, multicasting a single data stream over the air is straightforward; doing so requires only user selection, i.e., getting only the users in the corresponding MG to listen. However, neither providing multiple spatially multiplexed data streams within a single MG nor supporting concurrent MGs is as straightforward, because any interference caused by concurrent transmissions should be suppressed at each user. PLM seeks to overcome this channelization challenge through multi-user beamforming.

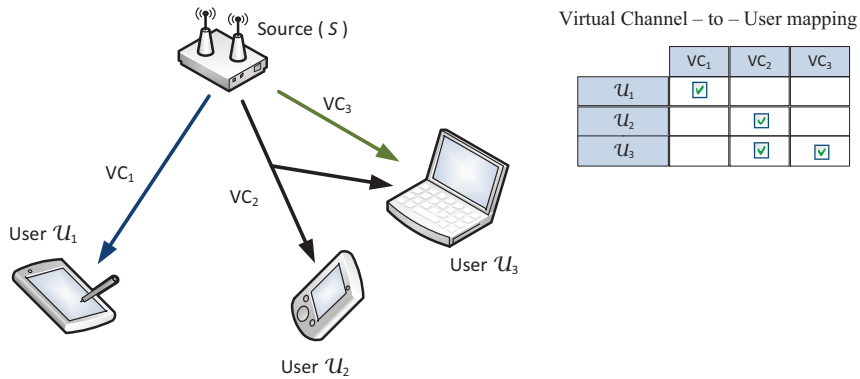


Figure 3.1: VC-to-User mapping in PLM.

PLM typically requires point-to-multipoint VCs (e.g., VC2 in Fig. 3.1), while conventional multi-user beamforming techniques, such as transmit zero forcing (ZF) [19] and block diagonalization (BD) [28], yield only multiple point-to-point VCs. Moreover with PLM, those point-to-multipoint VCs should match the desired VC-to-User mapping. Consequently, none of the known non-iterative beamforming techniques were readily applicable for PLM.

Iterative techniques for PLM have been investigated by considering both the single-antenna and multiple-antenna user configurations. References [69–75] focus on joint optimization of beamforming matrices to minimize performance criteria such as the signal to interference plus noise ratio and the mean squared error, subjected to constraints on, for example, the total transmit power. Performance analysis of certain multicast configurations has also been attempted [54, 76, 77]. However, non-iterative beamforming techniques, which are generally less computationally challenging to implement, have not been previously studied in the PLM literature.

The proposed approach is the first non-iterative beamforming technique for PLM.

**The chapter is organized as follows:** Section 3.2 introduces concepts pertaining to the novel approach for PLM proposed in Section 3.3. Section 3.4 provides a numerical example highlighting the feasibility of the approach. Section 3.5 concludes the discussion by highlighting directions for future research.

## 3.2 Background

### 3.2.1 Unicast vs. Multicast Virtual Channels

The VCs produced by conventional multiple-input multiple-output (MIMO) beamforming techniques are point-to-point; identify them as *unicast* VCs to emphasize that fact. Let the point-to-multipoint VCs catering to multiple users be designated *multicast* VCs. For example, the common virtual channels (CVCs) produced by GSVD beamforming (see Chapter 2) are multicast VCs.

In PLM, the total number of unicast and multicast VCs at a terminal may not exceed the available spatial DoFs. For example, in Fig. 3.1, which shows a source multicasting to three users, the source and  $\mathcal{U}_3$  should have at least 3 and 2 DoFs, respectively. This requirement is necessary but not sufficient because, as will be explained in Section 3.3, the channelization techniques could require additional DoFs to guarantee the orthogonality of the VCs.

### 3.2.2 Block Diagonalization

BD [28] produces multiple unicast VCs from a source to multiple users. It is examined here in detail because the proposed inter-MAG beamforming technique generalizes BD.

Consider a multiple antenna source terminal  $\mathcal{S}$  communicating with  $K > 1$  multiple antenna users  $\mathcal{U}_i, i \in \{1, \dots, K\}$ . Let  $\mathbf{H}_i$  be the  $\mathcal{S} \rightarrow \mathcal{U}_i$  MIMO channel and  $\tilde{\mathbf{H}}_i = (\mathbf{H}_1^T \dots \mathbf{H}_{i-1}^T \mathbf{H}_{i+1}^T \dots \mathbf{H}_K^T)^T$  for  $i \in \{1, \dots, K\}$ . Given a matrix  $\tilde{\mathbf{V}}_i^{(0)}$  whose columns span the subspace  $\text{Null}(\tilde{\mathbf{H}}_i) - \text{Null}(\mathbf{H}_i)$ , a matrix  $\mathbf{G}_i$  defined as  $\mathbf{G}_i = \mathbf{H}_i \tilde{\mathbf{V}}_i^{(0)}$  would be orthogonal to each  $\mathbf{H}_j$  for  $j \neq i$ . Therefore, by having  $\tilde{\mathbf{V}}_i^{(0)}$  as the leftmost factor of the transmit precoding matrix,  $\mathcal{S}$  may transmit

to  $\mathcal{U}_i$  without interfering with any other user  $\mathcal{U}_j$ . BD exploits this fact to achieve orthogonal communications with multiple users, by having  $\mathcal{S}$  transmit a linear combination of signals each thus precoded for a distinct user; this precoding makes the effective channel between  $\mathcal{S}$  and the users block diagonal, giving BD its name. Unlike transmit ZF, BD does not prevent MIMO receiver signal processing at the user terminals; therefore, BD yields a better performance. Moreover, BD requires no more antennas at the source than ZF [28, Sec. III.A]. Therefore, despite the increased complexity due to the two-phased approach, i.e., the approach assuring the orthogonality of the users, followed by channelization on top of the thus realized orthogonal effective channels, BD is preferred over ZF for multi-user MIMO. However, as illustrated in Example 3.1, the two-phased approach typically causes BD to produce fewer VCs than ZF.

**Example 3.1** Consider a  $\{2, 3, 2\} \times 6$  channel [28], representing a 6-antenna source and three users with 2, 3, and 2 antennas, respectively. Suppose that the corresponding MIMO channels are not rank-deficient. BD can produce 4 VCs, i.e., 1, 2, and 1 unicast VC(s) with the respective users. ZF does not hold since the source has less antennas than the user terminals, but it would hold and yield 6 VCs if a user antenna were disregarded (via antenna selection). Had the configuration been  $\{2, 3, 2\} \times 7$ , both schemes could have produced 7 VCs. •

Reference [78] suggests adaptively partitioning the set of user antennas to form correlated antenna groups, each possibly comprising antennas from more than one physical user. Although grouping together antennas from distinct users appears counterintuitive since doing so precludes MIMO receiver processing, this method inspired the notion of MAGs proposed here for PLM.

### 3.2.3 Multicast Groups

In multicasting, the same information is dispatched to all the users in a multicast group (MG). Consider a  $K$ -user MIMO downlink from source  $\mathcal{S}$ , where each  $\mathbf{H}_k$

represents the  $\mathcal{S} \rightarrow \mathcal{U}_k$  MIMO channel for  $k \in \{1, \dots, K\}$ . Let  $\mathcal{G} \subseteq \{1, \dots, K\}$  denote a MG of users  $\mathcal{U}_i, i \in \mathcal{G}$  receiving  $n > 0$  spatially multiplexed multicast VCs from  $\mathcal{S}$ . Define  $m = |\mathcal{G}|$ . If we assume that no interference occurs from outside this MG, multi-user beamforming can facilitate the corresponding VCs if a transmit precoding matrix  $\mathbf{W}$  and receiver reconstruction matrices  $\mathbf{R}_i, i \in \mathcal{G}$  can be found such that

- $\mathbf{D}_i = \mathbf{R}_i \mathbf{H}_i \mathbf{W}$  are diagonal for  $i \in \mathcal{G}$ , and
- at least  $n$  columns of  $\mathbf{D} = (\mathbf{D}_{i_1}^T \dots \mathbf{D}_{i_m}^T)^T$  for  $i_j \in \mathcal{G}$  have  $m$  non-zero elements.

Depending on the system design, the other columns of  $\mathbf{D}$  (if any) can be exploited as unicast VCs or multicast VCs serving some of the users.

In practice, a MG may not function in isolation; consequently, the orthogonality of concurrent MGs is also a concern. Complicating the matters further, the MG-to-User mapping, which depends on the end-user requirements, could be Many-to-Many: i.e., the MGs may partially overlap. Therefore, PLM poses a challenging design problem, for which a systematic solution is proposed in Section 3.3.

### 3.3 Signal Processing & System Design

Consider the  $\{M_1, \dots, M_K\} \times N$  multi-user MIMO downlink channel, corresponding to an  $N$ -antenna source  $\mathcal{S}$  multicasting to  $K$  users, with the  $i^{\text{th}}$  user  $\mathcal{U}_i$  having  $M_i$  antennas for  $i \in \{1, \dots, K\}$ . Suppose  $M = \sum M_i$ . Let  $\mathbf{H}_i \in \mathbb{C}^{M_i \times N}$  represent the  $\mathcal{S} \rightarrow \mathcal{U}_i$  MIMO channel. Define  $\hat{\mathbf{H}} = (\mathbf{H}_1^T \dots \mathbf{H}_K^T)^T$ .

Suppose that  $n$  unicast and multicast VCs,  $\text{VC}_k$  for  $k \in \{1, \dots, n\}$ , are realized, where  $n$  is upper bounded by  $\text{rank}(\hat{\mathbf{H}}) \leq \min(M, N)$ , which is the number of spatial DoFs  $\mathcal{S}$  has. Moreover, any user  $\mathcal{U}_i$  may receive no more than  $\text{rank}(\mathbf{H}_i) \leq M_i$  VCs. The Many-to-Many mapping between the users and the VCs, which is governed by the end-user requirements, is thus subjected to these DoF constraints. Therefore, the first hurdle in PLM is deciding if all of the required VCs can be supported without exhausting the spatial DoFs at each terminal. If not,

non-overlapping subsets of the VCs would have to be multiplexed in other orthogonal dimensions (e.g., in time). We do not dwell on this issue here, but take for granted that all the VCs can be spatially multiplexed.

### 3.3.1 Multicast Antenna Groups (MAGs)

On the one hand, the joint computation of the beamforming matrices for  $\mathcal{S}$  and the users  $\mathcal{U}_i, i \in \{1, \dots, K\}$ , which considers all the VCs, is optimal in terms of the DoF savings. However, the complexity of this computation might prohibit its use. Implementing the VCs separately, on the other hand, is simpler; but assuring their orthogonality (e.g., via BD) could be costly in terms of the spatial DoFs. Hence, a division coarser than the VC-level is desired where possible. Moreover, accommodating the Many-to-Many mappings between the VCs and the users, in general, requires partitioning the antennas of a given user so that the user may participate in multiple MGs. Therefore, the user-level is too coarse for the aforementioned division.

The solution proposed here is based on an abstract notion of multicast antenna groups (MAGs), a specialization of correlated antenna groups in reference [78], having the following characteristics.

1. VC-to-MAG relationship is Many-to-One:

A MAG supports one or more unicast/multicast VCs:  $\text{VC}_k, \exists k \in \{1, \dots, n\}$ ; each VC is associated with just one MAG. VCs catering to a certain subset of users may be accommodated in the same MAG to keep the number of MAGs small.

2. Antenna-to-MAG relationship is Many-to-One:

For each supported VC, a MAG has a sufficient number of antennas allocated from the corresponding users.

Let  $\Xi_i$  denote the set of antennas at user  $\mathcal{U}_i$  (excluding any antenna disregarded through antenna selection<sup>1</sup>) and  $\Theta_j$  represent the set of antennas associated with  $\text{MAG}_j$ , the  $j^{\text{th}}$  MAG.

---

<sup>1</sup> Antenna selection is not desirable in beamforming. However, leaving out certain user antennas could make it easier to assure the orthogonality of the MAGs.

- $|\Xi_i \cap \Theta_j|$  should be no less than the number of VCs in  $\text{MAG}_j$  catering to  $\mathcal{U}_i$ ;  $\Xi_i \cap \Theta_j \neq \phi$  iff there are VCs in  $\text{MAG}_j$  that cater to  $\mathcal{U}_i$ .
- $\Theta_j$ s form a partition of  $\bigcup_{\forall i} \Xi_i$ .

The MAGs provide a partitioning of the antennas lying between the VC-level and the user-level in granularity, enabling a compromise between the two extreme cases: beamforming for the whole system vs. considering the VCs one-by-one.

The proposed channelization scheme for implementing the MAGs and their VCs involves two phases:

- **Phase 1:** Inter-MAG beamforming:

The effective MIMO channel  $\mathbf{G}_j$  pertaining to each  $\text{MAG}_j$  is formed by concatenating the rows of  $\hat{\mathbf{H}}$  that correspond to the antennas in  $\Theta_j$ . Inter-MAG beamforming uses BD to make the communications over  $\mathbf{G}_j$ s orthogonal.

- **Phase 2:** Intra-MAG beamforming:

Since the elements in  $\Theta_j$  may come from more than one physical user, multi-user beamforming techniques are typically required for intra-MAG beamforming, i.e., beamforming within the MAGs.

### 3.3.2 Determination of MAGs

Given a PLM problem, the MAGs need to be determined first. The goal here is to reduce the PLM problem to manageable ‘sub-problems’ by breaking down the VC-to-User mapping to non-overlapping sub-mappings.

The VC-to-User mapping needs to be expanded first, by considering the choice of user antennas to support each VC. For the sake of simplicity, the antennas of a given user are assumed interchangeable.<sup>2</sup> Let  $\mathbf{\Gamma}_0$  be an  $M \times n$  binary matrix indicating the mapping the user antennas have with the VCs, such that

- the  $i^{\text{th}}$  antenna of  $j^{\text{th}}$  user corresponds to row number  $i + \sum_{k=1}^{j-1} M_k$  of  $\mathbf{\Gamma}_0$  for  $i \in \{1, \dots, M_j\}$  and  $j \in \{1, \dots, K\}$ ,

<sup>2</sup> Distinguishing between the antennas would require, for instance, considering the all permutations of antenna allocation to the MAGs, as well as the multiple-input single-output channel gains corresponding to the user antennas.

$$\begin{aligned}
\mathbf{\Gamma}_0 &= \begin{pmatrix} VC_1 & VC_2 & VC_3 & VC_4 \\ \mathbf{1} & 0 & 0 & 0 \\ 0 & 0 & 0 & \mathbf{1} \\ \times & \times & \times & \times \\ \hline 0 & \underline{\mathbf{1}} & 0 & 0 \\ 0 & 0 & \underline{\mathbf{1}} & 0 \\ \hline \bar{\mathbf{1}} & 0 & 0 & 0 \\ 0 & \bar{\mathbf{1}} & 0 & 0 \\ 0 & 0 & \bar{\mathbf{1}} & 0 \\ 0 & 0 & 0 & \bar{\mathbf{1}} \end{pmatrix} \begin{matrix} \leftarrow \mathcal{U}_1 \\ \leftarrow \mathcal{U}_2 \\ \leftarrow \mathcal{U}_3 \end{matrix} & \quad \mathbf{\Gamma}_1 = \begin{pmatrix} VC_1 & VC_2 & VC_3 & VC_4 \\ \mathbf{1} & 0 & 0 & 0 \\ \bar{\mathbf{1}} & 0 & 0 & 0 \\ 0 & \underline{\mathbf{1}} & 0 & 0 \\ 0 & \bar{\mathbf{1}} & 0 & 0 \\ 0 & 0 & \underline{\mathbf{1}} & 0 \\ 0 & 0 & \bar{\mathbf{1}} & 0 \\ 0 & 0 & 0 & \mathbf{1} \\ 0 & 0 & 0 & \bar{\mathbf{1}} \\ \times & \times & \times & \times \end{pmatrix} \\
& \text{(a)} & \quad \text{(b)} \\
\mathbf{\Gamma}_2 &= \begin{pmatrix} VC_1 & VC_4 & VC_2 & VC_3 \\ \mathcal{U}_1 & \mathbf{1} & & \\ & & \mathbf{1} & \\ \times & \times & & \\ \mathcal{U}_3 & \bar{\mathbf{1}} & & \\ & & \bar{\mathbf{1}} & \\ \hline \mathcal{U}_2 & & \underline{\mathbf{1}} & \\ & & & \underline{\mathbf{1}} \\ \mathcal{U}_3 & & \bar{\mathbf{1}} & \\ & & & \bar{\mathbf{1}} \end{pmatrix} \begin{matrix} \leftarrow \text{MAG}_1 \\ \leftarrow \text{MAG}_2 \end{matrix} \\
& \text{(c)}
\end{aligned}$$

Figure 3.2: A simple VC-to-User mapping involving three users and four multicast VCs. The non-zero entries in rows corresponding to individual users  $\mathcal{U}_1$ ,  $\mathcal{U}_2$ , and  $\mathcal{U}_3$  are indicated as  $\mathbf{1}$ ,  $\underline{\mathbf{1}}$ , and  $\bar{\mathbf{1}}$ , respectively.

- the columns of  $\mathbf{\Gamma}_0$  correspond to VCs, and
- each non-zero element in  $\mathbf{\Gamma}_0$  associates a VC with a corresponding antenna.

A MAG should have a sufficient number of antennas allotted from the respective users to support the VCs they receive. The antennas the users may have in excess of this number can be treated as *don't cares*<sup>3</sup> (designated as rows of ‘ $\times$ ’ on  $\mathbf{\Gamma}_0$ ) to gain more leeway in determining the MAGs. Thus, each row of  $\mathbf{\Gamma}_0$  will have a single unit element (i.e.,  $\mathbf{1}$ ); each column will have at least one unit element (Fig. 3.2a).

Since the VC-to-MAG relationship can be Many-to-One, the first step towards determining the MAGs is interchanging the rows of  $\mathbf{\Gamma}_0$  to make the non-zero ele-

<sup>3</sup>Once the MAGs are determined, those excess antennas can be assigned to arbitrary MAGs to avoid the loss of diversity benefits. However, where eliminating an excess antenna makes inter-MAG beamforming simpler, that antenna may be disregarded through antenna selection.

ments on each column adjacent and the resulting mapping  $\Gamma_1$  block diagonal. As with  $\Gamma_1$  of Fig. 3.2b, the don't cares can be disregarded during this process. Since each block in  $\Gamma_1$ 's structure may be interpreted as representing a MAG supporting a single VC,  $\Gamma_1$  corresponds to the VC-level division mentioned in Subsection 3.3.1. PLM based on a VC-level division is realizable irrespective of the VC-to-User mapping, provided that the source has sufficient DoFs to ensure the orthogonality of the MAGs.

The cost of inter-MAG beamforming makes it preferable to minimize the number of MAGs. Therefore, more than one VC may be associated with a MAG (e.g., the VCs serving similar sets of users may be grouped together), provided that the VC mapping within each MAG is realizable through any intra-MAG beamforming technique. The block diagonal form in  $\Gamma_2$  of Fig. 3.2c, obtained by interchanging rows and columns of  $\Gamma_1$ , for instance, has realizable mappings for each of its two MAGs. (In fact, GSVD beamforming can be used to realize the VCs.) Note how  $\mathcal{U}_3$ 's antennas are split between the two MAGs, highlighting why a user-level division is too coarse and the use of MAGs is needed.

Example 3.2 illustrates the VC realizations possible for the VC-to-User mapping in Fig. 3.2, highlighting the implications of the divide-and-conquer strategy of the proposed channelization scheme.

**Example 3.2** Let  $\mathbf{H}_1 \in \mathbb{C}^{3 \times N}$ ,  $\mathbf{H}_2 \in \mathbb{C}^{2 \times N}$ , and  $\mathbf{H}_3 \in \mathbb{C}^{4 \times N}$  represent the  $\mathcal{S} \rightarrow \mathcal{U}_1$ ,  $\mathcal{S} \rightarrow \mathcal{U}_2$ , and  $\mathcal{S} \rightarrow \mathcal{U}_3$  channels, where source  $\mathcal{S}$  has  $N$  antennas.

- **Possibility 1:** Based on  $\Gamma_2$ , the VCs can be realized with 2 MAGs:
  - MAG<sub>1</sub> using 3 antennas from  $\mathcal{U}_1$  and 2 antennas from  $\mathcal{U}_3$  to support VC<sub>1</sub> and VC<sub>4</sub>, and
  - MAG<sub>2</sub> using 2 antennas each from  $\mathcal{U}_2$  and  $\mathcal{U}_3$  to support VC<sub>2</sub> and VC<sub>3</sub>.

$\Gamma_0$  being a simple mapping, only  $\mathcal{U}_3$ 's antennas have to be split between the MAGs; similar VCs (e.g., VC<sub>1</sub> and VC<sub>4</sub>) are easily grouped into the

same MAG. The effective channel matrix for  $\text{MAG}_1$  is  $\mathbf{G}_1 \in \mathbb{C}^{5 \times N}$ . For example,  $\mathbf{G}_1$  could have rows of  $\mathbf{H}_1$  and the first 2 rows (say) of  $\mathbf{H}_3$ ; the matrix  $\mathbf{G}_2 \in \mathbb{C}^{4 \times N}$  corresponding to  $\text{MAG}_2$  may be similarly defined with rows of  $\mathbf{H}_2$  and remaining rows of  $\mathbf{H}_3$ ;

$$\text{i.e., } \mathbf{G}_1 = \begin{pmatrix} \mathbf{H}_1 \\ \{\mathbf{H}_3\}_{\mathcal{R}(1:2)} \end{pmatrix} \text{ and } \mathbf{G}_2 = \begin{pmatrix} \mathbf{H}_2 \\ \{\mathbf{H}_3\}_{\mathcal{R}(3:4)} \end{pmatrix}.$$

Supposing the channels are not rank-deficient, any  $N \geq 7$  can make the MAGs orthogonal. Had the excess antenna of  $\mathcal{U}_1$  (corresponding to the don't cares in  $\Gamma_2$ ) been disregarded,  $N = 6$  would have been sufficient to achieve the same VCs.

- **Possibility 2:** Alternatively, as implied by  $\Gamma_1$ , the system can be implemented with 4 MAGs, each supporting a distinct multicast VC. The requirement for orthogonality of the MAGs is  $N \geq 7$  even after disregarding the excess antenna. (It is  $N \geq 9$ , if that antenna is considered.) The effective channels  $\mathbf{G}_i, i \in \{1, \dots, 4\}$ , with each  $\mathbf{G}_i$  corresponding to  $\text{MAG}_i$ , which implements  $\text{VC}_i$ , would be of following (or similar) form:

$$\begin{aligned} \mathbf{G}_1 &= \begin{pmatrix} \{\mathbf{H}_1\}_{\mathcal{R}(1)} \\ \{\mathbf{H}_3\}_{\mathcal{R}(1)} \end{pmatrix}, & \mathbf{G}_2 &= \begin{pmatrix} \{\mathbf{H}_2\}_{\mathcal{R}(1)} \\ \{\mathbf{H}_3\}_{\mathcal{R}(2)} \end{pmatrix}, \\ \mathbf{G}_3 &= \begin{pmatrix} \{\mathbf{H}_2\}_{\mathcal{R}(2)} \\ \{\mathbf{H}_3\}_{\mathcal{R}(3)} \end{pmatrix}, & \text{and } \mathbf{G}_4 &= \begin{pmatrix} \{\mathbf{H}_1\}_{\mathcal{R}(2)} \\ \{\mathbf{H}_4\}_{\mathcal{R}(1)} \end{pmatrix}. \end{aligned}$$

Inter-MAG beamforming would make each MAG effectively single-input multiple-output, for which intra-MAG beamforming is trivial.

- **Possibility 3:** Multicasting at higher layers (by using multiple unicast VCs in place of each multicast VC) is also possible. Doing so requires  $N \geq 9$  if the excess antenna is considered, and  $N \geq 8$  if it is disregarded.

PLM is possible even when  $\mathcal{S}$  has fewer antennas than the users' total. Having fewer MAGs lowers the antenna requirement at  $\mathcal{S}$ , but makes intra-MAG beamforming more challenging. Therefore, a compromise is necessary with this divide-and-conquer strategy. •

### 3.3.3 Inter-MAG Beamforming

With transmit channel-state information (CSI), inter-MAG beamforming ensures the orthogonality of communications in distinct MAGs. This result is achieved by considering each MAG as a *virtual* user and applying a variant of BD. Let  $\mathbf{G}_j \in \mathbb{C}^{|\Theta_j| \times N}$  be the effective channel corresponding to each  $\text{MAG}_j$ . Consider  $\mathbf{V}_j^{(0)} \in \mathbb{C}^{N \times n_j}$  whose columns span the space  $\bigcap_{k \neq j} \text{Null}(\mathbf{G}_k) - \text{Null}(\mathbf{G}_j)$ ;  $n_j = \text{rank}(\hat{\mathbf{H}}) - \text{rank}(\tilde{\mathbf{G}}_j)$  gives the maximal number of VCs each  $\text{MAG}_j$  may support, where  $\tilde{\mathbf{G}}_j = (\mathbf{G}_1^T \dots \mathbf{G}_{j-1}^T \mathbf{G}_{j+1}^T \dots \mathbf{G}_K^T)^T$ . (Notably,  $\sum n_j$  cannot exceed the total spatial DoFs at  $\mathcal{S}$ .) Let  $r_j \leq n_j$  be the number of VCs end-users require each  $\text{MAG}_j$  to support.

- **Approach 1:** Consider each effective channel matrix  $\hat{\mathbf{G}}_j = \mathbf{G}_j \mathbf{V}_j^{(0)}$ , and compute a transmit precoding matrix  $\mathbf{W}_j$  along with the receiver reconstruction matrices by using a suitable intra-MAG beamforming technique. Then, the matrices  $\hat{\mathbf{W}}_j$ , each formed with selected  $r_j$  columns of  $\mathbf{V}_j^{(0)} \mathbf{W}_j$ , will jointly ensure that all VC-to-User mappings are realized.
- **Approach 2:** Alternatively,  $\hat{\mathbf{G}}_j$  may be defined as  $\mathbf{G}_j \left\{ \mathbf{V}_j^{(0)} \right\}_{\mathcal{C}(r_j)}$ ; the transmit precoding matrices computed for the respective intra-MAG beamforming schemes may be modified as  $\hat{\mathbf{W}}_j = \left\{ \mathbf{V}_j^{(0)} \right\}_{\mathcal{C}(r_j)} \mathbf{W}_j$ .

Approach 2 above apparently yields lower diversity gains than Approach 1 but sometimes simplifies intra-MAG beamforming (e.g., when  $r_j = 1$ ). The receiver reconstruction matrices produced by linear intra-MAG beamforming techniques require no modification with either approach.

### 3.3.4 Intra-MAG Beamforming

Intra-MAG beamforming jointly computes the precoding matrix  $\mathbf{W}_j$  and the reconstruction matrices  $\mathbf{R}_{j,i}, i \in \{1, \dots, K\}$  to implement the VCs within each  $\text{MAG}_j$ ; the orthogonalized effective channel  $\hat{\mathbf{G}}_j$  obtained through inter-MAG beamforming is used for this process.

Each row of  $\hat{\mathbf{G}}_j$  corresponds to a distinct antenna coming from a physical user being served by a VC associated with the  $\text{MAG}_j$ . Without a loss of generality,

assume that the rows corresponding to each user are adjacent and grouped together as blocks within  $\hat{\mathbf{G}}_j$ . That is,  $\hat{\mathbf{G}}_j = \left( \hat{\mathbf{G}}_{j,1}^T \dots \hat{\mathbf{G}}_{j,K}^T \right)^T$ , where each submatrix  $\hat{\mathbf{G}}_{j,i} \in \mathbb{C}^{|\Xi_i \cap \Theta_j| \times n_j}$ ,  $i \in \{1, \dots, K\}$  corresponds to antennas contributed by  $\mathcal{U}_i$  to  $\text{MAG}_j$  and possibly has zero rows (whenever  $\Xi_i \cap \Theta_j = \phi$ ).

Outlined below are three possibilities for intra-MAG beamforming.

- **Single-input multiple-output diversity combining:** This technique may be employed whenever the effective channel  $\hat{\mathbf{G}}_j$  is a column vector (i.e.,  $n_j = 1$ ). It is similar to diversity combining in a multi-user single-input multiple-output channel, and an arbitrary number of users can be catered to. A scalar  $\mathbf{W}_j = 1$  is used for precoding, while vectors  $\mathbf{R}_{j,i} = \hat{\mathbf{G}}_{j,i}^H$  facilitate maximal ratio combining [13, p.214]. The simplicity and the straightforwardness of this approach might even justify having a separate MAG for each VC whenever the DoFs at  $\mathcal{S}$  are adequate.
- **MIMO beamforming:** With trivial MAGs catering to a single physical user, intra-MAG beamforming reduces to beamforming for point-to-point MIMO channels. Eigenmode transmission based on the singular value decomposition (SVD) [8, Eqn. (5)], for instance, is a suitable candidate for this case.
- **GSVD beamforming:** GSVD beamforming (see Chapter 2) may be used with MAGs associated with two physical users. Depending on the VC-to-User sub-mapping for the MAG, rank reduction or antenna selection may be required, as outlined in Section 2.5, to realize the desired combination of the unicast (private) and multicast (common) VCs.

Intra-MAG beamforming for more general and complicated mappings is desired in terms of the spatial DoFs savings. However, non-iterative algorithms are not presently available for this purpose. Therefore, the MAGs determined in Subsection 3.3.2 should be simple enough for their intra-MAG beamforming to be realized by using one of the above possibilities.

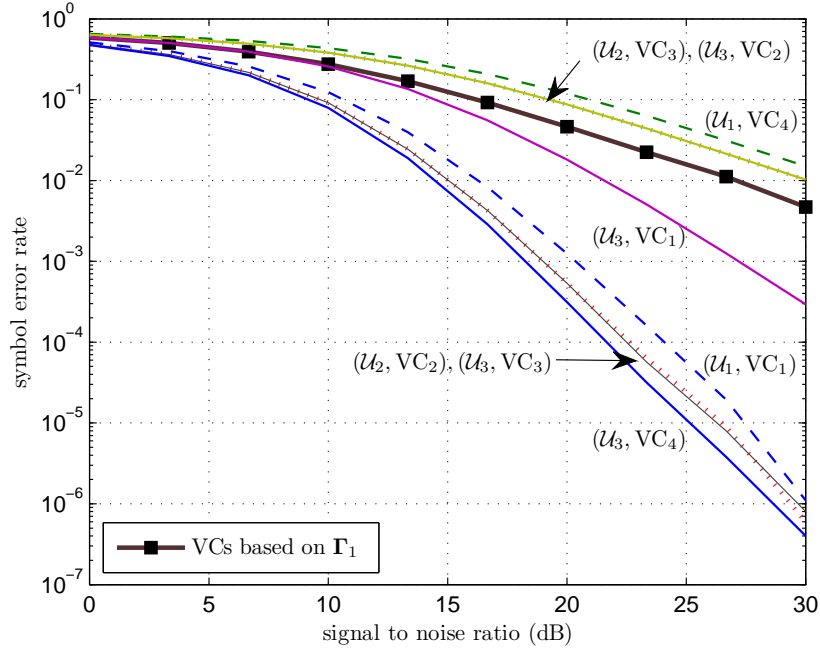


Figure 3.3: The SERs at each user in Example 3.2, assuming  $N = 7$  and PLM based on  $\Gamma_2$ . Each  $(\mathcal{U}_k, VC_j)$  designates the SER at the  $k^{\text{th}}$  user for the  $j^{\text{th}}$  VC. The curves for PLM based on  $\Gamma_1$  (solid with  $\blacksquare$  marker) overlap. QPSK modulation is used.

### 3.4 Numerical Results

The simulation-based symbol error rate (SER) performance results are presented here for the multi-user MIMO multicast configuration corresponding to Example 3.2.

Assumptions: Independent and identically distributed (i.i.d.) Rayleigh block fading is assumed for the  $\mathcal{S} \rightarrow \mathcal{U}_1$ ,  $\mathcal{S} \rightarrow \mathcal{U}_2$ , and  $\mathcal{S} \rightarrow \mathcal{U}_3$  MIMO channels. Monte Carlo simulation uses  $10^6$  channel realizations; a block of 10 quadrature phase shift keying (QPSK) modulated symbols per VC is transmitted for each channel realization. The average transmit power is normalized to be  $N$  power units.

Fig. 3.3 shows the SERs experienced by each user in Example 3.2.  $\mathcal{S}$  is assumed to have  $N = 7$  antennas so that the MAGs based on both the VC-to-User mappings  $\Gamma_1$  and  $\Gamma_2$  can be realized. Single-input multiple-output diversity combining is used with  $\Gamma_1$ -based MAGs; GSVD beamforming is used with  $\Gamma_2$ -based ones. In the  $\Gamma_1$ -

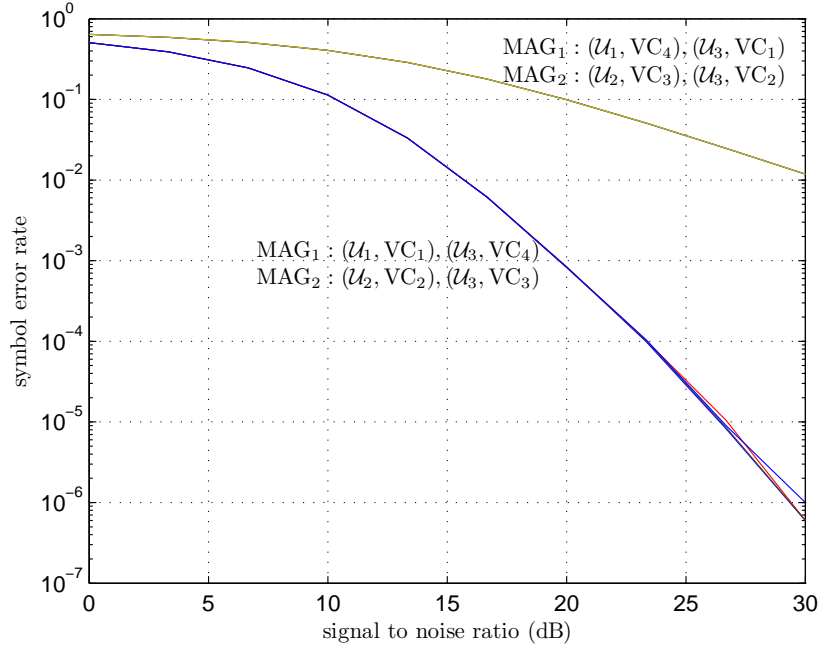


Figure 3.4: The SERs at each user in Example 3.2, assuming  $N = 6$  and PLM based on  $\Gamma_2$  — i.e., disregarding the excess antenna. Each  $(\mathcal{U}_k, \text{VC}_j)$  designates the SER at the  $k^{\text{th}}$  user for the  $j^{\text{th}}$  VC. QPSK modulation is used.

based 4-MAG implementation, all the VCs exhibit an identical SER performance. Although an exact analytical characterization of the SERs is not available for GSVD beamforming, the relative merits of the curves in Fig. 3.3 can be interpreted easily. For instance, consider  $\text{VC}_2$  and  $\text{VC}_3$  corresponding to  $\text{MAG}_2$  of Example 3.2. At any given moment, the signal to noise ratios (SNRs) for the multicast VCs produced by GSVD beamforming are in descending order for  $\mathcal{U}_2$  and in ascending order for  $\mathcal{U}_3$ . Therefore,  $\mathcal{U}_2$  experiences better performance (and a higher diversity order) for  $\text{VC}_2$  and worse performance for  $\text{VC}_3$ , whereas  $\mathcal{U}_3$  experiences the opposite. Similar observations can be made regarding  $\text{VC}_1$  and  $\text{VC}_4$  supported by  $\text{MAG}_1$ , even though the performance of  $\mathcal{U}_1$  and  $\mathcal{U}_3$  is dissimilar because of the asymmetry caused by the excess antenna at  $\mathcal{U}_1$ .

The effect of symmetry is evident in Fig. 3.4, which assumes  $N = 6$  and disregards the excess antenna altogether. As expected, all 4 VCs exhibit a similar SER performance; the relative merits of the VCs at a given user can be argued as before.

**Code 3.1** MATLAB code for  $\Gamma_2$ -based PLM implementation of Example 3.2.

```
% channel matrices
H1 = (randn(2,6)+1i*randn(2,6))/sqrt(2); % for U_1; MAG_1
H2 = (randn(2,6)+1i*randn(2,6))/sqrt(2); % for U_2; MAG_2
H3 = (randn(4,6)+1i*randn(4,6))/sqrt(2);
H3a = H3(1:2,:); H3b = H3(3:4,:); % for U_3; MAG_1, MAG_2
% compute basis for each null space (for inter-MAG beamforming)
G1 = [H1; H3a]; [~,S,V] = svd(G1); V02 = V(:,rank(S)+1:end);
G2 = [H2; H3b]; [~,S,V] = svd(G2); V01 = V(:,rank(S)+1:end);
% effective channel matrices
H1hat = H1 * V01;
H2hat = H2 * V02;
H3ahat = H3a * V01; H3bhat = H3b * V02;
% GSVD (intra-MAG) beamforming
% (adjusted for MATLAB GSVD implementation differences)
[V1,U1,X,~,~] = gsvd(H3ahat,H1hat); Q = X'; Qinvl = Q'/(Q*Q');
[V2,U2,X,~,~] = gsvd(H3bhat,H2hat); Q = X'; Qinvs = Q'/(Q*Q');
% joint beamforming matrices
W = [V01*Qinvs, V02*Qinvs]; % for transmission
R1 = U1'; R2 = U2'; R3 = blkdiag(V1,V2)'; % for reception
% fix order of antennas and VCs
R3 = R3([1,3,4,2],:); W = W(:,[1,3,4,2]);
% compute effective VC gains at each user
map = [R1*H1;R2*H2;R3*H3]*W;
inhibit = @(x)x.*(abs(x)>1e-15);
inhibit(real(map))+1i*inhibit(imag(map)) % display VC gains
```

**MATLAB output:**

```
>> ans =
    0.8615         0         0         0
         0         0         0    0.5441
         0    0.9473         0         0
         0         0    0.2772         0
    0.5077         0         0         0
         0    0.3203         0         0
         0         0    0.9608         0
         0         0         0    0.8390
```

Code 3.1 illustrates, in MATLAB script, the operations required to realize the mapping  $\Gamma_0$  of Fig. 3.2 by using PLM based on  $\Gamma_2$ .  $N = 6$  is assumed, and the excess antenna at  $\mathcal{U}_1$  is disregarded. The output ans on the MATLAB command line shows the VC-gains achieved for a single realization of i.i.d. Rayleigh faded MIMO channels. The correspondence of the non-zero entries of  $\Gamma_0$  (in Fig. 3.2) and the output confirms that the desired VC-to-User mapping is realized perfectly.

## 3.5 Conclusion

A two-phased, non-iterative, divide-and-conquer PLM scheme was proposed to implement an arbitrary VC-to-User mapping over a MIMO multi-user downlink. The scheme reduces a VC-to-User mapping into a set of non-overlapping sub-mappings, each represented by a multicast antenna group (MAG), such that the unicast and multicast VCs corresponding to these sub-mappings can be realized through non-iterative (intra-MAG) beamforming. The first phase, inter-MAG beamforming, uses a generalized form of BD to ensure the orthogonality of communications in different MAGs; the second phase, intra-MAG beamforming, realizes the VCs on top of the orthogonal effective channels produced by inter-MAG beamforming. Numerical results were provided to establish the viability of the proposed scheme for a sample VC-to-User mapping.

### **Future directions:**

- Only three candidate techniques were identified in Subsection 3.3.4 for intra-MAG beamforming. Non-iterative multi-user beamforming techniques that can realize more complicated sub-mappings (e.g., involving three users) still need to be developed.
- A comparison of the proposed approach with iterative PLM techniques is also of interest. The SER and sum-rate could be used as performance measures; the results would more definitively establish whether the proposed scheme is worth pursuing.
- The exact performance of the systems using the proposed scheme is mathematically tractable, at least for i.i.d. Rayleigh fading and with single-input multiple-output and SVD-based MIMO intra-MAG beamforming. Such analytic results are yet to be derived.

~

# Chapter 4

## Spatial Multipath Resolution

This chapter outlines spatial multipath resolution (SMR), a novel signal processing technique that exploits excess spatial degrees of freedom (DoFs) available at the receiver to combat multipath fading. SMR's pros and cons are highlighted by using applications with space time block codes (STBCs) and eigenmode transmission; the benefits of partial SMR and adaptive SMR are also highlighted.

### 4.1 Introduction

The inter-symbol interference (ISI) caused by frequency selective multipath fading (see Subsection 1.1.1) severely degrades the quality-of-service of multiple-input multiple-output (MIMO) wireless systems, especially at high data rates. The ISI is typically mitigated by using orthogonal frequency division multiplexing (OFDM) [9], the classic alternatives for which include time-domain equalization [14, Sec. 10.2], time-reversal [79], and maximum-likelihood sequence estimation [80]. In OFDM, the bandwidth is split into a number of narrowband subcarriers, each carrying data at a lower rate and thus avoiding the ISI. The latest wireless standards, including 3GPP LTE [38], WiGig [44], and WiMAX [39], use OFDM.

A MIMO receiver designed to meet certain minimal quality-of-services requirements could have spatial DoFs in excess to that required to meet the desired data rates and error rates under favorable channel conditions. Those 'excess' DoFs would remain unused, unless they are exploited for benefits other than diversity or multiplexing; SMR uses them to combat multipath fading.

SMR employs a unique rake receiver, which, unlike direct sequence code division multiple access receivers [81], which use code dimension, employs spatial signal processing (by using the space dimension) at the receiver fingers to extract the signal components received over individual paths. By appropriately delaying and then combining the extracted signal components, SMR transforms the received signal into an equivalent signal received over an effective MIMO channel undergoing flat fading. In other words, SMR *flattens* the effective MIMO channel, on top of which, MIMO channelization techniques (see Subsection 1.1.3), including eigenmode transmission [8] and STBCs [20], can be implemented. Thus, SMR can be considered as a single carrier alternative to OFDM. Moreover, it can supplement OFDM in, for example, the form of hybrid SMR–OFDM requiring fewer subcarriers than OFDM.

More specifically, SMR exploits the left nullspace of the MIMO channel taps to extract the multipath signal components, provided that the receiver has sufficiently more spatial DoFs than the transmitter. Consequently, perfect SMR requires the receiver to have as many antennas as the number of antennas at the transmitter multiplied by the number of multipaths. However, as demonstrated in Section 4.4, even *partial* SMR, i.e., resolving a smaller set of strongest multipath components by using a feasibly lesser number of receiver antennas, could significantly suppress the ISI.

Reference [49] proposes SMR, examines its performance with MIMO eigenmode transmission, and highlights the benefits of partial SMR. There, the transmit beamforming matrix  $\mathbf{W}$  and a set of receiver beamforming matrices  $\mathbf{R}_l$ s are jointly computed such that the  $\mathbf{R}_l$ s resolve the multipath signals, and along with  $\mathbf{W}$ , combining the appropriately delayed resolved signals yields orthogonal virtual channels (VCs) over a flattened effective MIMO channel.

In [48], the potential of MIMO STBC–SMR configurations and the benefits of *adaptive* SMR, i.e., adjusting the extent of partial SMR based on the channel state, are highlighted. The Alamouti code [82], which is the simplest of the STBCs and is used in wireless standards including the IEEE 802.11n [83] standard, is considered in [48]. With STBCs, only the combiner weights  $\mathbf{R}_l$ s need to be computed. There-

fore, unlike eigenmode transmission, the STBCs do not require transmit channel-state information (CSI); neither does SMR. This fact, along with the observation that having more antennas at the receiver is preferred with the STBCs<sup>1</sup> as well as the SMR, makes SMR more appealing with STBCs than with eigenmode transmission. Moreover, since SMR does not affect the STBC transmitter processing, the receiver may employ adaptive SMR without coordinating with the transmitter by using, for example, the error rate (determined by using an error-detection code), as a criterion for adaption.

**The chapter is organized as follows:** Section 4.2 details the system model of a MIMO STBC–SMR configuration and explains how SMR signal processing reduces the signal received over a multipath MIMO channel to that corresponding to the same STBC over a flattened effective MIMO channel. The symbol error rate (SER) simulation results are presented in Section 4.4 for the Alamouti STBC scheme, and the use of the practical multipath MIMO channel model outlined in Section 4.3 is assumed. The trade-off between the ISI reduction and diversity loss due to SMR is thereby examined; the prospects of adaptive SMR are also highlighted. Section 4.5 briefly summarizes eigenmode transmission with SMR [49]. The conclusion follows in Section 4.6.

## 4.2 Signal Processing

### 4.2.1 STBC over Multipath MIMO

Assumptions: Perfect CSI at the receiver (Transmit CSI is required only with beamforming) and block fading.

Consider a multipath MIMO channel given by

$$\mathbf{H}(k) = \sum_{l=0}^{L-1} \mathbf{H}_l \delta(k - \tau_l), \quad (4.1)$$

where  $L$  is the channel length, and  $\mathbf{H}_l \in \mathbb{C}^{N_r \times N_t}$  represents the channel matrix tap of the  $l^{\text{th}}$  strongest multipath component, such that  $\|\mathbf{H}_k\|_F \geq \|\mathbf{H}_l\|_F$  for  $k < l$  and

---

<sup>1</sup> For instance, the maximum achievable rate of orthogonal STBCs, given by  $1/2 + 1/n$  [84], where  $n = 2 \lceil N_t/2 \rceil$ , diminishes with the increasing number of transmit antennas  $N_t$ ; the diversity order of the STBCs improves linearly with the number of receiver antennas.

$k, l \in \{0, \dots, L-1\}$ . Let  $\tau_l$  be the corresponding discretized delay in time units, each equal to a symbol duration. Define  $m = \arg \min_l (\tau_l)$ . Conventionally,  $\mathbf{H}_0$  is deemed the desired path, and the others, the interfering paths.

Suppose a symbol vector  $\mathbf{S}^{(k)} \in \mathbb{C}^{N_s \times 1}$  is transmitted once every  $T$  time units, i.e., during the time units  $kT$  through  $((k+1)T-1)$  for  $k \geq 0$ , in the form of space time blocks  $\mathbf{X}^{(k)} \in \mathbb{C}^{N_t \times T}$ . The rate of the code is  $N_s/T$ . Denote by  $\mathbf{x}^{(j)} \in \mathbb{C}^{N_t \times 1}$  for  $j \geq 0$  the sub-block of space time coded symbols transmitted during the  $j^{\text{th}}$  time instance. Thus, we have  $\mathbf{X}^{(k)} = (\mathbf{x}^{(kT)} \mathbf{x}^{(kT+1)} \dots \mathbf{x}^{((k+1)T-1)})$  for  $k \geq 0$ .

Therefore, the sub-block of received symbols at the point of the first reception of a replica of  $\mathbf{x}^{(j)}$  is given by

$$\mathbf{y}^{(j)} = \sum_{l=0}^{L-1} \mathbf{H}_l \mathbf{x}^{(j-\tau_l+\tau_m)} + \mathbf{n}^{(j)}, \quad (4.2)$$

where  $\mathbf{n}^{(j)} \in \mathbb{C}^{N_r \times 1}$  is the corresponding additive noise at the receiver. Note that  $\mathbf{y}^{(j)}$  lags the transmission of  $\mathbf{x}^{(j)}$  by  $\tau_m$  time units. The conventional STBC receiver processes the  $\mathbf{y}^{(j)}$ s corresponding to each transmitted  $\mathbf{X}^{(k)}$  in order to obtain the estimates of  $\mathbf{S}^{(k)}$ . The ISI is manifested as inter-space time block interference and intra-space time block interference, making symbol detection quite challenging.

## 4.2.2 Receiver Design

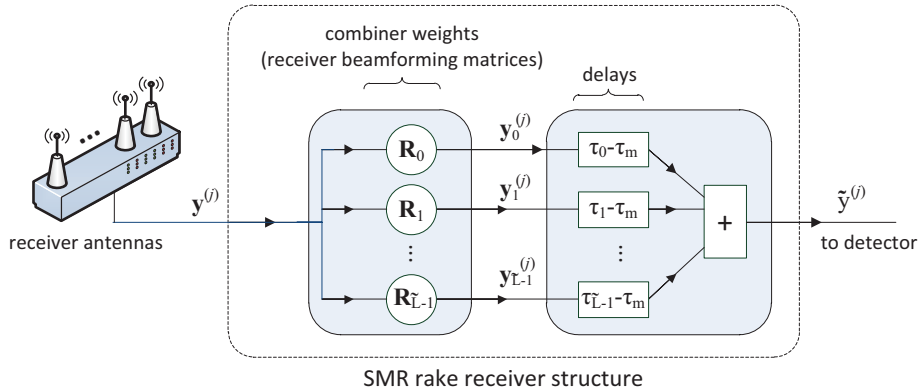


Figure 4.1: The basic rake receiver structure for SMR.

The proposed SMR rake receiver structure (Fig. 4.1) precedes STBC signal detection in the STBC-SMR receiver.

The matrices  $\mathbf{R}_l \in \mathbb{C}^{\hat{N}_r \times N_r}$ , defined as

$$\mathbf{R}_l \mathbf{H}_n = \mathbf{0}, \forall l \neq n \text{ and } \mathbf{R}_l \mathbf{H}_l \neq \mathbf{0}, \quad (4.3)$$

for  $l, n \in \{0, \dots, \tilde{L} - 1\}$ , represent the spatial signal processing for extracting the  $\tilde{L} \leq L$  strongest multipath components. The  $\mathbf{R}_l$ s also include the combiner weights (described in page 59); the *effective* number  $\hat{N}_r$  of receiver antennas after SMR depends on the choice of the combiner weights  $\mathbf{C}_l$ s.

Each thus extracted  $l^{\text{th}}$  path signal is given by  $\mathbf{y}_l^{(j)} = \mathbf{R}_l \mathbf{y}^{(j)}$ ; i.e.,

$$\mathbf{y}_l^{(j)} = \mathbf{R}_l (\mathbf{H}_l \mathbf{x}^{(j-\tau_l+\tau_m)} + \mathbf{n}^{(j)}) + \underbrace{\mathbf{R}_l \sum_{k=\tilde{L}}^{L-1} \mathbf{H}_k \mathbf{x}^{(j-\tau_k+\tau_m)}}_{\text{residual ISI}}, \quad (4.4)$$

where  $m = \arg \min_{l \in \{0, \dots, \tilde{L}-1\}} (\tau_l)$ .

The extracted signals are delayed, each  $\mathbf{y}_l^{(j)}$  by  $(\tau_l - \tau_m)$  time units, and then combined as in (4.5) to form a set of ISI reduced symbols  $\tilde{\mathbf{y}}^{(j)}$  corresponding to a single  $\mathbf{x}^{(j)}$ .

$$\begin{aligned} \tilde{\mathbf{y}}^{(j)} &= \sum_{l=0}^{\tilde{L}-1} \mathbf{y}_l^{(j+\tau_l-\tau_m)} & (4.5) \\ &= \underbrace{\sum_{l=0}^{\tilde{L}-1} \mathbf{R}_l \mathbf{H}_l \cdot \mathbf{x}^{(j)}}_{\mathbf{H}_{\text{eff}}} + \underbrace{\sum_{l=0}^{\tilde{L}-1} \mathbf{R}_l \mathbf{n}^{(j+\tau_l-\tau_m)}}_{\tilde{\mathbf{n}}^{(j)}} + \underbrace{\sum_{l=0}^{\tilde{L}-1} \sum_{k=\tilde{L}}^{L-1} \mathbf{R}_l \mathbf{H}_k \mathbf{x}^{(j-\tau_k+\tau_l)}}_{\text{residual ISI}} & (4.6) \end{aligned}$$

Note that the elimination of the residual ISI from (4.6) requires choosing  $\tilde{L} = L$ . However, the numerical results (see Section 4.4) indicate that even smaller  $\tilde{L}$ s eliminate a significant portion of the ISI.

$\mathbf{H}_{\text{eff}} \in \mathbb{C}^{\hat{N}_r \times N_t}$  in (4.6) is the flattened effective MIMO channel. Therefore, the space time block  $\mathbf{Y}^{(k)} = (\tilde{\mathbf{y}}^{(kT)} \tilde{\mathbf{y}}^{(kT+1)} \dots \tilde{\mathbf{y}}^{((k+1)T-1)})$  for  $k \geq 0$  represents the received signal corresponding to an input signal  $\mathbf{X}^{(k)}$  and an effective channel  $\mathbf{H}_{\text{eff}}$ . Thus, we have

$$\mathbf{Y}^{(k)} = \mathbf{H}_{\text{eff}} \mathbf{X}^{(k)} + \mathbf{N}^{(k)} + \text{residual ISI}, \quad (4.7)$$

where  $\mathbf{N}^{(k)} = (\tilde{\mathbf{n}}^{(kT)} \tilde{\mathbf{n}}^{(kT+1)} \dots \tilde{\mathbf{n}}^{((k+1)T-1)})$  is the effective additive noise.

Each  $\mathbf{R}_l$  can be found to satisfy (4.3) provided that the receiver has a sufficient number of antennas. Let  $\tilde{\mathbf{H}}_l = (\mathbf{H}_0 \dots \mathbf{H}_{l-1} \mathbf{H}_{l+1} \dots \mathbf{H}_{\tilde{L}-1})$  for  $l \in \{0, \dots, \tilde{L}-1\}$ ;  $\tilde{\mathbf{H}}_l = \mathbf{U}_l \Sigma_l \mathbf{V}_l^H$  is its singular value decomposition (SVD), and  $m_l = \text{rank}(\tilde{\mathbf{H}}_l)$ . Define  $\tilde{\mathbf{U}}_l = (\{\mathbf{U}_l\}_{\mathcal{C}(m_l+1:N_r)}, \mathbf{0}_l)$ , where  $\mathbf{0}_l \in \mathbb{C}^{N_r \times m_l}$  is a zero matrix, and we have  $\tilde{\mathbf{U}}_l$  orthogonal to each  $\mathbf{H}_k$  for  $k \neq l$ . Then

$$\mathbf{R}_l = \mathbf{C}_l (\tilde{\mathbf{U}}_l)^H, \quad (4.8)$$

$l \in \{0, \dots, \tilde{L}-1\}$  satisfy the orthogonality requirement (4.3) for the arbitrary combiner weights, represented by matrices  $\mathbf{C}_l \in \mathbb{C}^{\hat{N}_r \times N_r}$ .

As demonstrated in Section 4.4, the choice of the  $\mathbf{C}_l$ s affects not just the SER performance, but even the diversity order. Three possibilities are outlined below.

- **Possibility 1:** Using  $\mathbf{I}_{N_r}$  as the combiner weights appears to be the simplest choice, but doing so causes the rows  $(N_r - m_l)$  and onwards of each  $\mathbf{R}_l$  to be zero, thus making  $\hat{N}_r = N_r - \min_l(m_l)$  and each  $\mathbf{C}_l = \{\mathbf{I}_{N_r}\}_{\mathcal{R}(1:\hat{N}_r)}$ . Note that this  $\hat{N}_r$  is the smallest possible.
- **Possibility 2:** Another possibility is using  $\mathbf{C}_l = \mathbf{P}_l$ , where each  $\mathbf{P}_l \in \mathbb{C}^{N_r \times N_r}$  is a randomly chosen permutation matrix [5, p.25].
- **Possibility 3:** Cascading the resolved paths is yet another possibility. Doing so makes  $\hat{N}_r = (\tilde{L} \cdot N_r) - \sum_{l=0}^{\tilde{L}-1} m_l$  and yields the best SERs. Corresponding  $\mathbf{C}_l$ s are of the form  $(\mathbf{0}_{l,1} \mathbf{I}_{N_r - m_l} \mathbf{0}_{l,2})^T$ , where each  $\mathbf{0}_{l,1}$  has  $\sum_{k=0}^{l-1} (N_r - m_k)$  zero columns, and each  $\mathbf{0}_{l,2}$ ,  $\sum_{k=l+1}^{\tilde{L}-1} (N_r - m_k)$  zero columns.  $\hat{N}_r$  could exceed  $N_r$ ; however, since  $\mathbf{R}_l$ s are correlated, this  $\hat{N}_r$  would not necessarily increase the MIMO diversity.

Note that all three possibilities above are forms of equal gain combining. Other forms of combining are also possible. Given (4.7), the estimation of  $\mathbf{X}^{(k)}$  (and then, of  $\mathbf{S}^{(k)}$ ) requires only conventional STBC signal detection.

### 4.3 Multipath MIMO Channel Model

The ‘Omni-Tx, Rx-15°, NICTA’ scenario of the IEEE 802.15.3c NLOS (CM4) multipath single-input single-output model [85, Sec. 6.2.2] is extended here for MIMO. This model assumes multiple clusters of scatterers that surround the transmitter while forming a small angle ( $< 15^\circ$ ) at the receiver, and multiple rays arriving at the receiver after being scattered at each of those clusters. Parameters including the number of clusters, number of rays per each cluster, inter-cluster/inter-ray arrival delays, and decay rates of the gains are modeled as random variables.

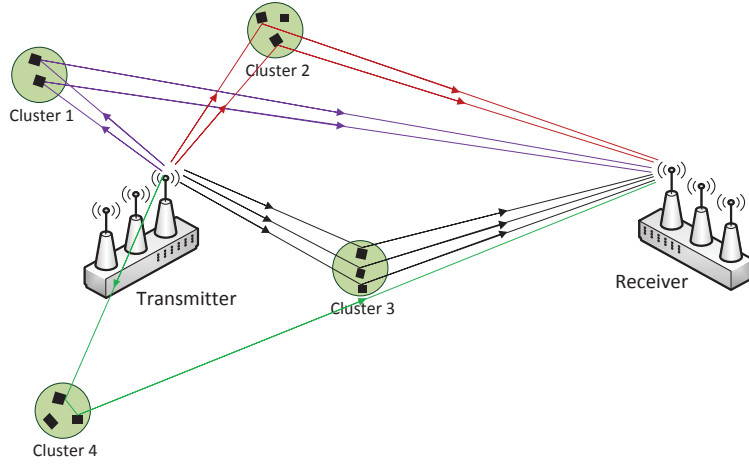


Figure 4.2: Ray-scattering in accordance to the multipath MIMO channel model in Section 4.3 and corresponding to the first transmit–receive antenna pair. Assumes four clusters, and for this specific antenna pair, 2, 2, 3, and 1 ray(s) scattering via the clusters 1 through 4, respectively.

The extension for MIMO is as follows (see Fig. 4.2). For a given channel realization, the scatterer clusters are assumed to be common to all transmit–receive antenna pairs; therefore, the inter-cluster parameters [85, Sec. 6.1] are considered common. The rays passing through each cluster, on the other hand, are assumed to be independent for each transmit–receive antenna pair. Thus, the intra-cluster parameters are independently instantiated for different transmit–receive antenna pairs. The resulting discrete multipath MIMO channel is normalized such that  $\sum_{l=0}^{L-1} \mathcal{E}\{\|H_l\|_F^2\} = 1$ . This extension should hold (approximately) where inter-antenna separation within the antenna arrays is significantly smaller than the distances between the transceivers and the scatterers. Note that  $L$ , the number of taps

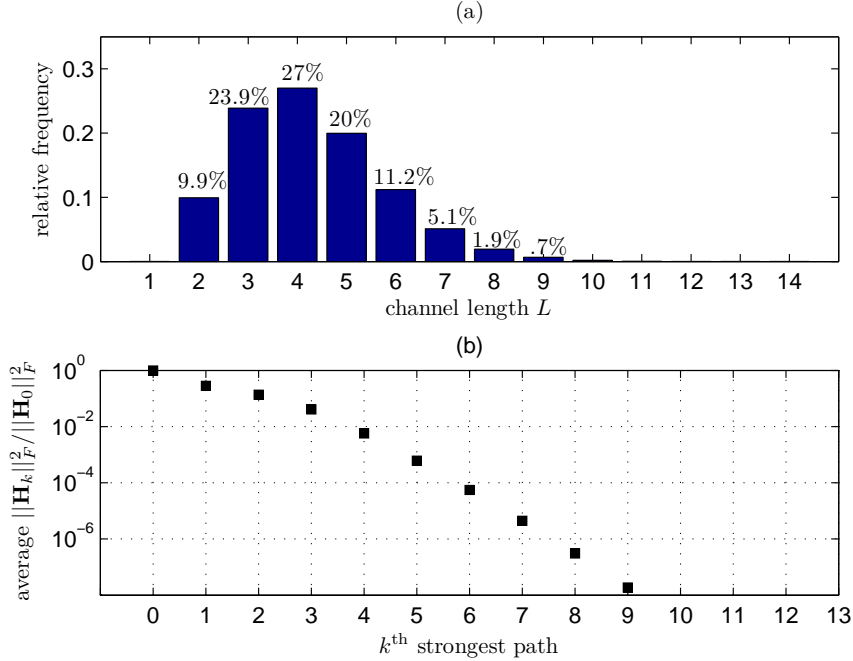


Figure 4.3: (a) Histogram of channel length  $L$  corresponding to a  $10 \times 2$  multipath MIMO channel. Mean length  $\mathcal{E}\{L\} = 4.25$ , and perfect SMR is possible for  $L \leq N_r/N_t = 5$  (i.e.,  $\approx 81\%$  the time). (b) Average relative strength  $\mathcal{E}\{\|\mathbf{H}_k\|_F^2 / \|\mathbf{H}_0\|_F^2\}$  of the  $k^{\text{th}}$  strongest multipath component.

in the multipath MIMO channel, varies between channel realizations. Fig. 4.3a gives the histogram of  $L$  for a  $10 \times 2$  MIMO channel based on this model (the model parameters are those assumed in Section 4.4).

Remark:

- The choice of the above channel model for this work is arbitrary; SMR is feasible irrespective of the channel model, provided that the receiver has sufficient DoFs.

## 4.4 Numerical Results (for STBC–SMR)

This section investigates the SER performance of SMR with STBCs by using Monte Carlo simulation. The Alamouti scheme [82], which has  $N_t = N_s = T = 2$  and

$$\mathbf{X}^{(k)} = \begin{pmatrix} \mathbf{s}_1^{(k)} & \mathbf{s}_2^{(k)*} \\ \mathbf{s}_2^{(k)} & -\mathbf{s}_1^{(k)*} \end{pmatrix}, \quad \text{where} \quad \mathbf{S}^{(k)} = \begin{pmatrix} s_1^{(k)} \\ s_2^{(k)} \end{pmatrix}, \quad (4.9)$$

is used for the purpose.

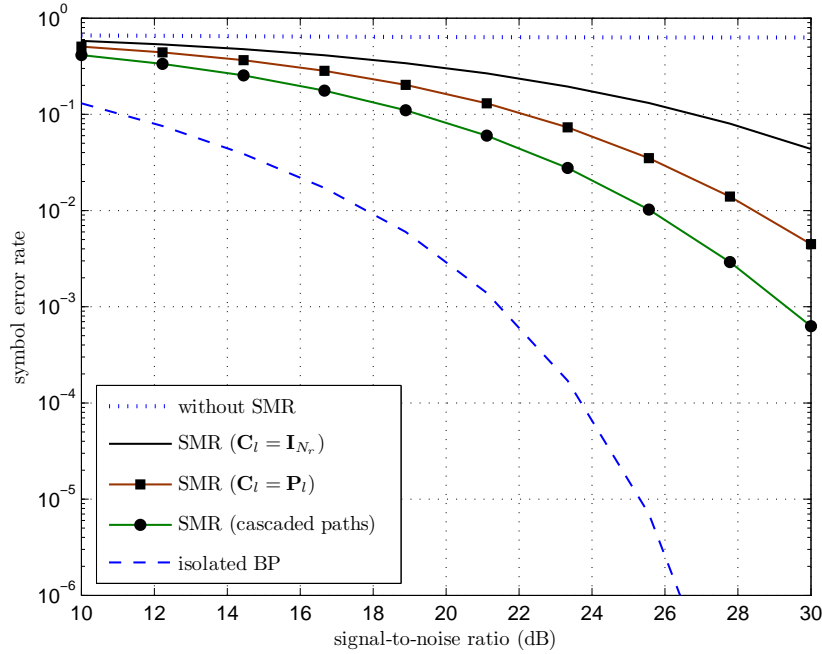


Figure 4.4: The SERs of SMR with STBC for  $N_r = 10$  and Alamouti code. The curves are shown for the cases (i) best path without SMR (dotted), (ii) SMR with  $C_l = I_{N_r}$  (solid), (iii) SMR with random permutation matrix  $P_l$  as  $C_l$  (solid, with ■ markers), (iv) SMR with cascaded resolved paths (solid, with ● markers), and (v) isolated best path (dashed). QPSK modulation is used.

Assumptions:  $10^6$  realizations of an  $N_r \times 2$  MIMO channel (based on the multipath channel model in Section 4.3) are simulated. The simulation parameters are those given under ‘Omni-Tx, Rx-15°, NICTA’ in [85, Table 4]; the shadowing effect, and hence, the parameters  $\sigma_c$  and  $\sigma_r$  therein are disregarded. Average numbers of 6 clusters and 6 rays per cluster are assumed. Unit receiver antenna gains are assumed irrespective of the angle of arrival; therefore, the angle spread  $\sigma_\phi$  in the model is irrelevant. Moreover, block fading with 100 quadrature phase shift keying (QPSK) modulated symbol pairs  $(s_1^{(k)}, s_2^{(k)})$  transmitted per each channel realization and perfect CSI are assumed. The symbol duration is 25 ns.

- Fig. 4.4 assumes  $N_r = 10$ . The dotted curve corresponds to conventional STBC decoding (i.e., decoding without SMR), which ignores multipath interference; detection fails utterly owing to the ISI, with SERs exceeding 60%

irrespective of the transmit signal to noise ratio (SNR). The dashed line represents conventional STBC reception of the best path disregarding the interfering paths; it provides an unachievable lower bound on the SER for performance comparison. (It fares the best because all receiver antennas contribute to MIMO diversity; moreover, sorting the paths by strength adds selection diversity.)

The solid lines correspond to (partial) SMR schemes attempting to resolve as many best paths as possible (up to a maximum of  $N_r/N_t = 5$  paths). The poor error performance and the loss of diversity correspond to spending spatial DoFs to resolve the paths. The choice of combiner weights  $\mathbf{C}_l$ s affects the performance significantly: cascading the resolved paths performs the best; randomly permuted  $\mathbf{C}_l$ s also outperform the use of  $\mathbf{C}_l = \mathbf{I}_{N_r}$ . The relative merits of the three combining possibilities can be explained in terms of the different  $\hat{N}_r$ s they yield. Error-floors are not observed because all paths are resolved  $\approx 81\%$  of the time, and the strongest disregarded path is on average about 30 dB weaker than the best path (Fig. 4.3b).

- Fig. 4.5 corresponds to the same simulation set-up as in Fig. 4.4, except that the channel length  $L$  is assumed to be at most 4 to guarantee perfect SMR. The SER performances of the three aforementioned combining possibilities are compared<sup>2</sup> here for the cases  $N_r = 10$  and  $N_r = 12$ . For the case  $N_r = 10$ , the relative merits observed in Fig. 4.4 prevail, with cascaded resolved paths producing the best performance. However, lower SERs are observed because the best path is stronger and the number of interfering paths is lower than before ( $\approx 19\%$  of the time). The SERs for the case  $N_r = 12$  are lower than those for  $N_r = 10$ . This result agrees with the intuition that having higher receiver DoFs is better than having lower ones.
- Since each multipath resolved reduces the effective number of receiver antennas by  $N_t = 2$ , thus limiting the MIMO diversity, it is not always desirable to resolve as many paths as possible. This premise is examined in Fig. 4.6

---

<sup>2</sup> Since the MIMO taps produced by the channel model do not scale linearly with  $N_r$ , the cases  $N_r = 10$  and  $N_r = 12$  are not strictly comparable. Nevertheless, qualitative comparison is warranted.

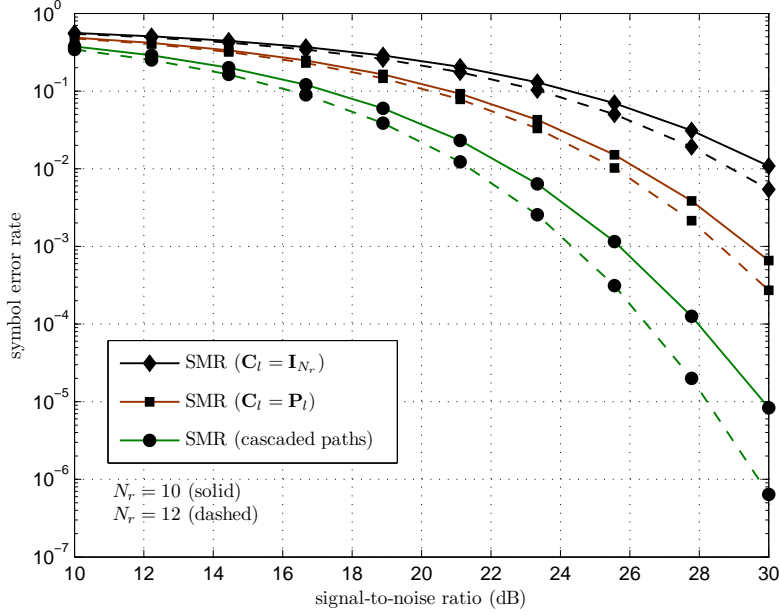


Figure 4.5: The SERs of SMR with STBC for Alamouti code and the cases  $N_r = 10$  (solid) and  $N_r = 12$  (dashed). The channel length is constrained not to exceed 4. The curves are shown for the cases: (i) SMR with  $C_l = \mathbf{I}_{N_r}$  (with  $\blacklozenge$  markers), (ii) SMR with random permutation matrix  $P_l$  as  $C_l$  (with  $\blacksquare$  markers), and (iii) SMR with cascaded resolved paths (with  $\bullet$  markers). QPSK modulation is used.

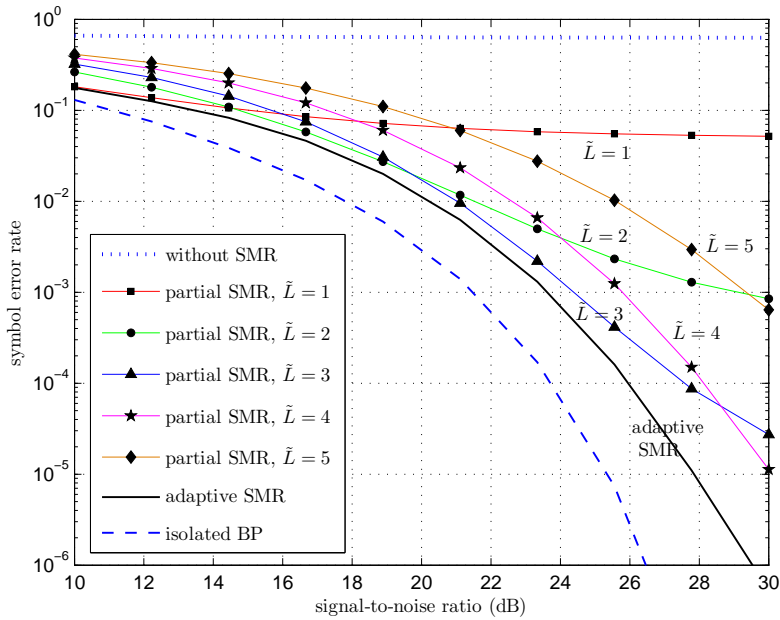


Figure 4.6: The SERs of partial and adaptive SMR with STBC for  $N_r = 10$  and Alamouti code. The curves are shown for the cases (i) best path without SMR (dotted), (ii) partial SMR, considering  $\tilde{L} \in \{1, \dots, 5\}$  paths (solid, with markers), (iii) adaptive SMR (solid, without markers), and (iii) isolated best path (dashed). QPSK modulation is used.

for the same simulation set-up as in Fig. 4.4. The solid curves with markers correspond to partial SMR resolving at most  $\tilde{L} \in \{1, \dots, N_r/N_t\}$  strongest paths. Note that, for a given curve,  $\tilde{L}$  is held fixed for all channel realizations. Resolving fewer paths (e.g.,  $\tilde{L} = 1, 2$ ) seems prudent at low SNRs, where additive noise dominates the interference, but the performance yields to residual interference as the SNR improves. Moreover, an optimal fixed  $\tilde{L}$  seems to exist ( $\tilde{L} = 4$ , in this case) at high SNRs, highlighting the conflicting effects of multipath and MIMO diversity in SMR.

Adapting  $\tilde{L}$  based on the instantaneous CSI, i.e., determining the optimal  $\tilde{L}$  every time the channel varies (and  $\mathbf{R}_l$ s are recomputed), results in even better error performance. The corresponding error performance (depicted by the solid curve without markers) is better than that of partial SMR based on *any* fixed  $\tilde{L}$  value. Adaptive SMR can be implemented by using error-detection codes for assessing the SER; however, a practicable algorithm for adapting  $\tilde{L}$  is not yet available.

## 4.5 Eigenmode Transmission with SMR

This section briefly outlines MIMO eigenmode transmission over SMR (see [49] for details). Here, the  $\mathbf{R}_l$ s are computed jointly with a transmit beamforming matrix  $\mathbf{W}$  such that

$$\mathbf{W} = \{\mathbf{V}\}_{\mathcal{C}(1:n)} \text{ and} \quad (4.10)$$

$$\mathbf{R}_l = \{\boldsymbol{\Sigma}\}_{\mathcal{D}(1:n)}^{-1} \left( \{\mathbf{U}\}_{\mathcal{C}(1:n)} \right)^H \mathbf{C}_l \left( \tilde{\mathbf{U}}_l \right)^H \text{ for } l \in \{0, \dots, \tilde{L}-1\}, \quad (4.11)$$

where  $\mathbf{H}_{\text{eff}} = \mathbf{U}\boldsymbol{\Sigma}\mathbf{V}^H$  is the SVD of  $\mathbf{H}_{\text{eff}}$  in (4.7), and  $n \leq \text{rank}(\mathbf{H}_{\text{eff}})$  is the number of VCs that needs to be realized.  $\mathbf{C}_l$  and  $\tilde{\mathbf{U}}_l$  are the same as in (4.8). Consequently, transmit CSI (or equivalently, feeding back  $\mathbf{W}$  computed at the receiver) becomes necessary, making adaptive SMR more challenging.

Fig. 4.7 depicts the SER performance of a  $10 \times 3$  MIMO configuration supporting three VCs,  $\text{VC}_k$  for  $k \in \{1, 2, 3\}$ , through eigenmode transmission. The multipath MIMO model and the assumptions are the same as in Section 4.4. Eigenmode

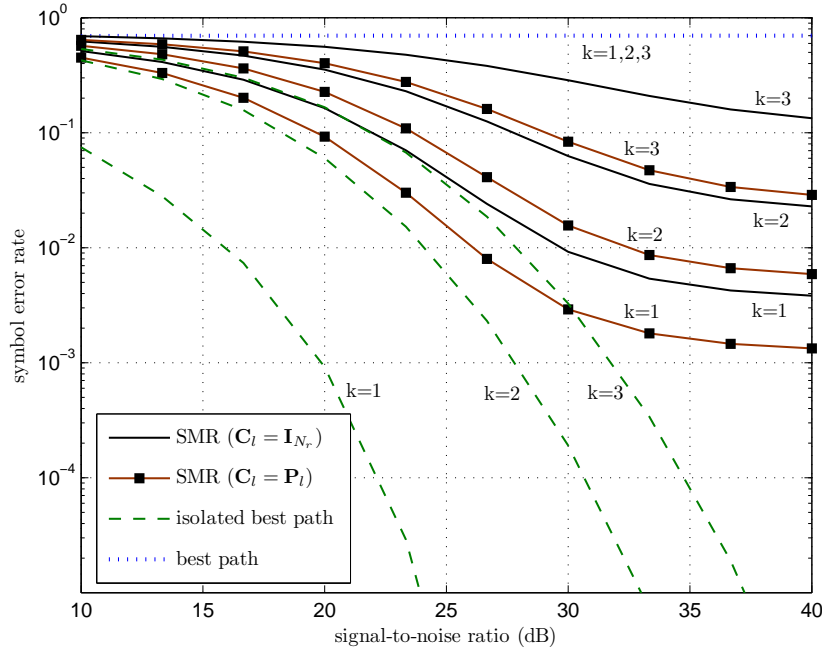


Figure 4.7: The SERs of  $VC_k$ ,  $k \in \{1, 2, 3\}$  in SMR with eigenmode transmission for  $N_t = 3$ ,  $N_r = 10$ , and  $n = 3$ . The curves are shown for the cases (i) SMR with  $C_l = \mathbf{I}_{N_r}$  (solid, without markers), (ii) SMR with random permutation matrix  $\mathbf{P}_l$  as  $C_l$  (solid, with markers), (iii) isolated best path (dashed), and (iv) best path (dotted). QPSK modulation is used.

transmission over the best path (corresponding to the dotted lines) becomes futile; the SER does not improve even at high SNRs. The dashed lines correspond to selecting the best path while assuming no multipath interference exists; they provide a hypothetical unachievable lower bound on the SERs for comparison purposes. The solid SER curves, corresponding to SMR, improve initially with the SNR but level off at high SNR, indicating that perfect multipath interference cancellation is impossible. This observation is as expected, since an average channel length of 4.27 could be observed [49], with more than the resolvable  $\lfloor (N_r - n)/N_t \rfloor + 1 = 3$  channel taps existing 66.21% of the time. This result shows that SMR is not very effective when the receiver does not have enough DoFs to resolve the strongest paths.

## 4.6 Conclusion

Spatial multipath resolution (SMR), a non-conventional use of spatial DoFs for mitigating multipath fading, was proposed. Unlike OFDM, SMR takes a single carrier approach, transforming the multipath MIMO channel into a flattened effective MIMO channel, on top of which any channelization scheme can be implemented. The SERs with MIMO STBC and eigenmode transmission were investigated to gain further insights into SMR. The trade-off between multipath and MIMO diversity was identified; partial and adaptive SMR were demonstrated as solutions.

### Future directions:

- Although SMR takes a single carrier approach, it could be used in hybrid SMR–OFDM configurations to reduce the number of subcarriers OFDM requires. This very promising approach should be investigated.
- Since SMR does not require transmit CSI, SMR is best used with channelization techniques not having that requirement, such as the STBCs. Moreover, the receiver can employ adaptive SMR transparent to the transmitter in such cases. Therefore, investigating similar channelization techniques such as spatial multiplexing (e.g., V-BLAST [86]) with SMR is of interest.
- The optimal choice of combiner weights  $C_l$ s also needs to be investigated.
- Capacity comparison with multi-carrier transmission too should be researched.

~

# Chapter 5

## Space Division Duplexing

This chapter investigates the error performance of multiple-input multiple-output (MIMO) eigenmode transmission alongside space division duplexing (SDD), i.e., the joint selection of beamforming matrices, to realize the virtual channels (VCs) while eliminating the self-interference. This chapter also highlights, through simulation, the implications of practical issues, including finite computational precision, finite analog-to-digital converter (ADC) resolution, and channel-estimation errors.

### 5.1 Introduction

Duplexing techniques exploit the degrees of freedom (DoFs) available in the time, frequency, or other suitable dimensions to facilitate simultaneous transmission and reception of data at a wireless terminal. Frequency division duplexing and time division duplexing techniques have been proven to be effective, and their applications are ubiquitous. Since the radio spectrum usually has a price-tag, and the extent and duration of its use (respectively associated with the frequency and time dimensions) also dictate how many wireless systems may coexist in a neighborhood, the DoFs in the time and frequency dimensions have an operational cost. Therefore, the frequency division duplexing and time division duplexing techniques, which split those DoFs between the transmit and receive directions, have half the spectral efficiency and cost-effectiveness of the alternative techniques using other dimensions (e.g., space and polarization) to achieve duplexing. Quantifying and addressing the practical challenges that presently preclude such alternatives are, therefore, of great

importance. This chapter investigates SDD in this context.

With SDD, the wireless terminals transmit and receive at the same time, using spatial signal processing to suppress the *self-interference* that the transmission causes on signal reception (and detection). SDD has been attempted with single-antenna systems [87, 88], but only with multiple antennas and MIMO signal processing can the terminals exploit the spatial DoFs to suppress the interference. Duplex MIMO repeaters [89] and relays [90–92] are already receiving attention, evidently because of the relaying’s potential for extending the coverage of existing/emerging MIMO compliant cellular and wireless data networks.

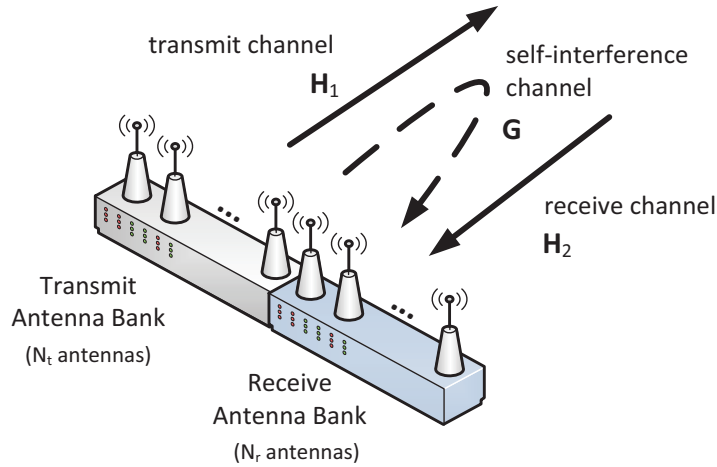


Figure 5.1: A MIMO terminal using SDD.

Even in a MIMO terminal using SDD (Fig. 5.1), a given antenna may not transmit and receive simultaneously over the same frequency band. Therefore, the antennas are partitioned to form two antenna banks dedicated, respectively, to transmission and reception (e.g.,  $N_t$  transmit antennas and  $N_r$  receive antennas); the excess DoFs at either bank [50, 90, 93] or the orthogonality of the spatial modes [94] can be used to mitigate the self-interference. Thus, SDD resembles near-end crosstalk cancellation in digital subscriber lines [95]. However, unlike the physical wire-pairs in a digital subscriber line, the VCs in a MIMO wireless system arise as a result of beamforming (see Subsection 1.1.4), making SDD more challenging than crosstalk cancellation. Moreover, the high signal attenuation in radio propagation creates significant practical challenges in the form of high amplifier dynamic range and ADC

resolution requirements, among others. Despite these challenges, new experimental evidence [50] demonstrating over 45 dB of self-interference suppression indicates the viability of SDD for, at least, short-range wireless systems such as the personal area networks.

**The chapter is organized as follows:** Section 5.2 outlines the signal processing involved, firstly for SDD, then for eigenmode transmission alongside it. The numerical results on the symbol error rate (SER) performance of selected MIMO SDD configurations are provided in Section 5.3; the detrimental effects of finite computational precision and finite ADC resolution on the SER are demonstrated. The conclusion follows in Section 5.4.

## 5.2 Signal Processing

### 5.2.1 Transmit vs. Receive SDD

Consider the singular value decomposition (SVD)  $\mathbf{G} = \mathbf{U}\mathbf{\Sigma}\mathbf{V}^H$  of a matrix  $\mathbf{G} \in \mathbb{C}^{m \times n}$ , where  $\mathbf{\Sigma} \in \mathbb{C}^{m \times n}$  is rectangular diagonal, and  $\mathbf{U} \in \mathbb{C}^{m \times m}$  and  $\mathbf{V} \in \mathbb{C}^{n \times n}$  are unitary. Let  $r = \text{rank}(\mathbf{G})$ . Whenever  $\mathbf{G}$  does not have full column-rank (i.e.,  $r < n$ ), the columns of  $\mathbf{V}^{(0)} = \{\mathbf{V}\}_{\mathcal{C}(r+1:n)}$  span the nullspace  $\text{Null}(\mathbf{G})$  such that  $\mathbf{G}\mathbf{V}^{(0)} = \mathbf{0} \in \mathbb{C}^{m \times (n-r)}$ . Similarly, the left nullspace  $\text{Null}(\mathbf{G}^T)$  is spanned by the columns of  $\mathbf{U}^{(0)} = \{\mathbf{U}\}_{\mathcal{C}(r+1:m)}$  such that  $(\mathbf{U}^{(0)})^H \mathbf{G} = \mathbf{0} \in \mathbb{C}^{(m-r) \times n}$ , if  $\mathbf{G}$  does not have full row-rank (i.e.,  $r < m$ ). The nullspace and the left nullspace exist simultaneously if  $\mathbf{G}$  is rank deficient — i.e.,  $r < \min(m, n)$ .

Suppose  $\mathbf{G}$  corresponds to the self-interference channel of a MIMO terminal using SDD (Fig. 5.1). Given a symbol vector  $\mathbf{x} \in \mathbb{C}^{n \times 1}$  to be transmitted, the self-interference component at the detector input is given by  $\mathbf{R}\mathbf{G}\mathbf{W}\mathbf{x}$ , where  $\mathbf{W} \in \mathbb{C}^{N_T \times n}$  and  $\mathbf{R} \in \mathbb{C}^{n \times N_R}$ , respectively, denote the transmit and receive signal processing (at the corresponding antenna banks). The self-interference can be nullified irrespective of  $\mathbf{x}$ , if either of the constraints

$$\mathbf{G} \cdot \mathbf{W} = \mathbf{0}, \text{ or} \tag{5.1a}$$

$$\mathbf{R} \cdot \mathbf{G} = \mathbf{0} \tag{5.1b}$$

can be enforced. The constraints (5.1a) and (5.1b) indicate three possibilities for implementing SDD at a terminal.

- **Transmit SDD:** Forming (the leftmost factor of)  $\mathbf{W}$  with columns of  $\mathbf{V}^{(0)}$  enforces (5.1a), and forces the transmitted signal  $\mathbf{W}\mathbf{x}$  to be orthogonal to  $\mathbf{G}$ . Since this approach requires  $\mathbf{G}$  to not have full-column rank, assigning more antennas for transmission than for reception is a sufficient condition to achieve Transmit SDD.
- **Receive SDD:** Likewise, forming (the rightmost factor of)  $\mathbf{R}$  by using rows of  $(\mathbf{U}^{(0)})^H$  enforces (5.1b), causing only the desired signal orthogonal to the row space of  $\mathbf{G}$  to be extracted. This approach requires  $\mathbf{G}$  to not have full-row rank. This condition is guaranteed if the majority of antennas are set aside for reception.
- **Joint Transmit and Receive SDD:** Simultaneously enforcing both (5.1a) and (5.1b), as in reference [90], requires  $\mathbf{G}$  to be rank-deficient. This result may be achieved only through proper antenna design and placement (e.g., by arranging the antenna banks such that a key-hole channel exists between them).

Since  $\mathbf{G}$  is not bidirectional, ‘Joint Transmit and Receive SDD’ appears redundant. Moreover, that approach complicates the computation of beamforming matrices for implementing VCs between two nodes employing SDD. Hence, only Transmit SDD and Receive SDD are hereafter considered; either scheme can be employed provided the appropriate antenna bank is assigned the greater number of antennas.

### 5.2.2 Eigenmode Transmission with SDD

Consider two MIMO terminals  $\mathcal{U}_i$  for  $i \in \{1, 2\}$  employing SDD (Fig. 5.2). Each  $\mathcal{U}_i$  has  $M_i$  antennas assigned to its transmit antenna bank, and  $N_i$ , to its receive antenna bank. (Note that the antennas in a given bank need not be physically adjacent.) Let the MIMO channel  $\mathcal{U}_i \rightarrow \mathcal{U}_{(3-i)}$ , existing between the transmit antenna bank of  $\mathcal{U}_i$  and the receive antenna bank of  $\mathcal{U}_{(3-i)}$ , be  $\mathbf{H}_i \in \mathbb{C}^{N_{(3-i)} \times M_i}$  for  $i \in \{1, 2\}$  and

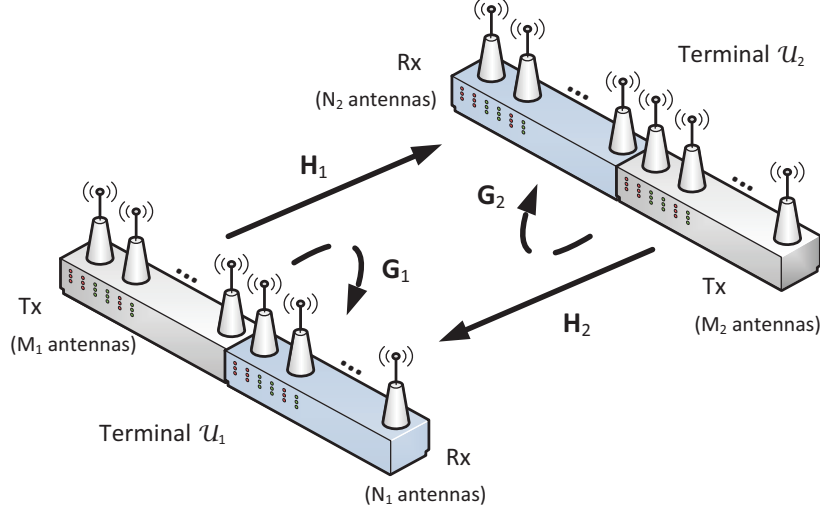


Figure 5.2: Eigenmode transmission alongside MIMO SDD.

the self-interference MIMO channel between the transmit–receive antenna banks of each  $\mathcal{U}_i$  be  $\mathbf{G}_i \in \mathbb{C}^{N_i \times M_i}$ . The  $\mathbf{G}_i$ s may or may not be rank-deficient. (Any rank deficiency would lower the spatial DoFs SDD costs.)

Suppose  $s_i$  VCs,  $\text{VC}_k$  for  $k \in \{1, \dots, s_i\}$ , need to be realized through eigenmode transmission from each  $\mathcal{U}_i$  to  $\mathcal{U}_{(3-i)}$ . Thus, the corresponding transmit and receiver beamforming matrices at each  $\mathcal{U}_i$  are  $\mathbf{W}_i \in \mathbb{C}^{M_i \times s_i}$  and  $\mathbf{R}_i \in \mathbb{C}^{s_{(3-i)} \times N_i}$  for  $i \in \{1, 2\}$ . Given a symbol vector  $\mathbf{x}_i \in \mathbb{C}^{s_i \times 1}$  precoded and transmitted from each  $\mathcal{U}_i$ , the signal  $\mathbf{y}_i \in \mathbb{C}^{s_{(3-i)} \times 1}$  fed to the signal detector of  $\mathcal{U}_i$  is given by

$$\mathbf{y}_i = \mathbf{R}_i (\mathbf{H}_j \mathbf{W}_j \mathbf{x}_j + \mathbf{G}_i \mathbf{W}_i \mathbf{x}_i + \mathbf{n}_i), \quad (5.2)$$

for  $i \in \{1, 2\}$  and  $j = (3 - i)$ .  $\mathbf{n}_i \in \mathbb{C}^{N_i \times 1}$  is the additive noise component of the received signal at  $\mathcal{U}_i$ . The term  $\mathbf{R}_i \mathbf{G}_i \mathbf{W}_i \mathbf{x}_i$  of (5.2) represents the self-interference after receiver processing.

Since the rank of a MIMO channel dictates the number of VCs it may support, the requirement

$$\text{rank}(\mathbf{H}_i) \geq s_i, \quad (5.3)$$

and either of the conditions

$$\text{nullity}(\mathbf{G}_i) \geq s_i \text{ or} \quad (5.4a)$$

$$\text{nullity}(\mathbf{G}_i^T) \geq s_{(3-i)} \quad (5.4b)$$

need to be satisfied for  $i \in \{1, 2\}$ .

Each terminal may exploit Transmit SDD or Receive SDD, thereby providing three possibilities:

- 1.) Transmit SDD implemented at both terminals,
- 2.) Receive SDD implemented at both terminals,
- 3.) Transmit SDD implemented at one terminal, and Receive SDD at the other.

### Case 1: Transmit SDD implemented at both terminals

Design requirements: A necessary, but not sufficient<sup>1</sup> condition for (5.3) is having  $N_{(3-i)} \geq s_i$ . The requirement (5.4a) can be met irrespective of rank ( $\mathbf{G}_i$ ) by ensuring that  $(M_i - N_i) \geq s_i$ . Where  $\mathbf{H}_i$ s are not rank-deficient, the requirements are satisfied for  $(M_i - s_i) \geq N_i \geq s_{(3-i)}$ .

**Example 5.1** Having  $M_i = 4$  and  $N_i = 2$ , for instance, guarantees two spatial modes in each direction, provided that  $\mathbf{H}_i, i \in \{1, 2\}$  are not keyhole channels. If communications were only from  $\mathcal{U}_1$  to  $\mathcal{U}_2$ , each terminal could have six VCs; but SDD yields only four VCs, two in each direction. Thus, SDD costs each terminal two spatial DoFs in terms of multiplexing gain. •

Beamforming matrices: Suppose the SVDs  $\mathbf{G}_i = \mathbf{U}_i \mathbf{\Sigma}_i \mathbf{V}_i^H$  hold for  $i \in \{1, 2\}$ . The columns of each  $\mathbf{V}_i^{(0)} = \{\mathbf{V}_i\}_{\mathcal{C}(\text{rank}(\mathbf{G}_i)+1:M_i)}$  span  $\text{Null}(\mathbf{G}_i)$ . Define<sup>2</sup>  $\hat{\mathbf{H}}_i = \mathbf{H}_i \mathbf{V}_i^{(0)}$  for  $i \in \{1, 2\}$ , and let their SVDs be  $\hat{\mathbf{H}}_i = \mathbf{Q}_i \mathbf{\Lambda}_i \mathbf{X}_i^H$ . The choice  $\mathbf{W}_i = \mathbf{V}_i^{(0)} \{\mathbf{X}_i\}_{\mathcal{C}(s_i)}$  and  $\mathbf{R}_{(3-i)} = \{\mathbf{Q}_i^H\}_{\mathcal{R}(s_i)}$  produces the VCs in both directions.

Remarks:

- The effective MIMO channel  $\hat{\mathbf{H}}_i$  is  $N_{(3-i)} \times \text{nullity}(\mathbf{G}_i)$ , and no longer  $N_{(3-i)} \times M_i$ , implying reduced diversity orders. The multiplexing gain is also reduced, since  $\text{rank}(\hat{\mathbf{H}}_i) \leq \min(\text{rank}(\mathbf{H}_i), \text{nullity}(\mathbf{G}_i))$ .

<sup>1</sup> Sufficient if  $\mathbf{H}_1$  and  $\mathbf{H}_2$  are not rank-deficient.

<sup>2</sup> Defining  $\hat{\mathbf{H}}_i = \mathbf{H}_i \{\mathbf{V}_i^{(0)}\}_{\mathcal{C}(s_i)}$  by using  $s_i$  columns from  $\mathbf{V}_i^{(0)}$  is also possible here; doing so would, however, yield lower diversity orders.

- Under Rayleigh fading, each  $\mathbf{H}_i$  is a complex Gaussian random matrix. Since  $\mathbf{V}_i$  is unitary,  $\hat{\mathbf{H}}_i$  will also be complex Gaussian irrespective of the distribution of  $\mathbf{G}_i$ s. Thus, the exact performance analysis of MIMO SDD under Rayleigh fading is straightforward.
- Channel estimation may be easily performed by, for example, time division duplexing the pilot signals, and estimating each  $\mathbf{G}_i, \mathbf{H}_i$  pair while  $\mathcal{U}_i$  transmits the pilots for  $i \in \{1, 2\}$ . Each  $\mathcal{U}_i$  should receive channel-state information (CSI) for  $\mathbf{H}_i$  from  $\mathcal{U}_{(3-i)}$ , compute  $\mathbf{W}_i$  and  $\mathbf{R}_{(3-i)}$  as outlined above, and convey  $\mathbf{R}_{(3-i)}$  and the gains  $\text{diag}(\mathbf{\Lambda}_i)$  back to  $\mathcal{U}_{(3-i)}$ .

### Case 2: Receive SDD implemented at both terminals

Design requirements: Where  $\mathbf{H}_i$ s are not rank-deficient, the requirements (5.3) and (5.4b) are satisfied for  $(N_i - s_{(3-i)}) \geq M_i \geq s_i$ .

Beamforming matrices : Suppose the SVDs  $\mathbf{G}_i = \mathbf{U}_i \mathbf{\Sigma}_i \mathbf{V}_i^H$  hold for  $i \in \{1, 2\}$ . Each  $\mathbf{U}_i^{(0)} = \{\mathbf{U}_i\}_{\mathcal{C}(\text{rank}(\mathbf{G}_i)+1:N_i)}$  would span  $\text{Null}(\mathbf{G}_i^T)$ . Define  $\hat{\mathbf{H}}_i = \left(\mathbf{U}_{(3-i)}^{(0)}\right)^H \mathbf{H}_i$  for  $i \in \{1, 2\}$ ; let their SVDs be  $\hat{\mathbf{H}}_i = \mathbf{Q}_i \mathbf{\Lambda}_i \mathbf{X}_i^H$ . The beamforming matrices  $\mathbf{W}_i = \{\mathbf{X}_i\}_{\mathcal{C}(s_i)}$  and  $\mathbf{R}_{(3-i)} = \left\{ \left(\mathbf{U}_{(3-i)}^{(0)} \mathbf{Q}_i\right)^H \right\}_{\mathcal{R}(s_i)}$  will yield the desired VCs.

Remarks:

- A loss of diversity and multiplexing gains occurs since the effective channel  $\hat{\mathbf{H}}_i$  is  $\text{nullity}(\mathbf{G}_{(3-i)}^T) \times M_i$  and  $\text{rank}(\hat{\mathbf{H}}_i) \leq \min(\text{rank}(\mathbf{H}_i), \text{nullity}(\mathbf{G}_{(3-i)}^T))$ .
- Interchanging the transmit–receive roles of each antenna transforms a Receive SDD configuration into a Transmit SDD configuration exhibiting equivalent SER performance, and vice versa. However, the implementation of Receive SDD appears simpler, because only the computed  $\mathbf{W}_i$ s need to be exchanged over the channel incurring an overhead.

### Case 3: Transmit SDD implemented at one terminal, Receive SDD at the other

Without a loss of generality, suppose that  $\mathcal{U}_1$  implements Transmit SDD while  $\mathcal{U}_2$  implements Receive SDD. The requirements (5.3), (5.4a), and (5.4b) are met if  $(M_1 - s_1) \geq N_1 \geq s_2$  and  $(N_2 - s_1) \geq M_2 \geq s_2$ . The effective channel for

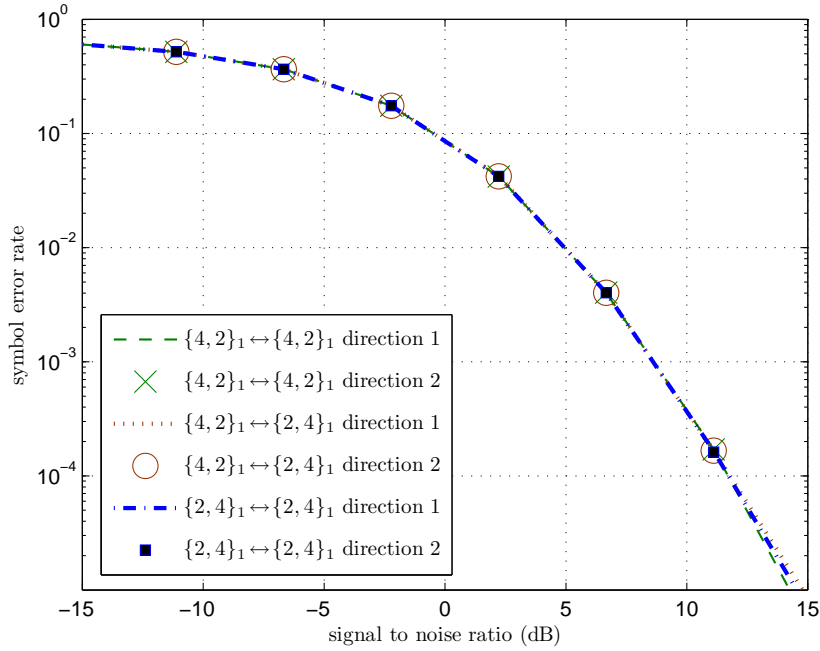


Figure 5.3: The SERs for VC<sub>1</sub> in either direction of  $\{M_1, N_1\}_1 \leftrightarrow \{M_2, N_2\}_1$  MIMO SDD configurations. The ‘direction  $i$ ’ is from  $\mathcal{U}_i$  to  $\mathcal{U}_{(3-i)}$  for  $i \in \{1, 2\}$ . QPSK modulation is used.

eigenmode transmission from  $\mathcal{U}_1$  to  $\mathcal{U}_2$  will be  $\hat{\mathbf{H}}_1 = \left(\mathbf{U}_2^{(0)}\right)^H \mathbf{H}_1 \mathbf{V}_1^{(0)}$ ; the channel  $\mathbf{H}_2$  can be used as it is in the other direction.

Remark:

- $\hat{\mathbf{H}}_1$  becomes  $\text{nullity}(\mathbf{G}_2^T) \times \text{nullity}(\mathbf{G}_1)$ , but  $\hat{\mathbf{H}}_2 = \mathbf{H}_2$  remains unchanged as  $N_1 \times M_2$  for the opposite direction.

### 5.3 Numerical Results

Denote by  $\{M_1, N_1\}_{s_1} \leftrightarrow \{M_2, N_2\}_{s_2}$  a MIMO configuration of terminals  $\mathcal{U}_1$  and  $\mathcal{U}_2$  (Fig. 5.2) supporting eigenmode transmission alongside SDD, such that  $M_i$  and  $N_i$  antennas are assigned, respectively, to the transmit and receive antenna banks of each  $\mathcal{U}_i$  for  $i \in \{1, 2\}$ , and  $s_i$  VCs are realized from  $\mathcal{U}_i$  to  $\mathcal{U}_{(3-i)}$ .

Fig. 5.3 depicts the SER of VC<sub>1</sub> in either direction, for the MIMO SDD configurations  $\{4, 2\}_1 \leftrightarrow \{4, 2\}_1$ ,  $\{4, 2\}_1 \leftrightarrow \{2, 4\}_1$ , and  $\{2, 4\}_1 \leftrightarrow \{2, 4\}_1$ .  $10^6$ -point Monte Carlo simulation is used.

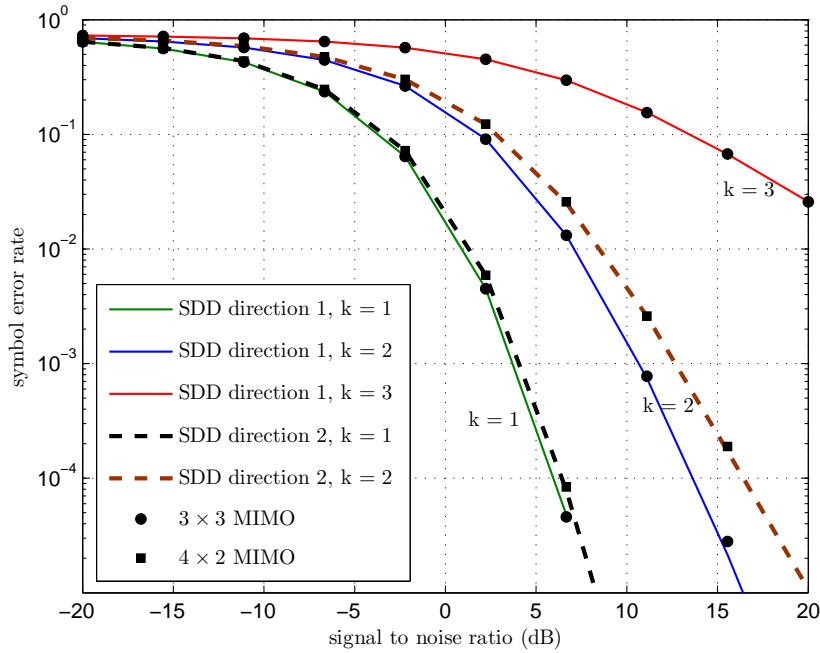


Figure 5.4: The SERs for each  $VC_k$  in either direction of the  $\{7, 4\}_3 \leftrightarrow \{5, 3\}_2$  MIMO SDD configuration. The ‘direction  $i$ ’ is from  $\mathcal{U}_i$  to  $\mathcal{U}_{(3-i)}$  for  $i \in \{1, 2\}$ . The SERs for VCs in  $3 \times 3$  MIMO ( $\bullet$ ) and  $4 \times 2$  MIMO ( $\blacksquare$ ) systems are shown for comparison. QPSK modulation is used.

Assumptions: Block fading with 10 quadrature phase shift keying (QPSK) modulated symbols per VC per channel realization. Independent and identically distributed (i.i.d.) Rayleigh faded  $\mathbf{H}_i$ s; the  $\mathbf{G}_i$ s are also i.i.d. Rayleigh faded but 100 dB stronger than the  $\mathbf{H}_i$ s.

All three configurations show an identical SER performance. This result is expected since the effective MIMO channel  $\hat{\mathbf{H}}_i$  in either direction is  $2 \times 2$  complex Gaussian for all three cases. This observation implies that the choice between Transmit SDD and Receive SDD does not affect the SER performance.

For the  $\{7, 4\}_3 \leftrightarrow \{5, 3\}_2$  MIMO SDD configuration, Fig. 5.4 illustrates more clearly the diversity and multiplexing gain reduction caused by SDD. (The assumptions are the same as for Fig. 5.3.) The VCs from  $\mathcal{U}_1$  to  $\mathcal{U}_2$  exhibit SERs identical to that of a  $3 \times 3$  MIMO channel; the opposite direction resembles a  $4 \times 2$  MIMO channel. This observation confirms the premise that each  $\hat{\mathbf{H}}_i$ , although of reduced dimensionality  $N_{(3-i)} \times \text{nullity}(G_i)$ , represents i.i.d. Rayleigh fading (just as the

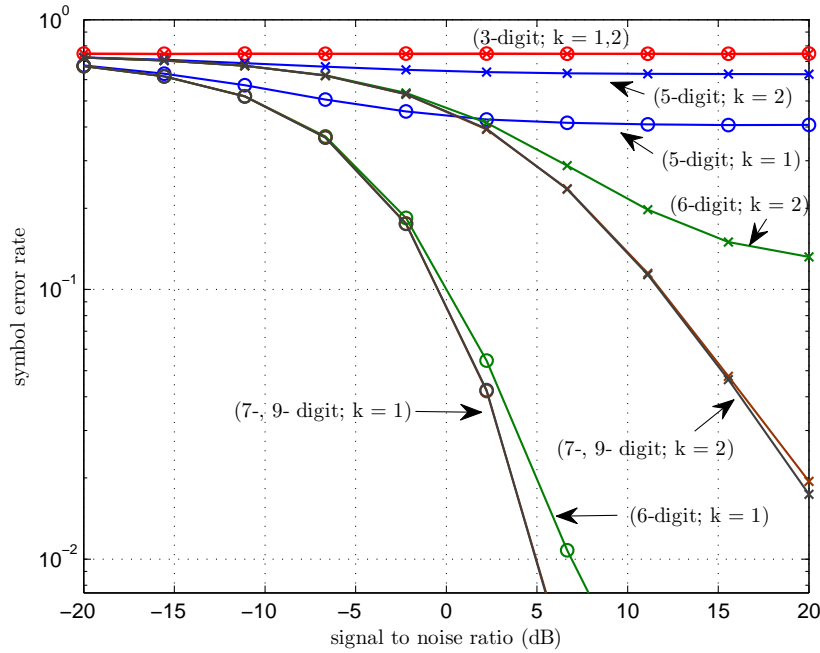


Figure 5.5: The effect of finite computational precision on the SERs for MIMO SDD eigenmode transmission. Considers each  $VC_k$  from  $\mathcal{U}_1$  to  $\mathcal{U}_2$  in the  $\{4, 2\}_2 \leftrightarrow \{4, 2\}_2$  configuration, for precisions of 3, 5, 6, 7, and 9 digits. QPSK modulation is used.

corresponding  $\mathbf{H}_i$  does). The loss of diversity gains is implicit. Since only 5 VCs are facilitated with 11 antennas at  $\mathcal{U}_1$  and 8 antennas at  $\mathcal{U}_2$ , a loss of three spatial DoFs for multiplexing can be concluded. These losses represent the cost of SDD.

From a mathematical point of view, the SDD techniques examined thus far perfectly suppress the self-interference. However, perfect self-interference suppression is infeasible because finite computational precision (in the transmitter and receiver signal processing) and quantization errors (at the ADCs) are in effect. They not only affect the signal processing directly, but also make the CSI used in the computations more imperfect.

Fig. 5.5 approximately<sup>3</sup> depicts how the number of significant digits of computation affects the SER, by using a  $\{4, 2\}_2 \leftrightarrow \{4, 2\}_2$  MIMO SDD configuration.  $10^5$ -point Monte Carlo simulation is used; the assumptions are the same as in Fig. 5.3. The error-floors indicate the presence of unmitigated interference. Apparently,

<sup>3</sup> Approximate, because the internal precision of the MATLAB `svd` routine was not restricted; its inputs and outputs were nevertheless truncated appropriately to control the precision.

self-interference does not get suppressed sufficiently for precisions of less than 6 digits; the effect of truncation errors (resulting from finite precision) is evident even at 6-digit precision. Nevertheless, the SERs improve rapidly as the number of significant digits of computation increases beyond that precision threshold. Presumably, this threshold is dictated by the ratio of transmit and receive signal strengths; e.g.,  $\log_{10}(\sqrt{100 \text{ dB}}) = \frac{1}{2}\log_{10}(10^{10}) = 5$ .

Low ADC resolution is also a significant concern because SDD requires that the receiver accurately resolve both the desired signal and the self-interference. The resolution governs the quantization errors thus affecting the SERs.

**Example 5.2** Suppose a complex Gaussian random variable  $X$  with a zero mean and  $2\sigma^2$  variance is digitized by using an  $n$ -bit uniform quantizer. The real and imaginary components of  $X$  lie in the  $(-8\sigma, 8\sigma)$  range, at  $\text{erf}(8/\sqrt{2}) = 1 - 1.2 \times 10^{-15}$  probability (i.e., practically 1). The quantizer will have a precision of  $\Delta = \frac{16\sigma}{2^n} = \frac{\sigma}{2^{n-4}}$ ; the corresponding maximum quantization error is  $\epsilon = \frac{\Delta}{2} = \frac{\sigma}{2^{n-3}}$ . •

Uniform quantization is unavoidable since the self-interference is additive; therefore, the maximum quantization error  $\epsilon \propto \frac{1}{2^n}$  should be insignificant with respect to both the desired and self-interference signal components. In other words, the ADC needs a wide dynamic range in the order of, for instance,  $\mathcal{E}\{\|\mathbf{G}_i\|_F\} / \mathcal{E}\{\|\mathbf{H}_i\|_F\}$ . Fig. 5.6 illustrates the effect of quantization errors on the SER for ADC resolutions 10, 12, 14, and 16 bits, and also considers their indirect effect on channel estimation.

Assumptions: The elements of  $\mathbf{H}_i$ s have unit variance, while those of  $\mathbf{G}_i$ s have 40 dB variance<sup>4</sup>. Midtread quantization at a dynamic range of  $16\sigma$  is considered, where  $\sigma = \sqrt{10^4/2}$ .  $10^6$ -point Monte Carlo simulation with 10 data symbols per VC per channel realization and 10 pilot symbols per transmit antenna per channel realization is assumed. The least square method is used for channel estimation. The other assumptions are the same as in Fig. 5.3.

<sup>4</sup> A duplex separation above 40 dB is not achievable with the ADC resolutions considered. Additional  $K$  dB separation requires approximately an extra  $\frac{1}{2}\log_2(10^{0.1K})$  bit precision at the ADC.

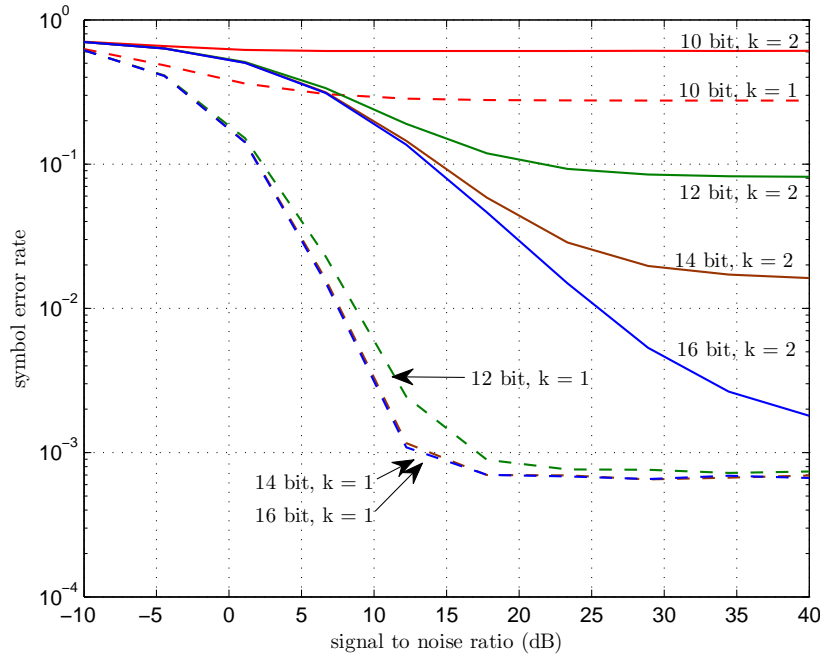


Figure 5.6: The effect of finite ADC resolution on the SERs for MIMO SDD eigenmode transmission. Considers each  $VC_k$  from  $\mathcal{U}_1$  to  $\mathcal{U}_2$  in the  $\{4, 2\}_2 \leftrightarrow \{4, 2\}_2$  configuration, for ADC resolutions of 10, 12, 14, and 16 bits. QPSK modulation is used.

The SER improves with finer ADC resolution (i.e., when more bits are output per sample). An abrupt degradation of error performance can be seen in the first VC ( $k = 1$ ) as the precision reduces from 12-bits to 10-bits. A possible reason for this result is that  $\log_2(16\sigma) = 10.14$ . The error-floors indicate the imperfections in the self-interference cancellation and channelization.

Quantization of the pilot symbols gives rise to channel-estimation errors, which indirectly but significantly contribute towards increasing the SERs. Fig. 5.7 confirms this fact by isolating the direct and indirect effects of quantization through SER comparison for the following cases. (The same MIMO SDD configuration and the assumptions as those in Fig. 5.6 and a 14-bit ADC are assumed.)

- **Case 1: ‘Ch Est + Qnt D&P’:** both the data and pilots are quantized.
- **Case 2: ‘Ch Est + Qnt D’:** data are quantized, but not the pilots.
- **Case 3: ‘Perf CSI + Qnt D’:** data are quantized, perfect CSI assumed.

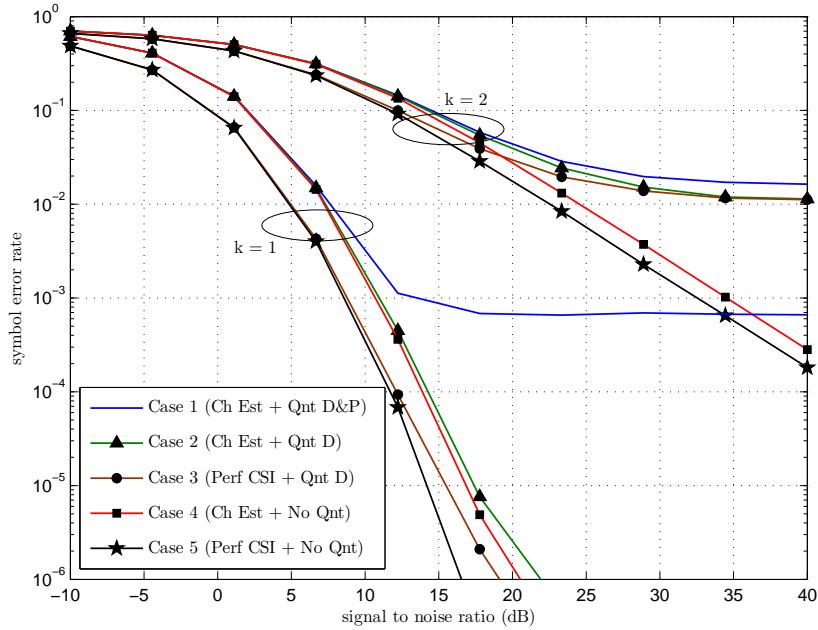


Figure 5.7: The interplay of channel-estimation errors and finite ADC resolution in MIMO SDD eigenmode transmission. Considers the SER of each  $VC_k$  from  $\mathcal{U}_1$  to  $\mathcal{U}_2$  in the  $\{4, 2\}_2 \leftrightarrow \{4, 2\}_2$  configuration, assuming a 14-bit ADC. Five cases reflecting realistic to idealistic assumptions on quantization and channel-estimation errors are compared. QPSK modulation is used.

- **Case 4: ‘Ch Est + No Qnt’:** neither data nor the pilots quantized.
- **Case 5: ‘Perf CSI + No Qnt’:** perfect CSI and no quantization.

Case 1 is realistic; Cases 2–5 depict more ideal scenarios. The SERs for Case 1 vs. Case 2 highlight the performance degradation due to quantization of the pilots. The quantization-induced channel-estimation errors are significant: an error-floor is observed with both the VCs for Case 1. The quantization of data appears to have a milder effect, since an error-floor is apparent for only  $k = 2$ . (Case 3 reinforces this conclusion.) Cases 4 and 5 disregard the quantization errors in order to isolate the effect of channel-estimation errors. An error-floor does not appear, evidently because the least square method of estimation improves with the signal to noise ratio (SNR). Thus, the effect of coarse ADC resolution is worsened by the increase in channel-estimation errors it causes.

## 5.4 Conclusion

Eigenmode transmission alongside MIMO space division duplexing (SDD) was investigated, and the possibilities of using Transmit SDD and Receive SDD were discussed. The loss of diversity and multiplexing benefits associated with SDD was demonstrated by using numerical results. Moreover, further insights were gained into the adverse effects of finite computational precision and finite ADC resolution, which are also manifested indirectly through increased channel-estimation errors.

The state-of-the-art general purpose ADCs operating above  $10^7$  samples per second have resolutions below 16-bits [96, 97]; as highlighted with numerical results, a 16-bit ADC restricts self-interference suppression capability to  $2^{16} \approx 50$  dB. Improving both the sampling rate and the resolution appears to be challenging presently, owing to high data rates and other factors including synchronization and jitter. The limited dynamic range of radio frequency amplifiers and the consequent non-linearities are also concerns. Therefore, SDD, as discussed here, will be feasible only when the hardware limitations are overcome.

Cellular systems typically involve long-range transmission; they could require duplex separations in excess of 100 dB. With lower duplex separations, SDD would likely be limited to short-range applications including personal/local area networks and femtocells in cellular systems.

### **Future directions:**

- Since SDD reduces the bidirectional wireless systems into two unidirectional, non-interfering MIMO systems of reduced dimensions, the exact performance analysis is mathematically tractable and could be attempted.
- Amplifier characteristics could be included in the simulations to assess the effect of amplifier non-linearities on the SER.

~

# Chapter 6

## Performance Analysis of MIMO Channel Inversion

In this chapter, a mathematical framework is developed to accurately characterize the per virtual channel (VC) received signal to noise ratio (SNR)  $\Lambda$  under channel inversion (CI) for an  $N_r \times N_t$  multiple-input multiple-output (MIMO) system. More specifically, the exact moment generating function (MGF) of  $\Lambda^{-1}$  is given for arbitrary  $N_t$  and  $N_r$ ; the exact probability density function (PDF) and cumulative distribution function (CDF) of  $\Lambda$ , as well as the symbol error rate (SER) for a class of modulation schemes, are characterized for the case  $\min(N_t, N_r) = 2$ . Although independent and identically distributed (i.i.d.) Rayleigh fading is assumed for the main results, the extension of some of the results for Rician fading and semi-correlated Rayleigh fading is briefly developed.

### 6.1 Introduction

Because the energy consumption is a major concern with wireless systems, power allocation schemes [12, Ch. 5] are used to appropriately allocate the transmit power among the individual channels in a multi-channel communication system. For instance, where the transmitter has channel-state information (CSI), the CI power allocation scheme ensures fairness, while maintaining the total instantaneous transmit power constant. More specifically, CI allocates power such that the instantaneous received SNR is identical for all channels. Although CI yields less capacity than the optimal water-filling power allocation, CI may be more suitable for ap-

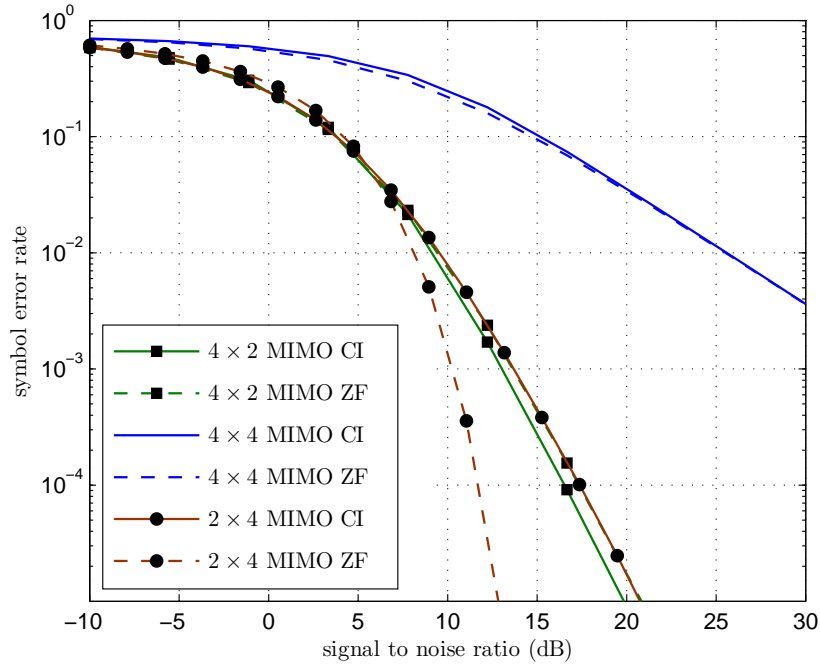


Figure 6.1: The SERs of  $N_r \times N_t$  MIMO systems —ZF vs. CI. Transmit ZF is used for the  $2 \times 4$  configuration, while ZF reception is used with the others. QPSK modulation is used.

plications with tight delay constraints. The temporal variants of CI can be used in single-carrier single-antenna systems [98]. The spatial variant [99] is applied across spatially multiplexed VCs in MIMO systems.

Hereafter, ‘CI’ refers to CI power allocation across the VCs produced by MIMO eigenmode transmission [8]. References [99–101] examine the basics of CI, while references [102, 103] investigate certain variants exhibiting improved capacity.

The similarities of CI and zero forcing (ZF) beamforming [19] are noteworthy. ZF simply inverts the channel at the transmitter or at the receiver. Transmit ZF causes the instantaneous transmit power to fluctuate unbounded, making its practical realization challenging; CI is immune to this issue. ZF reception employs non-unitary signal processing, which is susceptible to noise enhancement and correlated noise. CI, with only unitary receiver processing [99, 101], is free from these disadvantages. However, CI requires non-unitary transmit processing, and the average SER is the same as that of ZF reception, but is worse than that of transmit ZF. (Fig.

6.1 highlights these distinctions in terms of the SER performance.<sup>1)</sup> Moreover, signal processing for CI when the transmitter has more antennas than the receiver does not even require the singular value decomposition (SVD) of the channel matrix. Therefore, CI can be used as an easier-to-implement alternative to transmit ZF in MIMO and multi-user MIMO scenarios [104]. This work was motivated by the lack of exact performance results for MIMO CI in the literature.

**The chapter is organized as follows:** A mathematical framework for performance analysis of MIMO CI is presented in Section 6.2; the numerical results for i.i.d. Rayleigh fading follow in Section 6.3. Section 6.4 extends the analysis for Rician fading and semi-correlated Rayleigh fading. Section 6.5 concludes the chapter. Proof of the results is presented in Appendix B.

## 6.2 Mathematical Framework

Consider a MIMO system with  $N_t$  and  $N_r$  transmit and receive antennas; the channel matrix is  $\mathbf{H} \in \mathbb{C}^{N_r \times N_t}$ . Let  $m = \min(N_t, N_r)$ , and  $n = \max(N_t, N_r)$ . Define

$$\mathbf{W} = \begin{cases} \mathbf{H}\mathbf{H}^H, & N_t > N_r \\ \mathbf{H}^H\mathbf{H}, & N_t \leq N_r \end{cases}. \quad (6.1)$$

The eigenvalues  $\{\lambda_1, \dots, \lambda_m\} = \text{eig}(\mathbf{W})$  characterize the MIMO channel sufficiently. For instance, they relate to the received SNR along the  $m$  VCs under eigenmode transmission. By using CI, the total transmit power  $P$  is allocated as  $p_i$  to each  $i^{\text{th}}$  VC:  $\text{VC}_i$  for  $i \in \{1, \dots, m\}$ ;  $\lambda_i p_i = K$  is therefore identical for all VCs at a given time. Thus, we get

$$P = \sum_{i=1}^m p_i = K \sum_{i=1}^m \lambda_i^{-1}. \quad (6.2)$$

Let  $\Lambda = K/P$ . Then we get

$$\Lambda^{-1} = \sum_{i=1}^m \lambda_i^{-1} = \text{trace}(\mathbf{W}^{-1}). \quad (6.3)$$

---

<sup>1</sup>  $10^6$ -point Monte Carlo simulation with 100 quadrature phase shift keying (QPSK) symbols per VC per channel realization is used.

Assumptions: Eqn. (6.3) and the analysis based on it hold only under block fading assumptions, which permit averaging out the additive noise and transmitted data for each channel realization. Perfect transmit CSI and additive white Gaussian noise are also assumed.

The links between the transmit–receive antenna pairs are assumed to undergo i.i.d. Rayleigh fading. Thus,  $\mathbf{H} \in \mathbb{C}^{N_r \times N_t}$  becomes a complex Gaussian matrix;  $\mathbf{W}$  a rank  $m$  complex central Wishart matrix [8, 105] having  $n$  degrees of freedom; and  $\Lambda^{-1}$  the trace of an inverse-Wishart matrix.

### 6.2.1 Arbitrary $m \leq n$

The joint PDF of  $\lambda_i$  for  $i \in \{1, \dots, m\}$ , the unordered eigenvalues of  $\mathbf{W}$ , is given [105] by

$$f_{\lambda_1, \dots, \lambda_m}(\lambda_1, \dots, \lambda_m) = \frac{e^{-\sum_{i=1}^m \lambda_i}}{m! \mathcal{K}_{m,n}} \prod_{i=1}^m \lambda_i^{n-m} \prod_{1 \leq i < j \leq m} (\lambda_i - \lambda_j)^2, \quad (6.4)$$

where

$$K_{m,n} = \prod_{k=1}^m (m-k)! (n-k)!. \quad (6.5)$$

The joint PDF of ordered eigenvalues differs only by not having a factor  $\frac{1}{m!}$  in (6.4). All the unordered eigenvalues have the range  $[0, \infty)$ ; therefore, using their joint PDF simplifies further derivations.

The factor  $\prod_{1 \leq i < j \leq m} (\lambda_i - \lambda_j)^2$  in (6.4) may be expanded to obtain the more manipulable form

$$f_{\lambda_1, \dots, \lambda_m}(\lambda_1, \dots, \lambda_m) = \frac{e^{-\sum_{i=1}^m \lambda_i}}{m! \mathcal{K}_{m,n}} \left( \prod_{i=1}^m \lambda_i^{n-m} \right) \sum_{\substack{k_1, \dots, k_m \in \{0, \dots, 2(m-1)\} \\ \sum k_i = m(m-1)}} b(k_1, \dots, k_m) \lambda_1^{k_1} \dots \lambda_m^{k_m}. \quad (6.6)$$

The coefficients  $b(k_1, \dots, k_m)$ , corresponding to raising each  $\lambda_i$  to power  $k_i$  for  $i \in \{1, \dots, m\}$ , can be obtained by expanding the factor as a multivariate polynomial. The equality  $\sum_{i=1}^m k_i = m(m-1)$  is seen to hold for each term of this expansion.

**Theorem 6.1** *The MGF of  $\Lambda^{-1}$  (for arbitrary  $m \leq n$ ).*

Let  $\lambda_1, \dots, \lambda_m$  be the unordered eigenvalues of an  $m \times m$  complex central Wishart matrix having  $n$  degrees of freedom. The MGF of  $\Lambda^{-1}$  in (6.3) is given by

$$\mathcal{M}_{1/\Lambda}(s) = \frac{2^m s^{-\frac{mn}{2}}}{m! \mathcal{K}_{m,n}} \sum_{\substack{k_i \in \{0, \dots, 2(m-1)\} \\ \sum k_i = m(m-1)}} b(k_1, \dots, k_m) \prod_{i=1}^m \mathcal{K}_{k_i+n-m+1}(2\sqrt{s}). \quad (6.7)$$

**Proof:** See Appendix B. ■

### 6.2.2 Special Case: $m = 2$

This scenario occurs in any MIMO channel having two antennas at one end, and at least two antennas at the other. The MIMO downlink from a multi-antenna base station to two-antenna mobile station (as in the  $4 \times 2$  LTE downlink configuration [38]) is an example. Another is the multi-user MIMO downlink [104] from a multi-antenna base station to two single-antenna mobile stations. Because of antenna-spacing constraints, equipping a mobile terminal operating in cellular frequency bands (presently below 4 GHz) with more antennas is technically challenging at present; therefore, the case  $m = 2$  is realistic.

For the case  $m = 2$ , (6.4) reduces to

$$f_{\lambda_1, \lambda_2}(\lambda_1, \lambda_2) = \frac{1}{2\mathcal{K}_{2,n}} e^{-(\lambda_1 + \lambda_2)} (\lambda_1 - \lambda_2)^2 \lambda_1^{n-2} \lambda_2^{n-2}, \quad (6.8)$$

where  $\mathcal{K}_{2,n}$  simplifies to  $(n-1)!(n-2)!$ . The distribution of  $\Lambda$  in (6.3) can then be derived by using (6.8).

**Theorem 6.2** *The PDF of  $\Lambda$  (for  $m = 2$ ).*

Let  $\lambda_1, \lambda_2$  be the unordered eigenvalues of a  $2 \times 2$  complex central Wishart matrix having  $n$  degrees of freedom. The PDF of  $\Lambda$  in (6.3) is given by

$$f_{\Lambda}(x) = \frac{x^{2(n-1)} e^{-2x}}{\mathcal{K}_{2,n}} \sum_{k=0}^{2n} \binom{2n}{k} ((n-k-2x)\mathcal{K}_{k-n}(2x) + 2x\mathcal{K}_{k+1-n}(2x)). \quad (6.9)$$

**Proof:** See Appendix B. ■

**Corollary 6.1** *The CDF of  $\Lambda$  (for  $m = 2$ ).*

Let  $\lambda_1, \lambda_2$  be the unordered eigenvalues of a  $2 \times 2$  complex central Wishart matrix having  $n$  degrees of freedom. The CDF of  $\Lambda$  in (6.3) is given by

$$F_{\Lambda}(x) = \frac{2\sqrt{\pi}}{4^{2n}\mathcal{K}_{2,n}} \sum_{k=0}^{2n} \binom{2n}{k} \left[ 2(n-k) \mathcal{G}_{2 \ 3}^2 \left( 4x \mid_{3n-k-1, n+k-1, 0}^{1, 2n-0.5} \right) - \mathcal{G}_{2 \ 3}^2 \left( 4x \mid_{3n-k, n+k, 0}^{1, 2n+0.5} \right) + \mathcal{G}_{2 \ 3}^2 \left( 4x \mid_{3n-k-1, n+k+1, 0}^{1, 2n+0.5} \right) \right]. \quad (6.10)$$

**Proof:** See Appendix B. ■

Although used relatively infrequently in the wireless literature, Meijer  $\mathcal{G}$  function is well characterized [2, Sec. 9.3]. Moreover, it is directly available in the common computational environments including Mathematica, Maple, and MATLAB. Hence, the results can be easily evaluated at high precision.

## 6.3 Numerical Results

This section highlights a few applications of the characterization of  $\Lambda$  made in Section 6.2. Numerical results for different performance metrics are presented, establishing the validity of this characterization.

### 6.3.1 Arbitrary $m \leq n$

Further derivations based on the result (6.7) likely require the use of hypergeometric functions of multiple variables, and are not attempted here.<sup>2</sup> Having an exact expression for  $\mathcal{M}_{\Lambda^{-1}}(s)$  is more appealing for numerical evaluation of the performance metrics, for such an expression reduces the number of folded-integrals one may have to evaluate. The complimentary CDF of  $\Lambda$  that relates to the probability of outage, for instance, is given by [106]:

$$\bar{F}_{\Lambda}(x) = F_{\Lambda^{-1}}\left(\frac{1}{x}\right) = \frac{2}{\pi} \int_0^{\infty} \frac{\Re(\mathcal{M}_{\Lambda^{-1}}(j\omega))}{\omega} \sin\left(\frac{\omega}{x}\right) d\omega, \quad (6.11)$$

whose single integral can be evaluated by using a simple quadrature technique. Likewise, evaluating a single integral suffices to obtain the SER [107].

---

<sup>2</sup> Native support for special functions of an arbitrary number of variables is not currently available in standard computational environments such as MATLAB and Mathematica. Those functions are nevertheless implementable as cascaded infinite series.

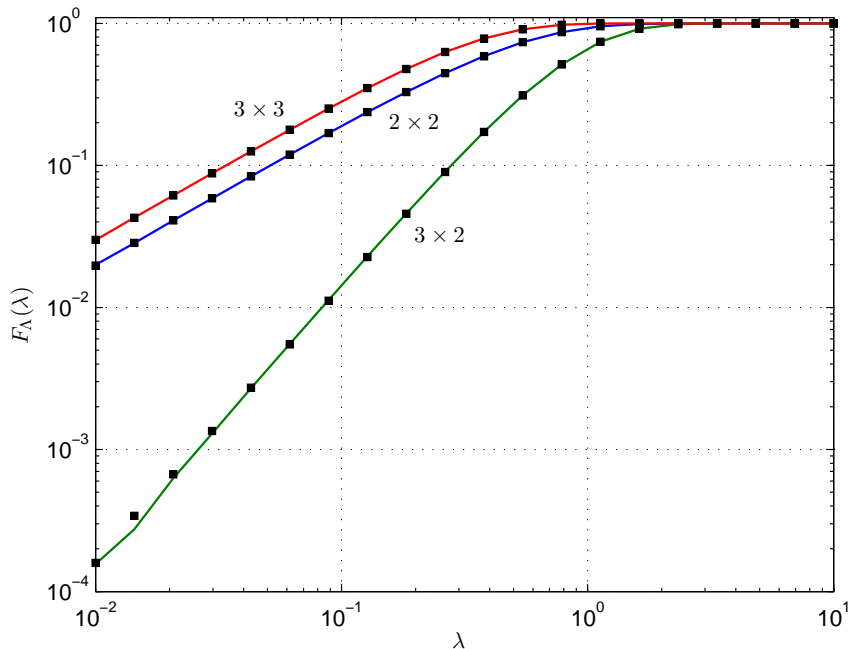


Figure 6.2: The CDF of  $\Lambda$  over  $\{2 \times 2, 3 \times 2, 3 \times 3\}$  MIMO systems using CI—numerical vs. simulated (■ markers).

Fig. 6.2 compares the CDF curves computed by using (6.11) against the  $10^6$ -point semi-analytic Monte Carlo simulation results for three MIMO configurations. The numerical values were computed by using the adaptive quadrature routine `quadl` in MATLAB after applying the variable transformation  $\omega = (1+t)^2/(1-t)^2$  to adjust the range of integration. Since CI holds reciprocity and performs similarly to a ZF receiver, the diversity order of CI can be deduced (from [108]) to be  $|N_t - N_r| + 1$ . The slope of CDF curves as  $\lambda \rightarrow 0$  agrees with this deduction.

### 6.3.2 Special Case: $m = 2$

This scenario is more tractable. Three applications of the mathematical framework are examined next, to indirectly verify Theorem 6.2 and Corollary 6.1.

#### Application 1: Ergodic Capacity

The capacity [12, Ch. 5] of the MIMO system being considered is given by a random variable  $C = \sum_{k=1}^2 \log_2(1 + p_i \lambda_i / N_0) = 2 \log_2(1 + P\Lambda)$ , where  $P$  denotes

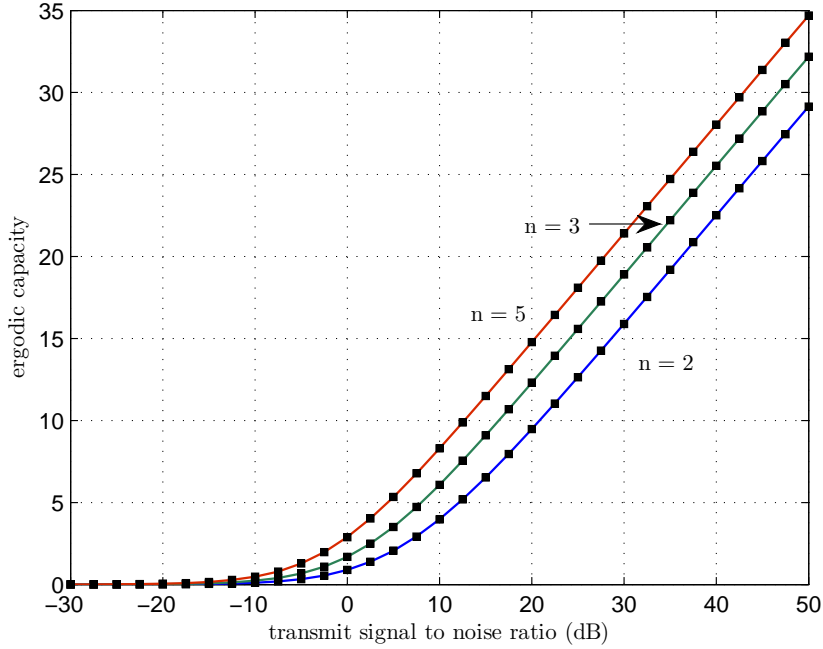


Figure 6.3: Ergodic capacity (bit/s/Hz) for a  $2 \times n$  MIMO system using CI—numerical vs. simulated (■ markers).

the transmit SNR (transmit power normalized by noise variance). Its average, the ergodic capacity  $\mathcal{E}_C\{C\}$  can be numerically computed as

$$\mathcal{E}_C\{C\} = \int_0^\infty c f_C(c) dc = 2 \int_0^\infty \log_2(1 + Px) f_\Lambda(x) dx \quad (6.12)$$

for any given  $P$ . Fig. 6.3 verifies the numerical values thus obtained for  $\mathcal{E}_C\{C\}$  for the cases  $n \in \{2, 3, 5\}$  against the  $10^5$ -point semi-analytic Monte Carlo simulation results. As expected, the ergodic capacity increases logarithmically with the transmit SNR (i.e., the capacity curves appear as straight lines at high transmit SNR, when the SNR is given in dB), and increases (non-linearly) with  $n$ .

### Application 2: Average SER

Since the receiver processing for CI leaves the distribution of additive Gaussian noise unaltered, the average SER  $P_e$  under many modulation schemes [14, Ch. 5] can be given by

$$P_e = \mu \mathcal{E}_\Lambda \left\{ \mathcal{Q} \left( \sqrt{2\nu\Lambda P} \right) \right\}, \quad (6.13)$$

where  $P$  is the transmit SNR, and  $\mu, \nu$  are constants dependent on the modulation scheme. For example,  $\mu = 1$  and  $\nu = 1$  give exactly the SER for binary phase shift keying modulation, while  $\mu = 2(M-1)/M$  and  $\nu = 3/(M^2-1)$  approximate those for other  $M$ -ary pulse amplitude modulation schemes. The SER for such systems can be analytically derived by using (6.13) and the distribution of  $\Lambda$ .

**Corollary 6.2** *Average SER (for  $m = 2$ ).*

Let  $\lambda_1, \lambda_2$  be the unordered eigenvalues of a  $2 \times 2$  complex central Wishart matrix having  $n$  degrees of freedom. The SER (6.13) is given by

$$P_e = \frac{\mu}{(4^{2n})\mathcal{K}_{2,n}} \sum_{k=0}^{2n} \binom{2n}{k} \left[ 2(n-k) \mathcal{G}_3^2 \left( \frac{4}{\nu P} \middle| \begin{matrix} 0.5, 1, 2n-0.5 \\ 3n-k-1, n+k-1, 0 \end{matrix} \right) - \mathcal{G}_3^2 \left( \frac{4}{\nu P} \middle| \begin{matrix} 0.5, 1, 2n+0.5 \\ 3n-k, n+k, 0 \end{matrix} \right) + \mathcal{G}_3^2 \left( \frac{4}{\nu P} \middle| \begin{matrix} 0.5, 1, 2n+0.5 \\ 3n-k-1, n+k+1, 0 \end{matrix} \right) \right]. \quad (6.14)$$

**Proof:** See Appendix B. ■

### Application 3: High SNR analysis

The diversity and coding gains of the system can be easily deduced [109, Prop. I] from the least order approximation of  $x$  on the PDF of  $\Lambda$ . For the MIMO system of concern, this approximation may be obtained, after some manipulations, by using [1, Eqn. (9.6.9)] on (6.9).

**Corollary 6.3** Let  $\lambda_1, \lambda_2$  be the unordered eigenvalues of a  $2 \times 2$  complex central Wishart matrix having  $n$  degrees of freedom. The least order approximation of the PDF of  $\Lambda$  in (6.3) is given by

$$f_{\Lambda}(x) = \frac{n}{2(n-2)!} x^{n-2} + o(x^{n-2}). \quad (6.15)$$

**Proof:** Evidently, only the  $k = 0$  term of the summation in (6.9) contributes to this approximation. Using the first term of each series expansion [1, Eqn. (4.2.1)] and [1, Eqn. (9.6.9)] followed by the selection of the least order term of  $x$  yields the result. ■

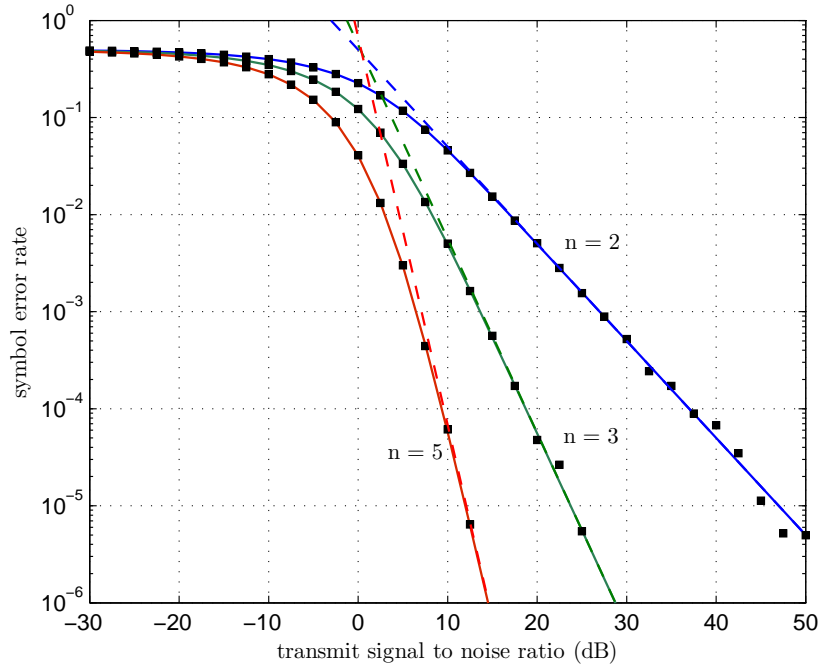


Figure 6.4: The SER for binary phase shift keying (i.e.  $\mu = \nu = 1$ ) over a  $2 \times n$  MIMO system using CI—analytical vs. simulated (■ markers). Asymptotes to curves are in dashed lines (—).

Fig. 6.4 illustrates for the cases  $n \in \{2, 3, 5\}$  how the exact analytic SER (6.14) for binary phase shift keying modulation compares with the  $10^5$ -point semi-analytic Monte Carlo simulation results. This figure also shows the asymptotes for the curves computed by using (6.15) based on reference [109]. A diversity order of  $(n - 1)$  is observed.

## 6.4 Extension to Rician and Semi-Correlated Rayleigh Fading (Case: $m = 2$ )

The joint PDF of the unordered eigenvalues of a complex central Wishart distribution resembles those of the non-central and semi-correlated central Wishart distributions [110]. Therefore, certain results presented in Section 6.2 can be generalized for these scenarios. Only the PDF results (for case  $m = 2$ ) are presented here; the derivation of the other results from them does not require a different approach from that used in the central Wishart case.

### 6.4.1 Rician Fading

Without a further loss of generality, let  $N_t = n \geq 2$  and  $N_r = 2$ . Suppose the resulting  $2 \times n$  channel matrix  $\mathbf{H}$  is of the form  $\mathbf{H} = a\mathbf{H}_{\text{sp}} + b\mathbf{H}_{\text{sc}}$ , where  $\mathbf{H}_{\text{sp}}$  represents the deterministic specular (line-of-sight) component,  $\mathbf{H}_{\text{sc}} \in \mathbb{C}^{2 \times n}$ , the random scatter component, and  $a^2 + b^2 = 1$ . The specular component is governed by the directional gains of the antennas, the presence of dominant multi-paths, etc.  $K = a^2 \|\mathbf{H}_{\text{sp}}\|_F^2 / b^2 \mathcal{E}\{\|\mathbf{H}_{\text{sc}}\|_F^2\}$  is the Rician factor [111];  $\mathbf{\Omega} = (a^2/b^2)\mathbf{H}_{\text{sp}}\mathbf{H}_{\text{sp}}^H$  is the non-centrality matrix. Let  $\{\lambda_1, \lambda_2\} = \text{eig}(\mathbf{H}\mathbf{H}^H)$  and  $\{\omega_1, \omega_2 | \omega_1 > \omega_2\} = \text{eig}(\mathbf{\Omega})$ . The joint distribution of the unordered eigenvalues  $\lambda_1, \lambda_2$  is given by [111, Eqn. (15)]

$$f_{\lambda_1, \lambda_2}(\lambda_1, \lambda_2) = \frac{e^{-(\omega_1 + \omega_2)} |\lambda_1 - \lambda_2| (\lambda_1 \lambda_2)^{\frac{n-2}{2}}}{2 (\omega_1 - \omega_2) (\omega_1 \omega_2)^{\frac{n-2}{2}}} e^{-(\lambda_1 + \lambda_2)} \left( \mathcal{I}_{n-2} \left( 2\sqrt{\omega_1 \lambda_1} \right) \mathcal{I}_{n-2} \left( 2\sqrt{\omega_2 \lambda_2} \right) - \mathcal{I}_{n-2} \left( 2\sqrt{\omega_2 \lambda_1} \right) \mathcal{I}_{n-2} \left( 2\sqrt{\omega_1 \lambda_2} \right) \right). \quad (6.16)$$

The PDF result corresponding to the case  $\omega_1 = \omega_2$  can be obtained by using the limiting operation  $\omega_1 \rightarrow \omega_2$  on (6.16).

Assume perfect transmit CSI and the CI scheme. Given transmit SNR  $P$ , the per channel received SNR  $\frac{b^2}{2} P \Lambda$  relates to  $\lambda_1$  and  $\lambda_2$  through (6.3).

**Theorem 6.3** *The PDF of  $\Lambda$ .*

Let  $\lambda_1, \lambda_2$  be the eigenvalues of a rank-2 complex non-central Wishart matrix having  $n$  degrees of freedom, and a non-centrality matrix  $\mathbf{\Omega}$ , whose eigenvalues are  $\{\omega_1, \omega_2 | \omega_1 > \omega_2 > 0\}$ . The PDF of  $\Lambda$  in (6.3) is given by

$$f_{\Lambda}(x) = \sum_{i=0}^{\infty} \sum_{j=0}^i \frac{g_{i,j}(\omega_1, \omega_2)}{(j+n-2)! (i-j+n-2)! j! (i-j)!} \sum_{p=0}^{i+2n-1} \binom{i+2n-1}{p} e^{-2x} x^{i+2n-2} (\mathcal{K}_{n+j-p}(2x) - \mathcal{K}_{n+j-p-1}(2x)), \quad (6.17)$$

where

$$g_{i,j}(\omega_1, \omega_2) = \frac{e^{-(\omega_1 + \omega_2)}}{(\omega_1 - \omega_2)} \left( \omega_1^j \omega_2^{(i-j)} - \omega_1^{(i-j)} \omega_2^j \right). \quad (6.18)$$

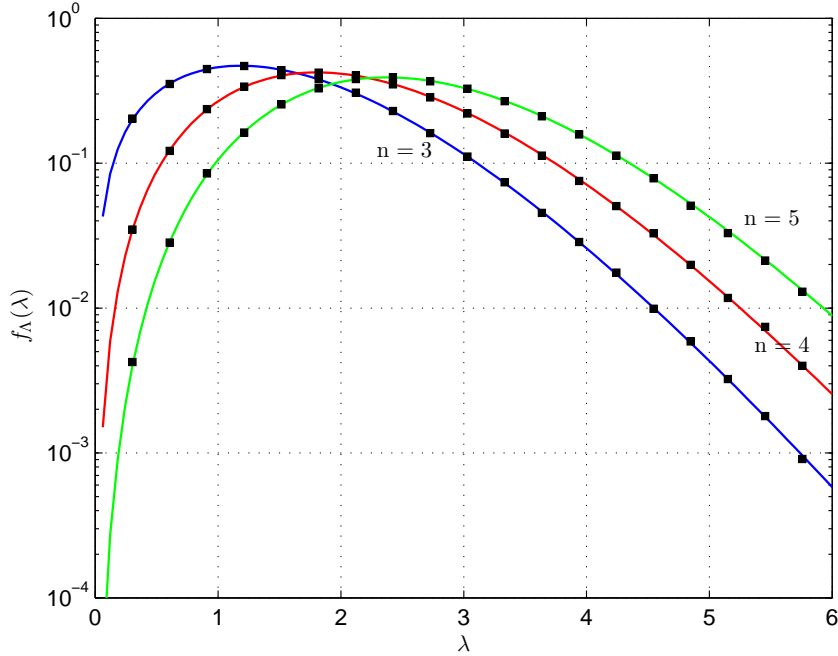


Figure 6.5: The PDF of  $\Lambda$  over  $2 \times n$  Rician faded MIMO systems using CI—analytical vs. simulated (■ markers). Rician fading is modeled by a rank-2 non-centrality matrix with eigenvalues  $[4, 1]$ .

**Proof:** The identity [1, Eqn. (9.6.10)] is used to expand each  $\mathcal{I}_n(\cdot)$  as an infinite series. Each term of the resulting cascaded infinite series is of a form similar to (6.9). Hence, the rest of the proof is similar to that of Theorem 6.2. ■

Fig. 6.5 verifies the analytical PDF results for  $2 \times n$  MIMO systems using CI under Rician fading against the  $10^6$ -point semi-analytic Monte Carlo simulation results. The non-centrality matrix has eigenvalues  $\omega_1 = 4$  and  $\omega_2 = 1$ .

Eqn. (6.17) gets simplified further for the case  $\omega_1 \neq 0, \omega_2 = 0$  and the limiting case  $\omega_1 \rightarrow \omega_2$ . The corresponding PDF expressions, along with the CDF and SER results, have been presented and verified in [45]. The least order approximation of the PDF result therein is reproduced below. The approximation shows that the diversity order is the same for both Rayleigh and Rician fading.

**Corollary 6.4** Let  $\lambda_1, \lambda_2$  be the eigenvalues of a rank-2 non-central complex Wishart matrix having  $n$  degrees of freedom, and a non-centrality matrix  $\Omega$ , whose eigenvalues are  $\{\omega_1, \omega_2 | \omega_1 > \omega_2 > 0\}$ . The first-order approximation of the PDF of  $\Lambda$  in

(6.3) is given by

$$f_{\Lambda}(x) = ax^{n-2} + o(x^{n-2}), \quad (6.19)$$

where

$$a = \frac{(n + \omega_1 - 1)e^{-\omega_2} - (n + \omega_2 - 1)e^{-\omega_1}}{2(\omega_1 - \omega_2)(n - 2)!}. \quad (6.20)$$

**Proof:** Similar to that of Corollary 6.3. ■

Note that the limit of  $a$  in (6.20) as  $\omega_1 \rightarrow \omega_2$  and  $\omega_2 \rightarrow 0$  is  $\frac{n}{2(n-2)!}$ , which corresponds to Rayleigh fading.

## 6.4.2 Min Semi-Correlated Rayleigh Fading

Semi-correlated MIMO channels [110] arise where only one of the set of transmit antennas and set of receive antennas is correlated. Such channels could result when the antenna spacing is constrained at one of the terminals because of, for example, the device size. Given the similarity corresponding joint eigenvalue distribution has to that of uncorrelated Rayleigh fading, the results from Section 6.2 can be extended for semi-correlated Rayleigh fading.

Assume min semi-correlated Rayleigh fading (i.e., correlation exists only at the terminal having fewer antennas) and suppose  $\min(N_t, N_r) = 2$ . Without a loss of generality, let  $N_t = n \geq 2$  and  $N_r = 2$ . The channel matrix becomes  $\mathbf{H} = \mathbf{\Sigma}^{1/2}\mathbf{H}_w$ , where  $\mathbf{H}_w \in \mathbb{C}^{N_r \times N_t}$  is complex Gaussian distributed;  $\mathbf{\Sigma}$  is the  $2 \times 2$  receive correlation matrix, whose ordered eigenvalues are  $\sigma_1$  and  $\sigma_2$  such that  $\sigma_2 > \sigma_1$ . The joint distribution of the ordered eigenvalues of  $\mathbf{H}\mathbf{H}^H$  is given by [112, Eqn. (17)]. Thus, we get the joint distribution of the unordered eigenvalues  $\{\lambda_1, \lambda_2\} = \text{eig}(\mathbf{H}\mathbf{H}^H)$  as

$$f_{\lambda_1, \lambda_2}(\lambda_1, \lambda_2) = \frac{K}{2} |\lambda_1 - \lambda_2| (\lambda_1 \lambda_2)^{n-2} \left( e^{-\left(\frac{\lambda_1}{\sigma_1} + \frac{\lambda_2}{\sigma_2}\right)} - e^{-\left(\frac{\lambda_1}{\sigma_2} + \frac{\lambda_2}{\sigma_1}\right)} \right), \quad (6.21)$$

where

$$K = \frac{(\sigma_1 \sigma_2)^{1-n}}{(n-1)!(n-2)!(\sigma_2 - \sigma_1)}. \quad (6.22)$$

The result for the case  $\sigma_1 = \sigma_2$  would be given by the limiting operation  $\sigma_2 \rightarrow \sigma_1$ . The distribution of  $\Lambda$  in (6.3) can be characterized as follows.

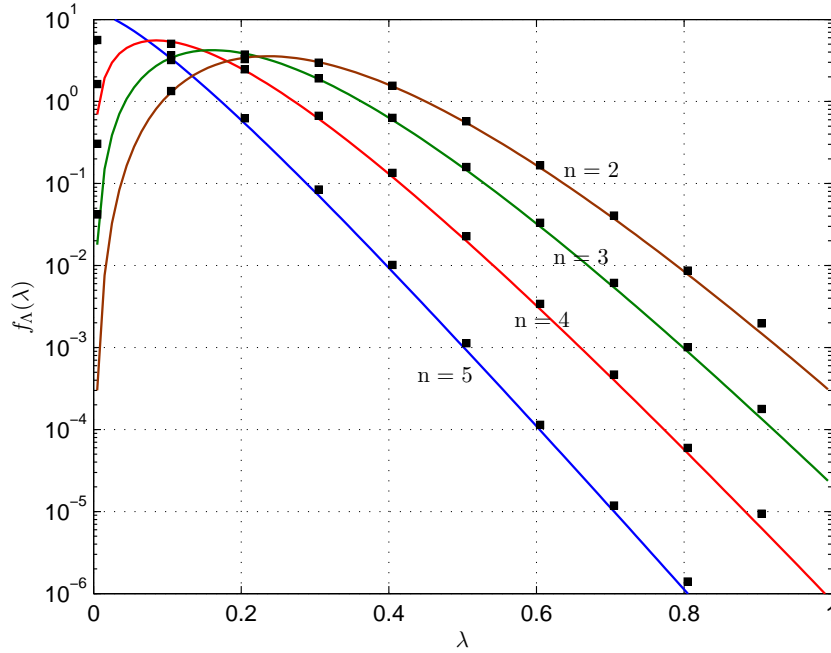


Figure 6.6: The PDF of  $\Lambda$  over  $2 \times n$  semi-correlated Rayleigh faded MIMO systems using CI—analytical vs. simulated (■ markers). Receive correlation matrix is assumed to have eigenvalues  $[.1, .3]$ .

**Theorem 6.4** *The PDF of  $\Lambda$ .*

Let  $\lambda_1, \lambda_2$  be the eigenvalues of a rank-2 complex central Wishart matrix having  $n$  degrees of freedom and a correlation matrix with eigenvalues  $\{\sigma_1, \sigma_2 | \sigma_2 > \sigma_1 > 0\}$ . The PDF of  $\Lambda$  in (6.3) is given by

$$f_{\Lambda}(x) = Kx^{2n-2}e^{-(1/\sigma_1+1/\sigma_2)} (\mathbb{I}_x(\sigma_1, \sigma_2, 0) - x\mathbb{I}_x(\sigma_1, \sigma_2, 1) - \mathbb{I}_x(\sigma_2, \sigma_1, 0) + x\mathbb{I}_x(\sigma_2, \sigma_1, 1)), \quad (6.23)$$

where

$$\mathbb{I}_x(\mu_1, \mu_2, a) = \sum_{k=0}^{2n-1} \binom{2n-1}{k} \left(\frac{\mu_1}{\mu_2}\right)^{\frac{k-n-a+1}{2}} \frac{\mathcal{K}_{k-n-a+1}\left(\frac{2x}{\sqrt{\mu_1\mu_2}}\right)}{x^a}. \quad (6.24)$$

**Proof:** Omitted given the similarity to that of Theorem 6.2. ■

Fig. 6.6 verifies the analytical PDF results for  $2 \times n$  MIMO systems by using CI against the  $10^8$ -point semi-analytic Monte Carlo simulation results. The receive correlation matrix has (arbitrarily chosen) eigenvalues  $\sigma_1 = 0.1$  and  $\sigma_2 = 0.3$ . The

special cases such as  $\sigma_1 = \sigma_2$ , as well as the CDF and SER results, are mathematically tractable, but not attempted here.

## 6.5 Conclusion

The performance of MIMO eigenmode transmission under the channel inversion (CI) power allocation scheme was examined. A mathematical framework was developed to characterize the received signal power  $\Lambda$  under CI. Assuming Rayleigh fading, the exact MGF of  $\Lambda^{-1}$  was developed for arbitrary  $N_t$  and  $N_r$ . Moreover, the exact PDF and CDF expressions were derived for the special case  $\min(N_t, N_r) = 2$ ; some of them were extended for Rician fading and semi-correlated Rayleigh fading. Numerical results, including the exact SER for the case  $\min(N_t, N_r) = 2$ , were provided to highlight possible applications of the framework and to gain insights into CI.

The observations confirm the intuition that CI has the diversity order of the weakest eigenmode, which is  $|N_t - N_r| + 1$  under both Rayleigh and Rician fading. It was also seen that ZF reception performs similarly to CI without requiring transmit CSI; hence, CI is not attractive when the receiver has more antennas than the transmitter. However, CI, given its finer control over the instantaneous transmit power, may be useful as an easier-to-implement alternative to transmit ZF for MIMO and multi-user MIMO configurations.

### Future directions:

- Certain analytic results based on Theorem 6.1 (for arbitrary  $m \leq n$ ), including the diversity order, appear to be mathematically tractable and could be derived.
- Performance comparison of CI and (transmit) ZF in multi-user MIMO configurations is also interesting. Here, CI would have to be applied on the effective MIMO channel the source has with all the users.

~

# Chapter 7

## Conclusion and Future Work

The similarities in the spatial, temporal, and frequency characterizations of wireless channels reveal the potential of the space dimension beyond the usual diversity–multiplexing benefits. Inspired by these similarities, this thesis focused on demonstrating non-conventional uses of the spatial degrees of freedom (DoFs).

- Chapter 2 of this thesis, for instance, proposed GSVD-based beamforming, a novel, non-iterative beamforming technique for the two-user multiple-input multiple-output (MIMO) downlink channel. This chapter also provided detailed insights into its performance by considering multicast and relaying applications.
- Next, a divide-and-conquer strategy to implement arbitrary physical-layer multicasting (PLM) configurations through non-iterative beamforming was proposed in Chapter 3. This strategy uses the notion of multicast antenna groups (MAGs) representing virtual grouping of user antennas and a two-phased beamforming strategy comprising inter-MAG beamforming and intra-MAG beamforming to systematically realize arbitrary virtual channel (VC)–to-User mapping.
- Chapter 4 introduced the use of space dimension for mitigating multipath fading, namely, spatial multipath resolution (SMR). Its use with space time block codes (STBCs) and eigenmode transmission was investigated; the possibilities and benefits of partial and adaptive SMR were examined.

- Space division duplexing (SDD), which is a promising, yet insufficiently explored use of space dimension, was investigated in Chapter 5. By considering eigenmode transmission under SDD, the benefits of SDD, as well as the extent certain hardware limitations including finite analog-to-digital converter (ADC) resolution contribute towards precluding SDD implementation, were assessed.
- Chapter 6 developed a mathematical framework for performance analysis of MIMO eigenmode transmission under the channel inversion power allocation scheme; detailed insights into the performance of such systems were provided.

Overall, this thesis demonstrated the feasibility, challenges, advantages, and disadvantages of certain non-conventional uses of spatial DoFs. The symbol error rate (SER) simulation results were usually used to quantify the performance; the exact analytic and numerical results were provided where possible to complement them.

Most non-conventional benefits of the space dimension are presently not viable because of practical challenges and the high cost of spatial DoFs. Nevertheless, the following trends could change this situation:

- Higher carrier frequencies (e.g., the 60 GHz ISM frequency band, as considered in the IEEE 802.15.3c [85] standard) reduce the antenna spacing required for uncorrelated reception, allowing more antennas to be accommodated in a terminal.

Challenges: However, higher frequencies have different propagation characteristics; further research on developing new MIMO techniques (and adapting existing ones) for such carriers is necessary.

- The complexity of MIMO signal processing increases more than linearly with the number of antennas. Therefore, relevant advancements in the electronics (e.g., [43]) are crucial for DoFs to become cost-effective.
- The ongoing research on large MIMO systems design is very promising. The complexity of signal processing algorithms is the main consideration in such

design.

Challenges: Novel uses of spatial DoFs, including those proposed in this research, need to be examined for large MIMO systems.

The future directions specific to the Chapters 2–6 are outlined in the chapters' conclusions. Common for all MIMO techniques is the need to coexist with the techniques for mitigating interference and frequency and/or time selective fading. Improving the robustness of beamforming techniques for imperfect channel-state information (CSI) is another requirement. Meeting those requirements while using the proposed techniques is a topic for future research. The proposed techniques do not exhaust the potential of the space dimension; investigating such unexplored possibilities is also of interest.

The untapped potential of spatial DoFs could be exploited in non-conventional applications such as those investigated in this thesis to improve next-generation wireless systems.

~

# Bibliography

- [1] M. Abramowitz and I. Stegun, *Handbook of Mathematical Functions*. Dover Publications, Inc., New York, 1970.
- [2] I. Gradshteyn and I. Ryzhik, *Table of Integrals, Series, and Products*, 7th ed. Academic Press, 2000.
- [3] A. Papoulis and S. U. Pillai, *Probability, Random Variables and Stochastic Processes*, 4th ed. New York, NY: McGraw-Hill Inc., Jan. 2002.
- [4] G. Strang, *Linear Algebra and Its Applications*, 2nd ed. Orlando, FL: Academic Press, Inc, 1980.
- [5] R. A. Horn and C. R. Johnson, *Matrix Analysis*, 1st ed. New York, NY: Cambridge University Press, 1985.
- [6] International Telecommunication Union. (2008, Mar.) Background on IMT-advanced. [Accessed: July 2012]. [Online]. Available: <http://www.itu.int/md/R07-IMT.ADV-C-0001/en>
- [7] *Technical Specification Group Radio Access Network; Evolved Universal Terrestrial Radio Access (E-UTRA); LTE physical layer; General description (Release 10)*, 3GPP TS 36.201 V10, Jan. 2011.
- [8] I. E. Telatar, "Capacity of multi-antenna Gaussian channels," Bell Laboratories, Lucent Technologies, Murray Hill, NJ, Tech. Rep., Oct. 1995.
- [9] L. Cimini Jr., "Analysis and simulation of a digital mobile channel using orthogonal frequency division multiplexing," *IEEE Trans. Commun.*, vol. 33, no. 7, pp. 665–675, Jul. 1985.

- [10] Cisco Corporation. (2011, Jun.) Cisco visual networking index: forecast and methodology, 2010–2015. [Accessed: April 2012]. [Online]. Available: [http://www.cisco.com/en/US/solutions/collateral/ns341/ns525/ns537/ns705/ns827/white\\_paper\\_c11-481360.pdf](http://www.cisco.com/en/US/solutions/collateral/ns341/ns525/ns537/ns705/ns827/white_paper_c11-481360.pdf)
- [11] *Information Technology - Open Systems Interconnection - Basic reference Model: The Basic Model*, ITU-T Recommendation X.200, 2004.
- [12] D. Tse and P. Viswanath, *Fundamentals of Wireless Communication*. New York, NY: Cambridge University Press, Jun. 2005.
- [13] A. Goldsmith, *Wireless Communications*, 1st ed. New York, NY: Cambridge University Press, 2005.
- [14] J. G. Proakis, *Digital Communications*, 5th ed. New York, NY: McGraw-Hill, Inc., 2007.
- [15] G. J. Foschini, “Layered space-time architecture for wireless communication in a fading environment when using multi-element antennas,” *Bell Labs Technical Journal*, vol. 5, no. 2, pp. 41–59, Autumn 1996.
- [16] A. M. Tulino and S. Verdú, *Random Matrix Theory and Wireless Communications*, 1st ed., ser. Foundations and Trends in Communications and Information Theory. Hanover, MA: now publishers, 2004, vol. 1.
- [17] R. Somaraju and J. Trunpf, “Degrees of freedom of a communication channel: using DOF singular values,” *IEEE Trans. Inf. Theory*, vol. 56, no. 4, pp. 1560–1573, Apr. 2010.
- [18] A. Host-Madsen and A. Nosratinia, “The multiplexing gain of wireless networks,” in *Proc. IEEE International Symposium on Information Theory (ISIT)*, Adelaide, Australia, Sep. 2005.
- [19] R. U. Nabar, O. Oyman, H. Bölcskei, and A. J. Paulraj, “Capacity scaling laws in MIMO wireless networks,” in *Proc. Allerton Conference on Communication, Control, and Computing*, Monticello, IL, Oct. 2003.

- [20] V. Tarokh, H. Jafarkhani, and A. R. Calderbank, "Space-time block codes from orthogonal designs," *IEEE Trans. Inf. Theory*, vol. 45, no. 5, pp. 1456–1467, Jul. 1999.
- [21] D. Chizhik, G. Foschini, and R. Valenzuela, "Capacities of multi-element transmit and receive antennas: correlations and keyholes," *Electron. Lett.*, vol. 36, no. 13, pp. 1099–1100, Jun. 2000.
- [22] L. Zheng and D. Tse, "Diversity and multiplexing: a fundamental tradeoff in multiple-antenna channels," *IEEE Trans. Inf. Theory*, vol. 49, no. 5, pp. 1073–1096, May 2003.
- [23] I. Gopal and R. Rom, "Multicasting to multiple groups over broadcast channels," in *Proc. Computer Networking Symposium*, Washington, DC, Apr. 1988, pp. 79–81.
- [24] *IEEE Standard for Information technology–Telecommunications and information exchange between systems Local and metropolitan area networks–Specific requirements Part 11: Wireless LAN Medium Access Control (MAC) and Physical Layer (PHY) Specifications*, IEEE Std 802.11n, Mar. 2012.
- [25] T. Cover, "Broadcast channels," *IEEE Trans. Inf. Theory*, vol. 18, no. 1, pp. 2–14, Jan. 1972.
- [26] D. J. Love, R. W. Heath Jr., and T. Strohmer, "Grassmannian beamforming for multiple-input multiple-output wireless systems," *IEEE Trans. Inf. Theory*, vol. 49, pp. 2735–2747, Oct. 2003.
- [27] L.-U. Choi and R. D. Murch, "A transmit preprocessing technique for multiuser MIMO systems using a decomposition approach," *IEEE Trans. Wireless Commun.*, vol. 3, no. 1, pp. 20–24, Jan. 2004.
- [28] Q. H. Spencer, A. L. Swindlehurst, and M. Haardt, "Zero-forcing methods for downlink spatial multiplexing in multiuser MIMO channels," *IEEE Trans. Signal Process.*, vol. 52, no. 2, pp. 461–471, Feb. 2004.

- [29] R. Chen, Z. Shen, J. G. Andrews, and R. W. Heath, "Multimode transmission for multiuser MIMO systems with block diagonalization," *IEEE Trans. Signal Process.*, vol. 56, no. 7, pp. 3294–3302, Jul. 2008.
- [30] Y. Wu, S. Zhou, and J. Wang, "Joint linear transmitter and receiver design for the downlink of multiuser MIMO systems," *IEEE Commun. Lett.*, vol. 9, no. 11, pp. 991–993, Nov. 2005.
- [31] A. Tarighat, M. Sadek, and A. Sayed, "A multi user beamforming scheme for downlink MIMO channels based on maximizing signal-to-leakage ratios," in *Proc. IEEE International Conference on Acoustics, Speech, and Signal Processing (ICASSP)*, Philadelphia, PA, Mar. 2005.
- [32] H. Weingarten, Y. Steinberg, and S. Shamai, "The capacity region of the Gaussian multiple-input multiple-output broadcast channel," *IEEE Trans. Inf. Theory*, vol. 52, no. 9, pp. 3936–3964, Sep. 2006.
- [33] Z. Pan, K.-K. Wong, and T.-S. Ng, "Generalized multiuser orthogonal space-division multiplexing," *IEEE Trans. Wireless Commun.*, vol. 3, no. 6, pp. 1969–1973, Nov. 2004.
- [34] J. Lee and N. Jindal, "Dirty paper coding vs. linear precoding for MIMO broadcast channels," in *Proc. Asilomar Conference on Signals, Systems and Computer*, Pacific Grove, CA, Oct. 2006, pp. 779–783.
- [35] T. Cover and A. E. Gamal, "Capacity theorems for the relay channel," *IEEE Trans. Inf. Theory*, vol. 25, no. 5, pp. 572–584, Sep. 1979.
- [36] A. Sendonaris, E. Erkip, and B. Aazhang, "User cooperation diversity—part I: system description," *IEEE Trans. Commun.*, vol. 51, no. 11, pp. 1927–1938, Nov. 2003.
- [37] A. Nosratinia, T. E. Hunter, and A. Hedayat, "Cooperative communication in wireless networks," *IEEE Commun. Mag.*, vol. 42, no. 10, pp. 74–80, Oct. 2004.

- [38] *Technical Specification Group Radio Access Network; Evolved Universal Terrestrial Radio Access (E-UTRA); LTE physical layer; General description (Release 9)*, 3GPP TS 36.201 V9.1, Apr. 2010.
- [39] *Air Interface for Fixed and Mobile Broadband Wireless Access Systems Amendment 2: Physical and Medium Access Control Layers for Combined Fixed and Mobile Operation in Licensed Bands and Corrigendum 1*, IEEE Std 802.16e-2005, Feb. 2006.
- [40] *Wireless Medium Access Control (MAC) and Physical Layer (PHY) Specifications for High Rate Wireless Personal Area Networks (WPANs) - Amendment 2: Millimeter-wave-based Alternative Physical Layer Extension*, IEEE Std 802.15.3c-2009, Oct. 2009.
- [41] *Technical Specification Group Radio Access Network; Evolved Universal Terrestrial Radio Access (E-UTRA) and Evolved Universal Terrestrial Radio Access Network (E-UTRAN); Overall description; Stage 2 (Release 10)*, 3GPP TS 36.300 V10.7, Mar. 2012.
- [42] J. Lee, J.-K. Han, and J. Zhang, "MIMO technologies in 3GPP LTE and LTE-Advanced," *EURASIP Journal on Wireless Communications and Networking*, Jul. 2009.
- [43] A. Valdes-Garcia, S. T. Nicolson, J.-W. Lai, A. Natarajan, P.-Y. Chen, S. K. Reynolds, J.-H. C. Zhan, D. G. Kam, D. Liu, and B. Floyd, "A fully integrated 16-element phased-array transmitter in SiGe BiCMOS for 60-GHz communications," *IEEE J. Solid-State Circuits*, vol. 45, no. 12, Dec. 2010.
- [44] Wireless Gigabit Alliance. (2010, Jul.) WiGig white paper - defining the future of multi-gigabit wireless communications. [Accessed: April 2012]. [Online]. Available: <http://wirelessgigabitalliance.org/?getfile=1510>
- [45] D. Senaratne and C. Tellambura, "Generalized singular value decomposition for coordinated beamforming in MIMO systems," in *Proc. IEEE Global Communication Conference (Globecom)*, Miami, FL, Dec. 2010.

- [46] —, “GSVD beamforming for two-user MIMO downlink channel,” *IEEE Trans. Veh. Technol.*, Jun. 2012, (submitted).
- [47] —, “Beamforming for physical layer multicasting,” in *Proc. IEEE Wireless Communications and Networking Conference (WCNC)*, Cancun, Mexico, Mar. 2011, pp. 176–1781.
- [48] —, “Spatial multipath resolution with space time block codes,” *IEEE Wireless Comm. Lett.*, vol. 1, no. 3, pp. 249–252, Jun. 2012.
- [49] —, “Spatial multipath resolution for MIMO systems,” *IEEE Wireless Comm. Lett.*, vol. 1, no. 1, pp. 10–13, Feb. 2012.
- [50] D. W. Bliss, P. A. Parker, and A. R. Margetts, “Simultaneous transmission and reception for improved wireless network performance,” in *Proc. IEEE Workshop on Statistical Signal Processing (SSP)*, Madison, WI, Aug. 2007.
- [51] D. Senaratne and C. Tellambura, “Beamforming for space division duplexing,” in *Proc. IEEE International Conference on Communications (ICC)*, Kyoto, Japan, Jun. 2011.
- [52] D. Senaratne, C. Tellambura, and H. A. Suraweera, “Performance analysis of MIMO channel inversion in Rayleigh fading,” *IEEE Trans. Veh. Technol.*, vol. 61, no. 3, pp. 1188–1196, Mar. 2012.
- [53] C. F. V. Loan, “Generalizing the singular value decomposition,” *SIAM Journal on Numerical Analysis*, vol. 13, no. 1, pp. 76–83, Mar. 1976.
- [54] S. Y. Park and D. J. Love, “Outage performance of multi-antenna multicasting for wireless networks,” *IEEE Trans. Wireless Commun.*, vol. 8, no. 4, pp. 1996–2005, Apr. 2009.
- [55] A. Khisti, G. Wornell, A. Wiesel, and Y. Eldar, “On the Gaussian MIMO wiretap channel,” in *Proc. IEEE International Symposium on Information Theory (ISIT)*, Nice, France, Jun. 2007.

- [56] R. Liu, T. Liu, H. Poor, and S. Shamai, "MIMO Gaussian broadcast channels with confidential messages," in *Proc. IEEE International Symposium on Information Theory (ISIT)*, Seoul, Korea, Jul. 2009.
- [57] Y. Fu, L. Yang, and Z. He, "Amplify-and-forward relaying scheme based on GSVD for MIMO relay networks," in *Proc. International Conference on Neural Networks and Signal Processing (ICNNSP)*, Zhenjiang, China, Jun. 2008.
- [58] C. C. Paige and M. A. Saunders, "Towards a generalized singular value decomposition," *SIAM Journal on Numerical Analysis*, vol. 18, no. 3, pp. 398–405, Jun. 1981.
- [59] K. Zyczkowski and H.-J. Sommers, "Truncations of random unitary matrices," *Journal of Physics A: Mathematical and General*, vol. 33, no. 10, pp. 2045–2057, Mar. 2000.
- [60] P. J. Forrester and M. Krishnapur, "Derivation of an eigenvalue probability density function relating to the Poincaré disk," *Journal of Physics A: Mathematical and Theoretical*, vol. 42, no. 38, pp. 1751–8121, Sep. 2009.
- [61] B. D. Sutton, "The stochastic operator approach to random matrix theory," Ph.D. dissertation, Department of Mathematics, Massachusetts Institute of Technology, Cambridge, MA, 2005.
- [62] A. Edelman and B. D. Sutton, "The beta-Jacobi matrix model, the CS decomposition, and generalized singular value problems," *Foundations of Computational Mathematics*, vol. 8, pp. 259–285, May 2008.
- [63] I. Dumitriu and A. Edelman, "Matrix models for beta ensembles," *Journal of Mathematical Physics*, vol. 43, pp. 5830–5847, Nov. 2002.
- [64] O. Munoz-Medina, J. Vidal, and A. Agustin, "Linear transceiver design in nonregenerative relays with channel state information," *IEEE Trans. Signal Process.*, vol. 55, no. 6, pp. 2593–2604, Jun. 2007.

- [65] Y. Rong and F. Gao, "Optimal beamforming for non-regenerative MIMO relays with direct link," *IEEE Commun. Lett.*, vol. 13, no. 12, pp. 926–928, Dec. 2009.
- [66] P. Popovski and H. Yomo, "Physical network coding in two-way wireless relay channels," in *Proc. IEEE International Conference on Communications (ICC)*, Glasgow, Scotland, Jun. 2007, pp. 707–712.
- [67] S. Katti, H. Rahul, W. Hu, D. Katabi, M. Médard, and J. Crowcroft, "XORs in the air: practical wireless network coding," in *Proc. ACM SIGCOMM conference on Applications, technologies, architectures, and protocols for computer communications*, Pisa, Italy, Sep. 2006, pp. 243–254.
- [68] B. Quinn and K. Almeroth, "IP multicast applications: challenges and solutions," RFC 3170, Sep. 2001. [Online]. Available: <http://tools.ietf.org/rfc/rfc3170.txt>
- [69] N. D. Sidiropoulos, T. N. Davidson, and Z.-Q. Luo, "Transmit beamforming for physical-layer multicasting," *IEEE Trans. Signal Process.*, vol. 54, no. 6, pp. 2239–2251, Jun. 2006.
- [70] E. Karipidis, N. D. Sidiropoulos, and Z.-Q. Luo, "Transmit beamforming to multiple co-channel multicast groups," in *Proc. IEEE International Workshop on Computational Advances in Multi-Sensor Adaptive Processing (CAMSAP)*, Puerto Vallarta, Mexico, Dec. 2005, pp. 109–112.
- [71] I. H. Kim, D. J. Love, and S. Y. Park, "Recursive covariance design for multiple antenna physical layer multicasting," in *Proc. IEEE Radio and Wireless Symposium*, Orlando, FL, Jan. 2008, pp. 555–558.
- [72] S. Shi, M. Schubert, and H. Boche, "Physical layer multicasting with linear MIMO transceivers," in *Proc. Conference on Information Sciences and Systems (CISS)*, Princeton, NJ, Jul. 2008, pp. 884–889.
- [73] E. Matakani, N. D. Sidiropoulos, and L. Tassiulas, "On multicast beamforming and admission control for UMTS-LTE," in *Proc. IEEE International*

*Conference on Acoustics, Speech, and Signal Processing (ICASSP)*, Las Vegas, NV, Mar. 2008, pp. 2361–2364.

- [74] N. Petrov, V. Poulkov, and G. Iliev, “Reduced computational complexity beamspace beamforming design for MIMO multicast systems,” in *Proc. International Conference on New Technologies, Mobility and Security (NTMS)*, Cairo, Egypt, Dec. 2009, pp. 158–162.
- [75] D. Tomecki, S. Stanczak, and M. Kaliszan, “Low complexity power control and beamforming for multigroup multicast MIMO downlink channel,” in *Proc. IEEE Wireless Communications and Networking Conference (WCNC)*, Budapest, Hungary, Apr. 2009.
- [76] S. Y. Park and D. J. Love, “Capacity limits of multiple antenna multicasting using antenna subset selection,” *IEEE Trans. Signal Process.*, vol. 56, no. 6, pp. 2524–2534, Jun. 2008.
- [77] N. Jindal and Z.-Q. Luo, “Capacity limits of multiple antenna multicast,” in *Proc. IEEE International Symposium on Information Theory (ISIT)*, Seattle, WA, Jul. 2006, pp. 1841–1845.
- [78] C. Masouros and E. Alsusa, “A transmitter-based beamforming scheme for the MIMO downlink employing adaptive channel decomposition,” in *Proc. IEEE Wireless Communications and Networking Conference (WCNC)*, Sydney, Australia, Apr. 2010.
- [79] C. Oestges, A. D. Kim, G. Papanicolaou, and A. J. Paulraj, “Characterization of space-time focusing in time-reversed random fields,” *IEEE Trans. Antennas Propag.*, vol. 53, no. 1, pp. 283–293, Jan. 2005.
- [80] G. Forney Jr., “Maximum-likelihood sequence estimation of digital sequences in the presence of intersymbol interference,” *IEEE Trans. Inf. Theory*, vol. 18, no. 3, pp. 363–378, 1972.

- [81] G. E. Bottomley, T. Ottosson, and Y.-P. E. Wang, "A generalized RAKE receiver for interference suppression," *IEEE J. Sel. Areas Commun.*, vol. 18, no. 8, pp. 1536–1545, Aug. 2000.
- [82] S. M. Alamouti, "A simple transmit diversity technique for wireless communications," *IEEE J. Sel. Areas Commun.*, vol. 16, no. 8, pp. 1451–1458, Oct. 1998.
- [83] *Wireless LAN Medium Access Control (MAC) and Physical Layer (PHY) Specifications - Amendment 5: Enhancements for Higher Throughput*, IEEE Std 802.11n, Oct. 2009.
- [84] X.-B. Liang, "Orthogonal designs with maximal rates," *IEEE Trans. Inf. Theory*, vol. 49, pp. 2468–2503, Oct. 2003.
- [85] S.-K. Yong, "TG3c channel modeling sub-committee final report," IEEE P802.15, Tech. Rep., 2007, [Accessed: April 2012]. [Online]. Available: <https://mentor.ieee.org/802.15/file/07/15-07-0584-01-003c-tg3c-channel-modeling-sub-committee-final-report.doc>
- [86] P. Wolniansky, G. Foschini, G. Golden, and R. Valenzuela, "V-BLAST: an architecture for realizing very high data rates over the rich-scattering wireless channel," in *URSI International Symposium on Signals, Systems, and Electronics (ISSSE 98)*, Pisa, Italy, Sep. 1998, pp. 295–300.
- [87] W. W. S. Wong and E. S. Sousa, "A CDMA mixed cellular architecture with space division duplex (SDD) for symmetric/asymmetric wireless communications," in *Proc. IEEE Wireless Communications and Networking Conference (WCNC)*, New Orleans, LA, Sep. 1999.
- [88] C. K. Ng, S. Khatun, B. M. Ali, S. S. Jamuar, and M. Ismail, "Space division duplex (SDD) system using smart antenna," in *Proc. IEEE International Workshop Antenna Technology: Small Antennas and Novel Metamaterials (IWAT)*, Singapore, Mar. 2005.

- [89] P. Larsson and M. Prytz, "MIMO on-frequency repeater with self-interference cancellation and mitigation," in *Proc. IEEE Vehicular Technology Conference (VTC Spring)*, Barcelona, Spain, Apr. 2009.
- [90] T. Riihonen, S. Werner, and R. Wichman, "Spatial loop interference suppression in full-duplex MIMO relays," in *Proc. Asilomar Conference on Signals, Systems and Computers*, Pacific Grove, CA, Nov. 2009.
- [91] J. Sangiamwong, T. Asai, J. Hagiwara, Y. Okumura, and T. Ohya, "Joint multi-filter design for full-duplex MU-MIMO relaying," in *Proc. IEEE Vehicular Technology Conference (VTC Spring)*, Barcelona, Spain, 2009.
- [92] T. Riihonen, S. Werner, and R. Wichman, "Transmit power optimization for multiantenna decode-and-forward relays with loopback self-interference from full-duplex operation," in *Proc. Asilomar Conference on Signals, Systems and Computers*, Pacific Grove, CA, Nov. 2011, pp. 1408–1412.
- [93] B. Chun and Y. H. Lee, "A spatial self-interference nullification method for full duplex amplify-and-forward MIMO relays," in *Proc. IEEE Wireless Communications and Networking Conference (WCNC)*, Sydney, Australia, Apr. 2010.
- [94] H. Ju, S. Lee, K. Kwak, E. Oh, and D. Hong, "A new duplex without loss of data rate and utilizing selection diversity," in *Proc. IEEE Vehicular Technology Conference (VTC Spring)*, Singapore, May 2008.
- [95] M. L. Honig, P. Crespo, and K. Steiglitz, "Suppression of near- and far-end crosstalk by linear pre- and post-filtering," *IEEE J. Sel. Areas Commun.*, vol. 10, no. 3, pp. 614–629, Apr. 1992.
- [96] Analog Devices. (2010, Sep.) "Analog to digital converters". [Accessed: April 2012]. [Online]. Available: <http://www.analog.com/en/analog-to-digital-converters/products/index.html>

- [97] Texas Instruments. “ADC GPS beta”. [Accessed: April 2012]. [Online]. Available: [http://focus.ti.com/en/multimedia/flash/selection\\_tools/adc/adc.html](http://focus.ti.com/en/multimedia/flash/selection_tools/adc/adc.html)
- [98] A. J. Goldsmith and P. P. Varaiya, “Capacity of fading channels with channel side information,” *IEEE Trans. Inf. Theory*, vol. 43, no. 6, pp. 1986–1992, Nov. 1997.
- [99] T. Haustein, C. von Helmolt, E. Jorswieck, V. Jungnickel, and V. Pohl, “Performance of MIMO systems with channel inversion,” in *Proc. IEEE Vehicular Technology Conference (VTC Spring)*, Birmingham, AL, May 2002.
- [100] E. Jorswieck, G. Wunder, V. Jungnickel, and T. Haustein, “Inverse eigenvalue statistics for Rayleigh and Rician MIMO channels,” in *Proc. IEE Seminar on MIMO: Communications Systems from Concept to Implementations*, London, UK, Dec. 2001.
- [101] V. Jungnickel, T. Haustein, E. Jorswieck, and C. von Helmolt, “A MIMO WLAN based on linear channel inversion,” in *Proc. IEE Seminar on MIMO: Communications Systems from Concept to Implementations*, London, UK, Dec. 2001.
- [102] V. Jungnickel, T. Haustein, V. Pohl, and C. von Helmolt, “Link adaptation in a multi-antenna system,” in *Proc. IEEE Vehicular Technology Conference (VTC Spring)*, Jeju, Korea, Apr. 2003.
- [103] C. B. Peel, B. M. Hochwald, and A. L. Swindlehurst, “A vector-perturbation technique for near-capacity multiantenna multiuser communication—part I: channel inversion and regularization,” *IEEE Trans. Commun.*, vol. 53, no. 1, pp. 195–202, Jan. 2005.
- [104] G. Caire and S. Shamai, “On the achievable throughput of a multiantenna Gaussian broadcast channel,” *IEEE Trans. Inf. Theory*, vol. 49, no. 7, pp. 1691–1706, Jul. 2003.

- [105] A. T. James, "Distributions of matrix variates and latent roots derived from normal samples," *The Annals of Mathematical Statistics*, vol. 35, no. 2, pp. 475–501, Jun. 1964.
- [106] A. H. Nuttall, "Alternate forms for numerical evaluation of cumulative probability distributions directly from characteristic functions," *Proc. IEEE*, vol. 58, no. 11, pp. 1872–1873, Nov. 1970.
- [107] C. Tellambura, M. Soysa, and D. Senaratne, "Performance analysis of wireless systems from the mgf of the reciprocal of the signal-to-noise ratio," *IEEE Commun. Lett.*, vol. 15, no. 1, pp. 55–57, Jan. 2011.
- [108] D. Gore, R. Heath Jr., and A. Paulraj, "On performance of the zero forcing receiver in presence of transmit correlation," in *Proc. IEEE International Symposium on Information Theory (ISIT)*, Lausanne, Switzerland, Jun. 2002.
- [109] Z. Wang and G. Giannakis, "A simple and general parameterization quantifying performance in fading channels," *IEEE Trans. Commun.*, vol. 51, no. 8, pp. 1389–1398, Aug. 2003.
- [110] L. Ordoez, D. Palomar, and J. Fonollosa, "Ordered eigenvalues of a general class of Hermitian random matrices with application to the performance analysis of MIMO systems," *IEEE Trans. Signal Process.*, vol. 57, no. 2, pp. 672–689, Feb. 2009.
- [111] P. J. Smith and L. M. Garth, "Exact capacity distribution for dual MIMO systems in Ricean fading," *IEEE Commun. Lett.*, vol. 8, no. 1, pp. 18–20, Jan. 2004.
- [112] M. Chiani, M. Z. Win, and A. Zanella, "On the capacity of spatially correlated MIMO Rayleigh-fading channels," *IEEE Trans. Inf. Theory*, vol. 49, no. 10, pp. 2363–2371, Oct. 2003.
- [113] A. Erdelyi, W. Magnus, F. Oberhettinger, and F. G. Tricomi, *Tables of Integral Transforms*, ser. Bateman Manuscript Project, California Institute of Technology. McGraw-Hill Book Company, Inc, 1954, vol. 1.

- [114] I. Wolfram Research. The Wolfram functions site. [Accessed: April 2012]. [Online]. Available: <http://functions.wolfram.com/07.34.21.0002.01>
- [115] Y. Chen and C. Tellambura, "Distribution functions of selection combiner output in equally correlated Rayleigh, Rician, and Nakagami-m fading channels," *IEEE Trans. Commun.*, vol. 52, no. 11, pp. 1948–1956, Nov. 2004.

~

# Appendix A

## Proof for Diversity Order with GSVD beamforming

The proof of Theorem 2.1 is given below.

**Proof:** Consider GSVD beamforming over MIMO channels  $\mathbf{H}_1 \in \mathbb{C}^{m \times n}$  and  $\mathbf{H}_2 \in \mathbb{C}^{p \times n}$  undergoing independent and identically distributed (i.i.d.) Rayleigh fading, corresponding to users  $\mathcal{U}_1$  and  $\mathcal{U}_2$ , respectively.

Suppose  $\text{rank}((\mathbf{H}_1^H, \mathbf{H}_2^H)) = k \leq \min(m, p)$ .

The variable transformation  $\gamma_i = \alpha_i^2, i \in \{1, \dots, k\}$  on (2.4) gives the ordered joint probability density function (PDF)  $f_\gamma(\gamma_1, \dots, \gamma_k)$  as

$$f_\gamma(\gamma_1, \dots, \gamma_k) \propto \prod_{i=1}^k \gamma_i^{m-k} (1 - \gamma_i)^{p-k} \cdot \prod_{1 \leq i < j \leq k} (\gamma_i - \gamma_j)^2, \quad (\text{A.1})$$

for  $1 \geq \gamma_1 \geq \gamma_2 \geq \dots \geq \gamma_k \geq 0$ .

Integrating out  $\gamma_i, i \neq r$  of (A.1), as follows, yields the marginal PDF of  $\gamma_r$ .

$$f_{\gamma_r}(\gamma_r) \propto \underbrace{\int_{\gamma_{r+1}=0}^{\gamma_r} \int_{\gamma_{r+2}=0}^{\gamma_{r+1}} \dots \int_{\gamma_k=0}^{\gamma_{k-1}}}_{(k-r) \text{ cascaded integrations}} \times \underbrace{\int_{\gamma_{r-1}=\gamma_r}^1 \int_{\gamma_{r-2}=\gamma_{r-1}}^1 \dots \int_{\gamma_1=\gamma_2}^1}_{(r-1) \text{ cascaded integrations}} \times f_\gamma(\gamma_1, \dots, \gamma_k) d\gamma_1 \dots d\gamma_{r-1} d\gamma_{r+1} \dots d\gamma_k \quad (\text{A.2})$$

Note that  $f_{\gamma_r}(\gamma_r)$  will be a polynomial of  $\gamma_r$  alone, and that we are interested only in its *least order term*.

The joint PDF (A.1) is a homogeneous multivariate polynomial of  $\gamma_i$ 's, and, given any of its terms, integration by each  $\gamma_i$  raises the corresponding degree by

1. Since each of the  $(k - r)$  cascaded integrations involving  $\gamma_i, i > r$  has 0 as the lower limit of integration and  $\gamma_{i-1}$  as the upper limit, each integration increases the degree of  $\gamma_r$  in the resulting expression by one. As a result, the degree of the least order term of  $f_{\gamma_r}(\gamma_r)$  gets incremented by  $(k - r)$ . By contrast, having a non-zero constant of 1 as the upper limit of integration, none of the  $(r - 1)$  remaining cascaded integrals (corresponding to  $\gamma_i, i < r$ ) has any effect on the degree of  $\gamma_r$  in the desired least order term. Thus, we need to consider only the powers of  $\gamma_i, i \geq r$  in the integrand for diversity order analysis.

Also, for our purpose,

$$\prod_{i=1}^k \gamma_i^{m-k} (1 - \gamma_i)^{p-k} = \prod_{i=r}^k \gamma_i^{m-k} + \text{higher order terms}, \quad (\text{A.3})$$

which contributes  $(m - k)(k - r + 1)$  degrees to the least order term. The sum of degrees of  $\gamma_i, i \geq r$  in the factor  $\prod_{1 \leq i < j \leq k} (\gamma_i - \gamma_j)^2$  of (A.1) is minimal in its term corresponding to  $\prod_{i=1}^{k-1} \gamma_i^{2(k-i)}$ . That term yields  $2 \sum_{i=r}^{k-1} (k - i) = (k - r)(k - r + 1)$  degrees towards the diversity order.

Thus, the degree of  $\gamma_r$  in the least order term of  $f_{\gamma_r}(\gamma_r)$  comes to

$$n_r = (m - k)(k - r + 1) + (k - r)(k - r + 1) + (k - r) \quad (\text{A.4a})$$

$$= (m - r + 1)(k - r + 1) - 1. \quad (\text{A.4b})$$

The term  $(k - r)$  in (A.4a) represents the increment due to the  $(k - r)$  cascaded integrations.

From (A.4b) and using [109], we get the diversity order of the  $r^{\text{th}}$  common virtual channel (CVC) for user  $\mathcal{U}_1$  to be  $n_r + 1 = (m - r + 1)(k - r + 1)$  for  $r \in \{1, \dots, k\}$ , completing the proof. ■

~

## Appendix B

# Proofs of Theorems on MIMO Channel Inversion

This Appendix presents the proofs of Theorems 6.1, 6.2 and Corollaries 6.1, 6.2.

**Proof: (Theorem 6.1)** *The MGF of  $\Lambda^{-1}$  (arbitrary  $m \in \mathcal{Z}^+$ ).*

The moment generating function (MGF) of  $\Lambda^{-1}$  is given by the  $m$ -folded integral:

$$\mathcal{M}_{1/\Lambda}(s) = \int_{\lambda_1=0}^{\infty} \cdots \int_{\lambda_m=0}^{\infty} e^{-\sum_{i=1}^m \frac{1}{\lambda_i} s} f_{\lambda_1, \dots, \lambda_m}(\lambda_1, \dots, \lambda_m) d\lambda_1 \cdots d\lambda_m. \quad (\text{B.1})$$

Substituting (6.6) into (B.1) and simplifying with [113, Eqn. 4.5.1.(9)], we get

$$\begin{aligned} \mathcal{M}_{1/\Lambda}(s) &= \frac{1}{m! \mathcal{K}_{m,n}} \sum_{\substack{k_1, \dots, k_m \in \{0, \dots, 2(m-1)\} \\ \sum k_i = m(m-1)}} b(k_1, \dots, k_m) \\ &\quad \prod_{i=1}^m \int_{\lambda_i=0}^{\infty} \lambda_i^{k_i+n-m} e^{-\left(\lambda_i + \frac{s}{\lambda_i}\right)} d\lambda_i \\ &= \frac{1}{m! \mathcal{K}_{m,n}} \sum_{\substack{k_1, \dots, k_m \in \{0, \dots, 2(m-1)\} \\ \sum k_i = m(m-1)}} b(k_1, \dots, k_m) \\ &\quad \prod_{i=1}^m \left( 2s^{-\frac{k_i+n-m+1}{2}} \mathcal{K}_{k_i+n-m+1}(2\sqrt{s}) \right), \quad (\text{B.2}) \end{aligned}$$

and hence, (6.7). ■

**Proof: (Theorem 6.2)** *The PDF of  $\Lambda$  (case:  $m = 2$ ).*

From the definition of the cumulative distribution function (CDF),

$$\begin{aligned}
F_{\Lambda}(x) &= \mathcal{P} \left[ \frac{\lambda_1 \lambda_2}{\lambda_1 + \lambda_2} \leq x \right] = \mathcal{P} [\lambda_1(\lambda_2 - x) \leq \lambda_2 x] \\
&= \int_0^x \underbrace{\bar{F}_{\lambda_1|\lambda_2} \left( \frac{\lambda_2 x}{\lambda_2 - x} \middle| \lambda_2 \right)}_{\doteq 1} f_{\lambda_2}(\lambda_2) d\lambda_2 \\
&\quad + \int_x^{\infty} F_{\lambda_1|\lambda_2} \left( \frac{\lambda_2 x}{\lambda_2 - x} \middle| \lambda_2 \right) f_{\lambda_2}(\lambda_2) d\lambda_2. \\
\therefore \bar{F}_{\Lambda}(x) &= \int_x^{\infty} \bar{F}_{\lambda_1|\lambda_2} \left( \frac{\lambda_2 x}{\lambda_2 - x} \middle| \lambda_2 \right) f_{\lambda_2}(\lambda_2) d\lambda_2. \tag{B.3}
\end{aligned}$$

Differentiating (B.3) with respect to  $x$ , we get

$$\begin{aligned}
f_{\Lambda}(x) &= \int_x^{\infty} \frac{\lambda_2^2}{(\lambda_2 - x)^2} f_{\lambda_1|\lambda_2} \left( \frac{\lambda_2 x}{\lambda_2 - x} \middle| \lambda_2 \right) f_{\lambda_2}(\lambda_2) d\lambda_2 \\
&= \int_x^{\infty} \frac{\lambda_2^2}{(\lambda_2 - x)^2} f_{\lambda_1, \lambda_2} \left( \frac{\lambda_2 x}{\lambda_2 - x}, \lambda_2 \right) d\lambda_2 \\
&= \int_0^{\infty} \left( \frac{t+x}{t} \right)^2 f_{\lambda_1, \lambda_2} \left( \frac{x(t+x)}{t}, t+x \right) dt. \tag{B.4}
\end{aligned}$$

Substituting (6.8) into (B.4), and using the Binomial expansion and [2, Eqns. (3.471.9, 8.471.1)], we get

$$\begin{aligned}
f_{\Lambda}(x) &= \frac{1}{2\mathcal{K}_{2,n}} \int_0^{\infty} \left( \frac{t+x}{t} \right)^2 e^{-\frac{(t+x)^2}{t}} \\
&\quad \left( \frac{(t+x)^2(t-x)^2}{t^2} \right) \left( \frac{x(t+x)^2}{t} \right)^{n-2} dt \\
&= \frac{1}{2\mathcal{K}_{2,n}} x^{n-2} e^{-2x} \\
&\quad \sum_{k=0}^{2n} \binom{2n}{k} x^{2n-k} \int_0^{\infty} \frac{(t-x)^2}{t^{n+2-k}} e^{-\left(t+\frac{x^2}{t}\right)} dt \\
&= \frac{1}{\mathcal{K}_{2,n}} x^{2(n-1)} e^{-2x} \sum_{k=0}^{2n} \binom{2n}{k} \\
&\quad \left( (n-k-2x)\mathcal{K}_{k-n}(2x) + 2x\mathcal{K}_{k+1-n}(2x) \right). \tag{B.5}
\end{aligned}$$

■

**Proof: (Corollary 6.1)** *The CDF of  $\Lambda$  (case:  $m = 2$ ).*

Consider the following integral, which can be simplified into a single Meijer  $\mathcal{G}$  function [2, Sec. 9.3], first by using [2, Eqn. (9.34.4)], and then, by applying [114, Eqn. (7.34.21.2.1)] with a substitution  $u \doteq 2t$ .

$$\begin{aligned} \int_0^x t^\mu \mathcal{K}_\nu(t) e^{-t} dt &= \sqrt{\pi} \int_0^x t^\mu \mathcal{G}_{1 \ 2}^{2 \ 0} (2t \mid_{-\nu, \nu}^{0.5}) dt \\ &= \frac{\sqrt{\pi}}{2^{\mu+1}} \int_0^{2x} u^\mu \mathcal{G}_{1 \ 2}^{2 \ 0} (u \mid_{-\nu, \nu}^{0.5}) du \\ &= \frac{\sqrt{\pi}}{2^{\mu+1}} \mathcal{G}_{2 \ 3}^{2 \ 1} (2x \mid_{\mu-\nu+1, \mu+\nu+1, 0}^{1, \mu+1.5}). \end{aligned} \quad (\text{B.6})$$

Now let us consider the CDF of  $\Lambda$ :

$$\begin{aligned} F_\Lambda(x) &= \int_0^x f_\Lambda(t) dt \\ &= \frac{1}{\mathcal{K}_{2,n}} \sum_{k=0}^{2n} \binom{2n}{k} \left( (n-k) \int_0^x t^{2n-2} e^{-2t} \mathcal{K}_{k-n}(2t) dt \right. \\ &\quad \left. - 2 \int_0^x t^{2n-1} e^{-2t} \mathcal{K}_{k-n}(2t) dt + 2 \int_0^x t^{2n-1} e^{-2t} \mathcal{K}_{k+1-n}(2t) dt \right). \end{aligned} \quad (\text{B.7})$$

Applying the result of (B.6), in (B.7), we get (6.10). ■

**Proof: (Corollary 6.2)** *The SER (case:  $m = 2$ ).*

Equation (6.13) can be simplified as follows by using integration by parts and Leibniz's rule for differentiation [115, Eqn. (32)].

$$P_s = \int_0^\infty \mu \mathcal{Q}(\sqrt{2\nu x P}) dF_\Lambda(x) = \mu \int_0^\infty \frac{e^{-\nu P x}}{\sqrt{2\pi}} \cdot \frac{\sqrt{2\nu P}}{2\sqrt{x}} F_\Lambda(x) dx. \quad (\text{B.8})$$

Consider the integral

$$\begin{aligned} \mathbb{I}(q, \alpha, \beta, \gamma) &= \int_0^\infty x^{-0.5} e^{-qx} \mathcal{G}_{2 \ 3}^{2 \ 1} (4x \mid_{\beta, \gamma, 0}^{1, \alpha}) dx \\ &= \mathcal{L} \left\{ x^{-0.5} \mathcal{G}_{2 \ 3}^{2 \ 1} (4x \mid_{\beta, \gamma, 0}^{1, \alpha}) \right\} \Big|_{s=q}, \end{aligned} \quad (\text{B.9})$$

where  $q, \alpha, \beta, \gamma$  are positive reals, and  $\mathcal{L} \{ \cdot \}$  denotes the Laplace transform.

Eqn. (B.9) can be solved by using [113, Eqn. (4.23.34)] to get

$$\mathbb{I}(q, \alpha, \beta, \gamma) = q^{-0.5} \mathcal{G}_{3 \ 3}^{2 \ 2} \left( \frac{4}{q} \mid_{\beta, \gamma, 0}^{0.5, 1, \alpha} \right). \quad (\text{B.10})$$

Substituting (6.10) into (B.8) and using (B.10) completes the proof. ■

~